ISSN: 2764-5886
e-ISSN: 2764-622X

Volume 9· N° 2 · February 2026

Journal of Bioengineering, Technologies and Health

An Official Publication of
SENAI CIMATEC

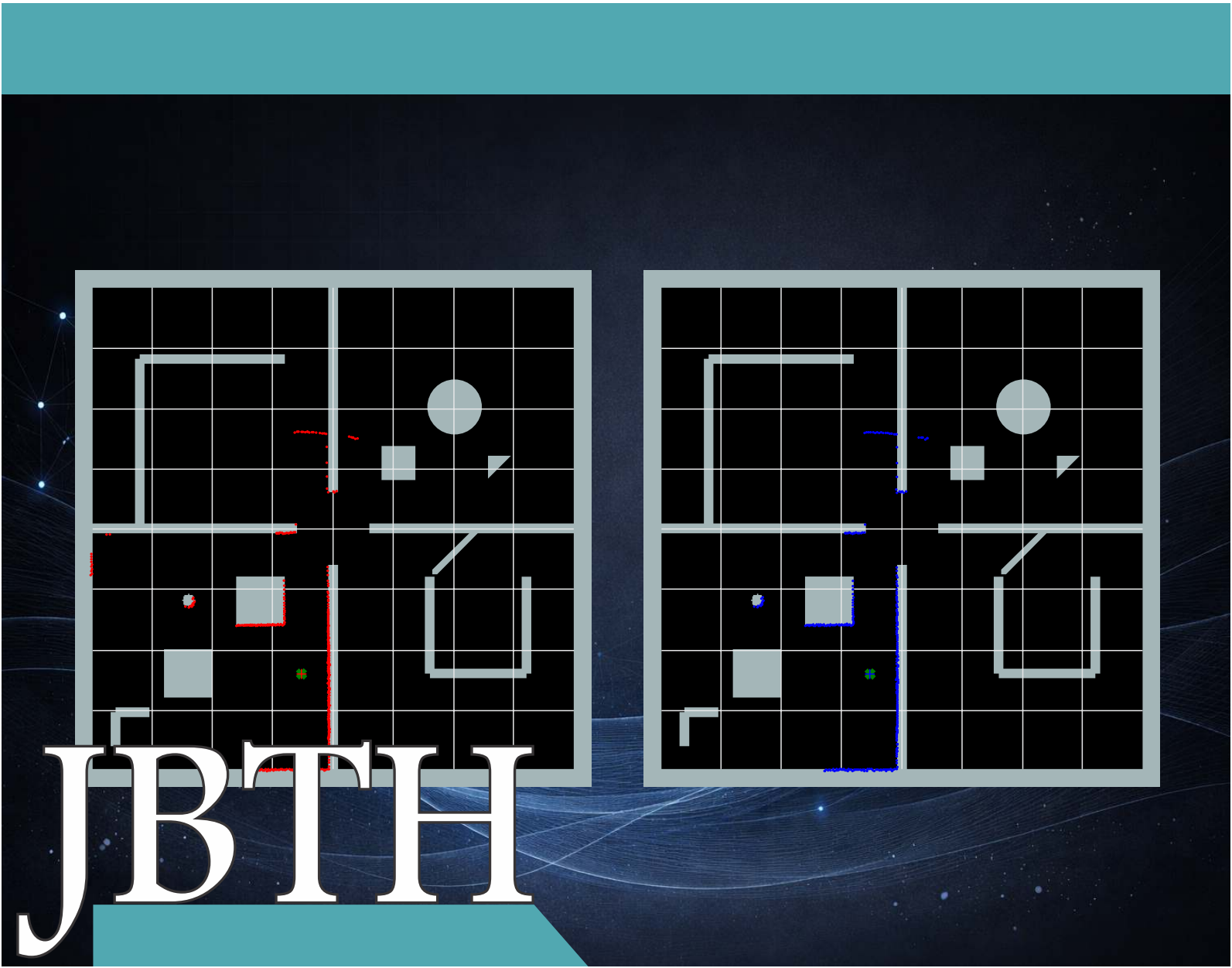

ISSN: 2764-5886 / e-ISSN 2764-622X

Volume 9 • Number 2 • February 2026

JOURNAL OF BIOENGINEERING TECHNOLOGIES AND HEALTH

An Official Publication of SENAI CIMATEC

PUBLISHED BY SENAI CIMATEC

Sistema FIEB | SENAI CIMATEC
PELO FUTURO DA INOVAÇÃO

February 2026
Printed in Brazil

JOURNAL OF BIOENGINEERING TECHNOLOGIES AND HEALTH

An Official Publication of SENAI CIMATEC

JOURNAL OF BIOENGINEERING TECHNOLOGIES AND HEALTH

Volume 9 • Number 2 **SUMMARY** *February 2026*

Original Articles

Original Case Study

Systematic Review

The Journal of Bioengineering, Technologies and Health (JBTH) is an official publication of the SENAI CIMATEC University (Serviço Nacional de Aprendizagem Industrial - Universidade Centro Integrado de Manufatura e Tecnologia). It is published montly (January to December) in English by SENAI CIMATEC University – Avenida Orlando Gomes, 1845, Piatã, Zip Code: 41650-010, Salvador-Bahia-Brazil; phone: (55 71) 3879-5501. The editorial offices are at SENAI CIMATEC University.

Editorial Office

Correspondence concerning subscriptions, advertisements, claims for missing issues, changes of address, and communications to the editors should be addressed to the Deputy Editor, Dr. Roberto Badaró, SENAI CIMATEC University (Journal of Bioengineering, Technologies and Health – JBTH) – Avenida Orlando Gomes, 1845, Piatã, Zip code: 41650-010, Salvador-Bahia-Brazil; phone: (55 71) 3879-5501; or sent by e-mail: jbth@fieb.org.br / jbth.cimatec@gmail.com.

Permissions

Postmaster

Send address changes to JBTH, Avenida Orlando Gomes, 1845, Piatã, Zip Code: 41650-010, Salvador-Bahia-Brazil.

Information by JBTH-SENAI CIMATEC University
Address: Avenida Orlando Gomes, 1845, Piatã, Zip Code: 41650-010, Salvador-Bahia-Brazil
Home-page: www.jbth.com.br
E-mail: jbth@fieb.org.br / jbth.cimatec@gmail.com
Phone: (55 71) 3879-5501 / 3879-5500 / 3879-9500

DOI:10.34178

ISSN: 2764-5886 / e-ISSN 2764-622X

COVER: Figure 5. Alignment in the best-case scenario. 2D Pose Optimization with Genetic Algorithms and Particle Swarm Optimization: A Comparative Analysis for Robotic Localization by Henrique Nunes Teixeira et al. J Bioeng. Tech. Health 2026;9(2):110.

Production of LLDPE and Sisal Composites via 3D Printing

Mariana Souza[1]*, Vinícius Oliveira[1], Lucas Horiuchi[1], Ana Paula Gonçalves[1], Paulo Romano Correia[1], Rodrigo Polkowski[1]
[1]TRL9 Lab; Salvador, Bahia, Brazil

3D printing is a processing technique that presents an interesting possibility for obtaining various materials, with advantages such as lower cost and design adaptation. Various materials are used for printing, including polymers. However, some difficulties can be faced due to the characteristics of the processed materials, such as their mechanical propertie (tensile strength and strain at maximum load). In this context, composite materials formed by linear low-density polyethylene (LLDPE) and sisal fibers in natura and chemically treated with sodium hydroxide solutions were obtained via extrusion (initially on a twin-screw printer to obtain the masterbatch, a single-screw printer to manufacture the filaments and a 3D printer to obtain the test specimens) with the aim of developing new materials and contributing to aspects related to LLDPE processing in the context of additive manufacturing. The specimens were mechanically evaluated through tensile testing, revealing that the control formulation exhibited greater tension at maximum force than the composites, as well as greater strain at maximum load. Comparing the materials with fiber addition without treatment and with treatment with sodium hydroxide at different content, it was observed that the treatment did not lead to significant differences in the evaluated mechanical properties. Thus, although the processing was successful, resulting in intact specimens, fiber treatments under the evaluated conditions were not sufficient to obtain improved mechanical properties.
Keywords: Natural Fibers. LLDPE. Composite Material. 3D Printing.

Additive manufacturing, also known as 3D printing or rapid prototyping, has been around for decades. However, it was initially an expensive and unviable technology for the general market. However, with advances in the 21st century, costs have dropped significantly, enabling the introduction of 3D printing into various sectors [1].

3D processing has undergone significant expansion in recent years, being widely used worldwide and increasingly applied to mass customization and production of any type of design in areas such as agriculture, healthcare, the automotive and aerospace industries [2].

Aspects associated with 3D printing such as less material waste, ease of manufacturing, lower post-processing rate and energy efficiency make the process sustainable for industrial use [3].

Since the origin of additive manufacturing (AM) there has been a growing interest in this technology for polymers and their composites, driven by advantages such as high efficiency, resolution and customization, however this type of processing requires certain conditions of these materials such as physical and rheological properties, providing limited application of AM in several industries [4]. Several polymers are used in 3D printing processes, such as PLA and PETG [5,6].

Polyolefins and polyolefin elastomers are widely used in various applications, however, they present challenges for use in 3D printing such as excessive softness, shrinkage, warping and low mechanical properties, which limits their application [7]. Other critical issues related to fused deposition (FDM) polyolefin 3D printing are low bed adhesion and low interlayer adhesion. However, the addition of filler can help reduce warpage and increase the strength of printed parts [8].

Low-density polyethylene (LLDPE) is a polymer characterized by medium crystallinity, presenting moderate rigidity and mechanical strength [9].

Some studies have used materials composed of LLDPE obtained by 3D printing [7,10], however, compared to other polymers, the number of studies is still incipient and, therefore, works that propose to investigate possibilities for this material can

Received on 18 November 2025; revised 20 January 2026.
Address for correspondence: Mariana Souza. TRL9 LAB Testing and Technical Analysis. Salvador, Bahia, Brazil. Zipcode:40210-630. E-mail: mariana.costa@trl9.tech.

J Bioeng. Tech. Health 2026;9(2):78-82

contribute with new paths in terms of additive manufacturing of different polymers, expanding the range of uses.

Regarding the addition of vegetable fibers to the LDPE matrix, the study developed by Wearn [11] addresses that components such as lignin and hemicellulose present in these fibers can hinder their adhesion to the polymer matrix, emphasizing that the removal of these compounds in adequate proportions from coconut fibers reduces their hydrophilicity and facilitates coupling to the LDPE. Still according to Wearn [11] the most commonly used chemical treatment for vegetable fibers is alkaline extraction using a sodium hydroxide solution, which is responsible for removing some components from the surface of the fibers, such as lignin and hemicellulose.

Some studies have already proposed to evaluate the effect of mercerization treatment of lignocellulosic biomass in composites involving low-density polyethylene (LDPE) such as castor cake [12], coconut fiber [11], in addition to publications involving linear low-density polyethylene (LLDPE) and natural fibers such as areca fiber [13] and ground hemp fibers [14].

However, the 3D printing process of composites formed by natural fibers and an LLDPE matrix is a field that can be contributed to, aiming to collaborate with the expansion of printing possibilities for this polyolefin, in addition to adding value to a lignocellulosic residue, in this case using residues from sisal processing.

Fiber is the main commercial product, corresponding to 4% of the weight of the sisal leaf, and among the co-products are mucilage, juice and short fibers, also called loofah, corresponding to, respectively, 15; 80 and 1%. In terms of production volume, Brazil is the main world producer, with Bahia ranking first [15].

Therefore, this work aims to produce composites of LLDPE and sisal fibers in natura and chemically treated via 3D printing, with the materials obtained being mechanically evaluated by tensile test.

Materials and Methods

The composites were prepared by mixing LLDPE (Braskem, ML3602U resin) and sisal fibers, totaling 04 formulations composed of both natural fibers and fibers chemically treated with sodium hydroxide solution at different concentrations (5 and 12.5%). For the treated fibers, a 1:20 ratio was used, with a 5% fiber content in each of the composites (Table 1).

The extrusion to obtain the masterbatch occurred in a co-rotating twin-screw extruder (DR.16.40.AX from AX Plásticos), with the temperature profile was 100/150/170/180/190/190/195/200/195 °C and screw rotation speed to 120 rpm. After extrusion, the materials were granulated. Then, the production of the filaments occurred, using a Filmaq 3D single-screw extruder, speed 18.5 rpm, temperature 185 ºC.

The production of the specimens of tensile tests, prepared in accordance with ASTM D638 type IV, were carried out on a 3D printer (Prusa Research MK3S+), through the following printing parameters: nozzle diameter: 0.6 mm, printing and printing bed temperature, respectively, 190 and 123 °C; printing speed: 30 mm/s; rectilinear pattern, orientation: 0% and infill density 100%.

The specimens were tested on an EMIC universal testing machine model DL200MF with a 2 kN load cell and a test speed of 50 mm/min, with five

Table 1. Formulation of LLDPE/sisal composites.

Formulation	LLDPE (%)	Natural fiber (%)	Treated fiber 5%	Treated fiber 12.5%
F1	100.0	–	–	–
F2	95.0	5.0	–	–
F3	95.0	–	5.0	–
F4	95.0	–	–	5.0

replicates being prepared for each formulation. The properties analyzed were tensile strength (MPa) and strain at maximum load (%). The tensile tests results were analyzed by the Tukey test ($p<0.05$) to compare means.

Results and Discussion

The 3D-printed specimens are shown in Figure 1. The images of the composites demonstrate that it was possible to obtain specimens without the presence of macroscopic defects, requiring future scanning electron microscopy analyses and dimensional analysis of the test specimens to identify aspects such as the distribution of matrix fibers and variation in dimensions, respectively.

In terms of processability, the adjustments made during printing, in addition to the development of a PETG substrate for subsequent deposition of the composites, were also essential for printing. The PETG surface enabled layer-by-layer deposition of the material, minimizing the shrinkage effect characteristic of LLDPE, with this surface being removed immediately after the 3D printing process. Figure 2 shows the test specimens obtained via 3D printing after performing a tensile test.

The results of the tensile strength (MPa) and strain at maximum load (%) of the different formulations are presented in Table 2.

When evaluating the mechanical properties of the specimens printed via 3D processing, it was observed that the pure polymer differs statistically from the composites in relation to the properties evaluated, except for the strain at maximum load (%) in which the composite F2 is statistically equal to the control formulation – F1, while the composites did not present any significant difference between them.

Evaluating the composites exclusively, it can be stated that the addition of fibers, whether made with raw material or with material treated with sodium hydroxide solution at different concentrations, did not contribute to mechanical changes in the materials under the conditions evaluated in the present study. Therefore, for these samples, mercerization did not contribute to greater fiber adhesion and dispersion to the matrix reflecting similar results, regardless of the chemical treatment used.

Figure 1. Tensile specimens obtained via 3D printing.

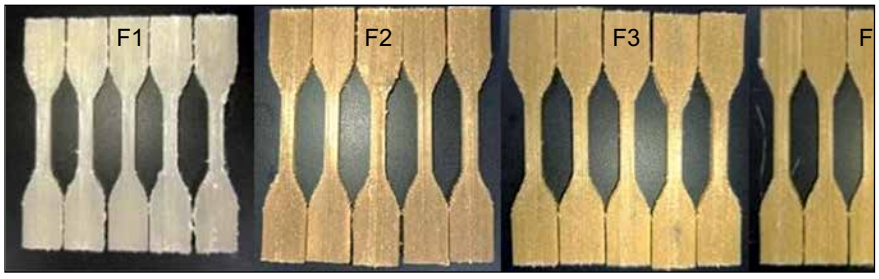

Figure 2. Test specimens obtained via 3D printing after performing a tensile test.

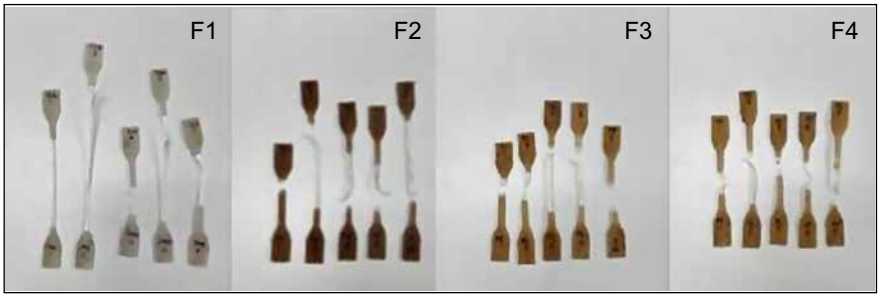

Table 2. Mechanical performance of composite materials.

Formulation	Tensile strength (MPa)	Strain at maximum load (%)
F1	14.83± 0.77a	31.92±2.96a
F2	13.56±0.44b	26.88±1.20ab
F3	13.50±0.50b	26.56±0.72b
F4	13.38±0.36b	28.88±1.04b

Means followed by the same letter do not differ statistically from each other using the Tukey test at 95% confidence interval.

Rocha and colleagues (2020) evaluated the mechanical properties of composites formed by LDPE/PHB and castor bean cake treated via mercerization with 5 and 10% calcium hydroxide solutions. They observed that the chemical treatments contributed to improved properties due to better adhesion properties between interfaces. The authors also revealed that the lower concentration solution probably contributed to better results, attributing the inferior performance of the materials added with fibers treated with higher concentrations of sodium hydroxide to the compromised integrity of the fibers.

The evaluation of coconut fibers treated with 10% sodium hydroxide solution [11] revealed that in terms of tensile properties, the composites with different contents, 5 e 10%, presented maximum stress values inferior compared to pure LDPE. Although it is expected that the removal of components such as lignin and hemicellulose through alkaline treatment would contribute to increased adhesion between filler and matrix [11].

In terms of the strain at maximum load parameter, it was observed that materials F3 and F4, which correspond to the composites in which fibers treated with sodium hydroxide solution at different concentrations were added, presented a lower capacity to deformation than pure LDDPE. A decrease in deformation in composites involving lignocellulosic fibers is a possible effect.

A material produced by Lemos [16] based on PLA and lignocellulosic fibers evaluated through tensile testing showed a decrease in mechanical strength when compared to the control material. This result was attributed to the presence of short fibers dispersed in the matrix, which may have caused a discontinuity, thus hindering the distribution and transfer of the applied stress, leading to a reduction in the maximum stress supported by the biocomposites. Regarding elongation, a decrease in this parameter was observed, which was intensified by the increase in the content of added natural fiber.

There was an increase in stiffness of the fiber composite produced by Wearn [11], reflected in a higher tensile modulus since, according to the authors, the addition of coconut fiber makes the material more rigid due to the stress it is capable of withstanding. Another point raised is that coconut fibers, when compared to other lignocellulosic materials, have a high lignin content, thus reducing the average tensile strength and increasing the material's stiffness.The addition of fiber also reduced the ductility of the samples since there was a lower deformation rate of the composites up to the maximum tensile stress [11].

In evaluating mechanical properties, Lemos and Martins (2014) [16] explored how the insertion of a rigid phase, such as wood fibers, can increase the rigidity of the polymer blend. They emphasized, through the evaluated references, that a relevant point for materials of this nature is the surface treatment, since this modifies the lignin content through the use of alkaline solutions of sodium hydroxide andhypochlorite. Therefore, the surface chemical treatment of the fibers can substantially affect the thermal, mechanical, and adhesion properties between the polymer matrix and the fibers, which are dependent on factors such as reagent concentrations and temperature. In the present work, only the sodium hydroxide

concentration parameter at room temperature was evaluated, and the study can be expanded in the future to investigate different chemical treatment temperatures and their effect, for example, aiming to present new perspectives for the addition of natural fibers in LLDPE, thus contributing to the aggregation of value of an agro-industrial residue, in addition to collaboration for the field of composite production via 3D printing.

Conclusion

Composite materials composed of LLDPE and sisal fibers were obtained through 3D printing, demonstrating the potential of additive manufacturing for processing various materials. The mercerized (chemically treated) fibers were obtained, however, the necessary reinforcing effect was not observed in the materials evaluated, requiring further studies to improve the characteristics of these composites.

Acknowledgement

The authors are grateful to the TRL9 – LAB, Company, LAPESCA-UFBA and Brazilian Research Agency-CNPq.

References

1. Attaran M. The rise of 3-D printing: the advantages of additive manufacturing over traditional manufacturing. Bus Horiz. 2017;60:677-688. doi:10.1016/j.bushor.2017.05.011
2. Shahrubudin N, et al. An overview on 3D printing technology: technological, materials and applications. Procedia Manuf. 2019;35:1286-1296. doi:10.1016/j.promfg.2019.06.089
3. Jandyal A, et al. 3D printing – a review of processes, materials and applications in Industry 4.0. Sustain Oper Comput. 2022;3:33-42. doi:10.1016/j.susoc.2021.09.004
4. Park S, et al. 3D printing of polymer composites: materials, processes, and applications. Matter. 2022;5:43-76. doi:10.1016/j.matt.2021.10.018
5. Alex Y. Comprehensive study of PLA material extrusion 3D printing optimization and its comparison with PLA injection molding through life cycle assessment. Sustain Mater Technol. 2025;43:e01222. doi:10.1016/j.susmat.2024.e01222
6. Santana L, et al. A comparative study between PETG and PLA for 3D printing through thermal, chemical and mechanical characterization. Matéria (Rio J). 2018;23(4). doi:10.1590/S1517-707620180004.0601
7. Liu T, et al. Influence of LLDPE on the mechanical properties improvement of 3D printed POE/LLDPE blends. J Vinyl Addit Technol. 2024. doi:10.1002/vnl.22099
8. Verma N, et al. Fused deposition modeling of polyolefins: challenges and opportunities. Macromol Mater Eng. 2023;308. doi:10.1002/mame.20220042
9. Canevarolo Jr SV. Ciência dos polímeros: um texto básico para tecnólogos e engenheiros. São Paulo: Artliber; 2002.
10. Peng Z, et al. FDM-3D printing LLDPE/BN@GNPs composites with double network structures for high-efficiency thermal conductivity and electromagnetic interference shielding. Compos Part B Eng. 2023;251:110491. doi:10.1016/j.compositesb.2022.110491
11. Wearn YN. Coconut fiber/LDPE composites: effect of surface treatment of coconut fibers to produce green composites. Matéria (Rio J). 2020;25(1). doi:10.1590/S1517-707620200001.0873
12. Rocha MC, et al. Mercerization effect on the properties of LDPE/PHB composites reinforced with castor cake. Polímeros. 2020;30(4). doi:10.1590/0104-1428.07720
13. Vishnu KA, et al. Areca fiber reinforced LLDPE biocomposite. Mater Today Proc. 2020;24. doi:10.1016/j.matpr.2020.03.619
14. Zelca Z, et al. LLDPE and natural fiber composites characterization using AFM. IOP Conf Ser Mater Sci Eng. 2017;251:012086. doi:10.1088/1757-899X/251/1/012086
15. Severino LS, et al. Proposta de um modelo de produção sustentável e competitivo para o sisal brasileiro. Campina Grande: Embrapa Algodão; 2023.
16. Lemos AL, et al. Development and characterization of polymeric composites based on poly(lactic acid) and natural fibers. Polímeros. 2014;24:190-197. doi:10.4322/polimeros.2014.047

Structural Sizing of Wing Spar in Fixed-Wing Unmanned Aerial Vehicle Concept Using Tsai-Hill Failure Criterion

Hariel Dumont Dias Sousa[1*], Jefferson dos Reis do Carmo[1], Mateus Baqueiro Mendonça O'Dwyer[1], Kauan Dantas Brito da Silva[1], Guilherme Prazeres Matos de Souza[1], Douglas Lima Silva[2], Bruno de Sousa Silva[2]

[1]SENAI CIMATEC University, Center of Competence in Aeronautical Engineering and Drones; [2]SENAI CIMATEC University, Department of Industrial Product Development; Salvador, Bahia, Brazil

The structural design for a Fixed-Wing Unmanned Aerial Vehicle (UAV) begins with preliminary aeronautical calculations driven by the mission profile. This profile defines key requirements such as endurance, cruise altitude, and payload capacity, which in turn guide the estimation of gross weight, wing loading, and power-to-weight ratio. These parameters determine the wing planform area, span, and aspect ratio, optimizing aerodynamic efficiency. Based on these definitions, wing load calculations are performed, accounting for distributed loads from lift and any concentrated loads from internal masses. Bending moment, shear force, and torsional moment diagrams along the span are obtained for the most critical load case. The results contribute to the subsequent structural design phase. With the maximum loads identified, the sizing of the stringers (longitudinal stiffeners installed along the wing skin). For this purpose, the reinforced shell model was adopted, composed of a core and flanges in polymer matrix composite material and fiber reinforcement, with assumptions of symmetry and linear loading. The stringers are sized to withstand buckling and axial compression, considering the maximum bending moment and the section centroid position. The cross-section of the profiles was selected based on the relationship between structural weight and stiffness. This process ensures that the structure withstands in-flight loads with minimum weight, applying the Tsai-Hill failure criterion. Using a numerical computing code to assess multiple geometries, the optimal configuration achieved reduced structural weight while maintaining an adequate minimum safety margin.

Keywords: UAV. Load Calculations. Structural Sizing. Stringers. Tsai-Hill.

Abbreviations: UAV, Unmanned Aerial Vehicle.

In the conceptual design phase of an aircraft, aerodynamics guides critical decisions such as the selection of the airfoil profile, the definition of fuselage geometry, and the configuration of control surfaces. In his study, Raymer [1] concludes that these elements directly influence the lift, drag, and moment coefficients, which are decisive for the aircraft's flight behavior and operational envelope. As Barros [2] states that performance targets are an essential part of aircraft design, the study of the aircraft structure becomes necessary to validate the conceptual design.

The main structural component of the wing is the spar, responsible for carrying bending, torsional, and distributed loads along the wingspan. Therefore, the present study aims to analyze the structural sizing of a wing spar in a Fixed-Wing Unmanned Aerial Vehicle (UAV) concept, applying the Tsai–Hill failure criterion.

Materials and Mtehods

The method was based on three main pillars: preliminary aeronautical calculations, wing load analysis, and main spar sizing. The structural assessment under critical conditions aims to determine key parameters such as deflection, torsion, ultimate loads, failure modes, load combinations, and life-cycle analysis. By understanding the structural behavior under variable loading conditions, it becomes possible to predict potential failure modes and define mitigation strategies, thereby contributing to the continuous improvement of the design.

Received on 15 October 2025; revised 10 January 2025.

Address for correspondence: Hariel Dumont Dias Sousa. Av. Orlando Gomes, 1845, Piatã, Salvador, Bahia, Brazil. Zipcode: 41650-010. E-mail: neon.951@hotmail.com.

J Bioeng. Tech. Health 2026;9(2):83-90

Preliminary Aeronautical Calculations

In his study, Raymer [1] defined that the initial phase of aircraft development is driven by the mission concept, which determines the key design decisions. In this context, the mission serves as the guiding factor for preliminary aeronautical calculations. As a case study, a UAV designed for coastal surveillance was considered, defining its baseline geometry as well as aerodynamic and propulsion characteristics.

Through benchmarking, existing UAV designs with similar mission requirements were analyzed in order to establish performance targets and structural parameters. The initial parameters for the aeronautical calculations were set based on standard and commercially available values for UAVs with comparable operational profiles.

For Raymer [1], the actual empty weight will be calculated by estimating and summing the weights of all aircraft components. Based on this, initial estimates for Maximum Takeoff Weight (MTOW), empty weight, and payload capacity were carried out. The basic dimensions (wing area, wingspan, and fuselage length) were estimated using data from similar aircraft, along with parameters such as wing loading, aspect ratio, and thrust-to-weight ratio. These were used to analyze the constraint diagram, correlating thrust-to-weight and wing loading to determine the feasible wing area and preliminary power requirements for the project.

Given that the intended mission is surveillance, the operational goal is to maximize endurance, following the methodology derived from the Breguet endurance equation, according to Raymer [1].

Wing Load Calculations

For the definition of limit loads, the method described in Barros [2] was adopted, based on JAR-VLA 333 [3]. Initially, a free-body diagram was developed to map all forces and moments acting on the UAV during steady, level flight, as shown in Figure 1. The diagram includes thrust force (T), drag force (D), weight force (W), wing lift force (Lw), vertical stabilizer lift force (Lev), horizontal stabilizer lift force (Lht), moment generated by wing lift (Mw), and the moment generated by horizontal stabilizer lift and the aerodynamic center (AC).

Subsequently, a flight envelope, also known as a V–n diagram, was developed to define the operational limits of the aircraft. The envelope consists of both maneuver and vertical gust diagrams. By developing the maneuver diagram, it was possible to determine the operating speeds, including stall speed (VS), maneuvering speed (VA), cruise speed (VC), and dive speed (VD), following the JAR-VLA 335 [4] reference. However, due to the absence of a defined propulsion system, the maximum speed was determined based on the legal limit for UAVs

Figure 1. Free-body diagram of a UAV.

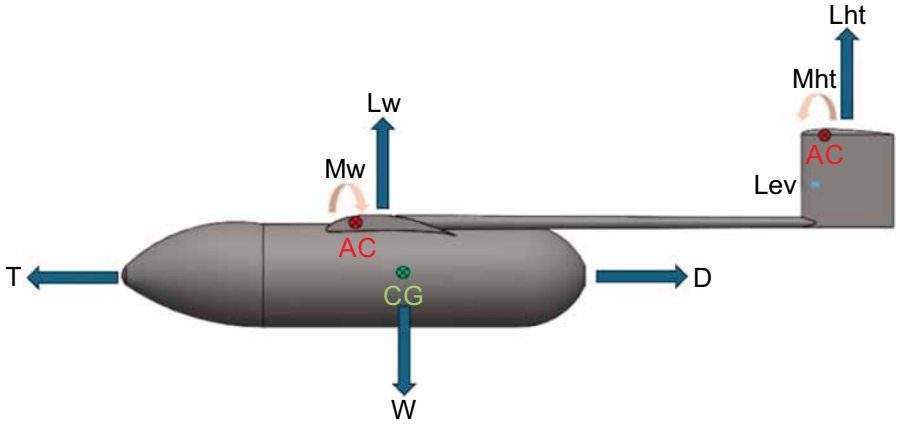

in Brazil, according to DECEA's AC100-40 [5], corresponding to 33.33 m/s.

The maximum (nmax) and minimum (nmin) load factors were initially defined in accordance with JAR-VLA 337 [6]. However, since this regulation was intended for manned aircraft, the prescribed values did not meet the design requirements. Therefore, based on the method described in Rosa [7], the nmax and nmin values were adjusted to better suit the project specifications. Table 1 presents the values used for the development of the maneuver diagram.

For the development of the vertical gust diagram, several factors influencing the forces acting on the aircraft throughout all phases of flight were considered. Among these forces, the gust load stands out, characterized by sudden and temporary changes in velocity that can lead to increased structural loads due to abrupt variations in dynamic pressure, according to Raymer [1].

The study focused exclusively on strictly vertical gusts, as they directly influence the increase or decrease of the load factor. According to JAR-VLA 341 [8], gust loads must be calculated using a gust gradient (Ude) of 15.24 m/s. However, since this standard was primarily intended for analyses of commercial aircraft, adopting this value would result in an overly conservative V-n diagram, leading to an unnecessarily robust and heavy UAV.

Nevertheless, NACA Report NR-692 [9] indicates that, for altitudes below 1,066.8 meters, gust velocities do not exceed 7.62 m/s, with over 95% of recorded measurements being below 6.10 m/s. The report also provided gust gradient (Ude) data as a function of altitude, allowing interpolation and derivation of equations.

Therefore, to define the parameters, a reference altitude of 150 meters and an operational radius of 30 km were adopted. As a result, Ude was determined as 8.06 m/s for cruise speed (VC) and 4.03 m/s for dive speed (VD). Subsequently, the calculation of positive and negative gust-induced load factors (ngust+ and ngust–) and their respective parameters was carried out following the procedures described in JAR-VLA 341 [8]. The obtained values are presented in Table 2.

Upon completion of the diagrams, a provisional V-n diagram (using estimated values) could be developed, serving as a guide for all load analysis and simulation processes. The diagram is illustrated in Figure 2.

For proper structural sizing, a load combination analysis must be performed based on individually calculated load effects. This study was essential because, during flight, the UAV will be subjected to loads that generate various combined forces, such as shear forces, bending moments, and torsional moments at a single point. Gust-induced loads must be analyzed separately, without the influence of other load effects. After selecting the critical cases from the flight envelope, the acting loads and moments for each selected condition could be extracted.

For this purpose, the method of Barros [2] was followed, which employs the Stender chord method. This method was based on the aerodynamic lift distribution and wing geometry to estimate the resulting internal loads. The analysis of all cases within the V-n diagram and the extraction of their

Table 1. Parameters for the maneuvering diagram.

Symbol	Definition	Value	Value
VS	Stall speed	11.84 m/s	42.62 km/h
VC	Cruise speed	30.00 m/s	108.00 km/h
VD	Dive speed	37.50 m/s	135.00 km/h
VA	Maneuvering speed	20.51 m/s	73.83 km/h
nmax	Maximum load factor	3.00	-
nmin	Minimum load factor	-1.00	-

Table 2. Parameters for the gust diagram.

Symbol	Definition	Value [-]
ug	Aircraft mass ratio	11.4367
Kg	Gust alleviation factor	0.6013
ngust + VC	Load factor due to positive gust at VC	5.9005
ngust - VC	Load factor due to negative gust at VC	-3.9005
ngust + VD	Load factor due to positive gust at VD	4.0628
ngust - VD	Load factor due to negative gust at VD	-2.0628

Figure 2. Provisional V-n diagram.

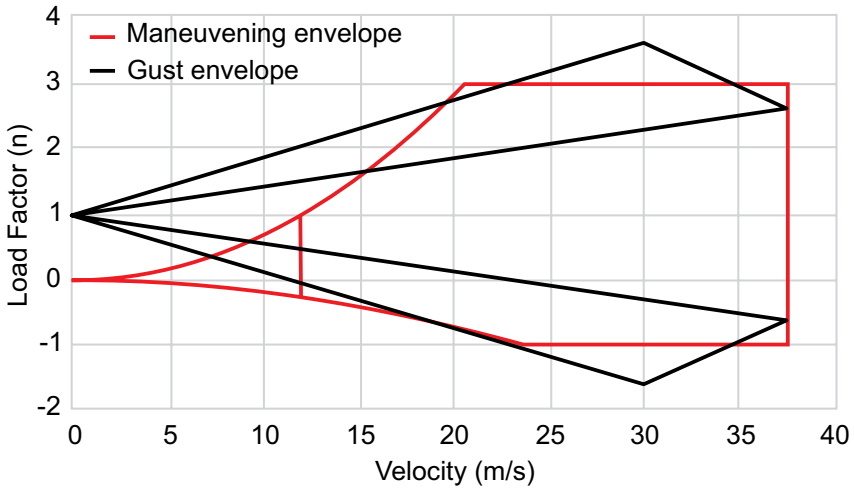

corresponding limit loads was of utmost importance, as they guide the aircraft's structural sizing.

The design safety factor (FOS) is a coefficient applied conservatively to assist in the UAV structural design. Structures must be designed to withstand loads multiplied by the safety factor, ensuring robustness beyond expected operational conditions. The safety factor adopted for the UAV structural design is defined as 1.5 to provide limited safety margins, in accordance with JAR-VLA 303 [10] standard.

Ultimate Loads are obtained by multiplying Limit Loads by the safety factor. They represent the maximum load that the structure can sustain before failure and are used in structural testing for verification and validation purposes. These ultimate loads were applied throughout the entire semi-wingspan and, at the end of the analysis, Table 3 presents the Ultimate Loads based on the highest loads found.

With this study completed, the detailed structural design process can begin, considering the identified critical loads.

Sizing of the Stringer

Tahir [11], in his study, addresses the Failure Criterion as being used to evaluate the structural capacity to support a given load, regardless of

Table 3. Ultimate loads based on the highest limit loads found.

Type of Load	Limit Loads	FOS	Ultimate Loads
Shear Force	585 N	1.5	877.5 N
Bending Moment	573 N.m	1.5	859.5 N.m
Twisting Moment	142 N.m	1.5	213 N.m

the occurrence of failure. The Tsai-Hill failure theory is an adaptation of the Von Mises theory for applications in anisotropic materials, such as unidirectional composite laminates. It considers the interactions between the stress components in the blade, allowing failure prediction based on distortion energy, according to Talreja [12]. Therefore, this criterion was employed to guide the preliminary sizing of the wing spar, as represented by Equation 1.

$$\left(\frac{\sigma_1}{X}\right)^2 - \left(\frac{\sigma_1 \cdot \sigma_2}{X^2}\right) + \left(\frac{\sigma_2}{Y}\right)^2 + \left(\frac{\tau_{12}}{S}\right)^2 \leq 1 \quad (1)$$

In the case where the left-hand term, also known as the Tsai-Hill index, is less than or equal to 1, the developed structure can withstand the loads. If the term is greater than 1, failure will occur. This criterion considers the interaction between normal and shear stresses, being simple for application in initial design simulations and providing an approximate elliptical failure envelope, which would be useful for preliminary safety assessments.

For the spar, a box configuration was selected because it distributes more material away from the neutral axis, and consequently provides greater bending resistance. The cross-section was divided into two parts, as shown in Figure 3.

For the determination of the properties required in the calculation of the Tsai-Hill index, a study of strength of materials was necessary. In the geometric property of an area, the centroid is analyzed, which refers to the point that defines its geometric center, as defined by Hibbeler [13]. To determine the area moment of inertia of the hollow rectangular section, used in bending analysis, Equation 2 was applied, based on Hibbeler [13].

$$I = \frac{\left(B \cdot H^3 - b \cdot h^3\right)}{12} \quad (2)$$

For the torsion analysis, it was necessary to calculate the polar moment of inertia of the hollow rectangular section, as represented in Equation 3, expressed by Hibbeler [13].

$$J = \frac{(B \cdot H^3 - b \cdot h^3)}{12} + \frac{(H \cdot B^3 - h \cdot b^3)}{12} \quad (3)$$

For Hibbeler [13], the safety factor was used to ensure that structural elements operate within acceptable stress limits, providing a margin against unexpected failures due to variations in materials, loads or operating conditions.

In this project, a wing with a semi-span of 2.33 m was considered, subjected to a distributed load along the span, representing the aerodynamic load generated during flight. To increase the analysis resolution, the load was discretized into 100 equally spaced points, allowing calculation of the bending moment and torque at each section along the wing.With the definition of the moments of inertia, it was possible to calculate the normal

Figure 3. Spar cross-sections.

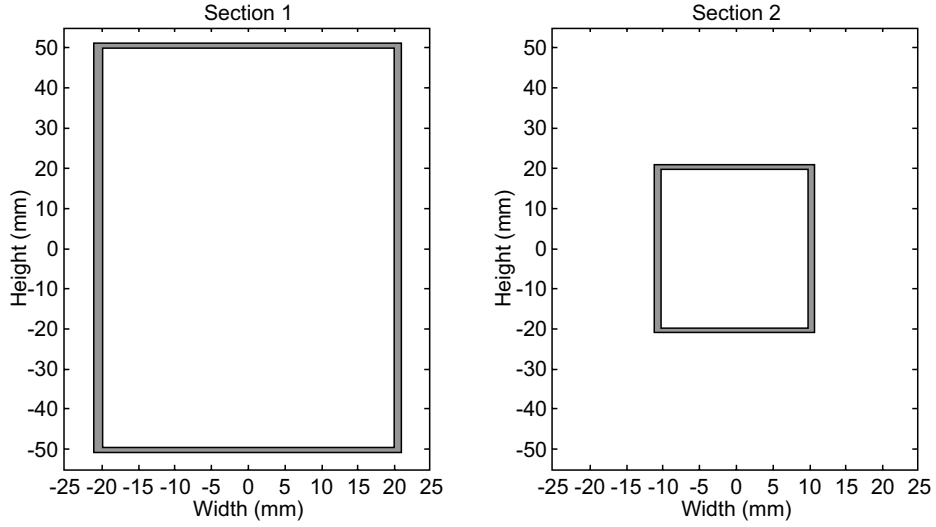

stress due to bending and the shear stress due to torsion, expressed by Hibbeler [13]. The formulas are represented in Equations 4 and 5, respectively.

$$\sigma = \frac{M_f \cdot \left(\frac{D}{2}\right)}{I} \cdot 10^{-6} \quad (4)$$

$$\tau_{max} = \frac{M_t \cdot \left(\frac{D}{2}\right)}{J} \cdot 10^{-6} \quad (5)$$

For the calculation of the Tsai-Hill index, it was necessary to determine the in-plane principal stresses and the maximum in-plane shear stress. The principal stresses correspond to the maximum and minimum normal stress values that occur at a point, on planes where the shear stress is zero. The maximum shear stress represents the highest absolute value that the shear stress can reach on any plane passing through that point. In his study, Timoshenko [14] uses Mohr's circle, which is a graphical tool that allows visualizing the plane stress state, providing intuitively and accurately the values of the principal stresses and the maximum shear stress, expressed by Hibbeler [13].

The principal stresses and maximum shear stress are determined from Equations 6 and 7, respectively.

$$\sigma_{1,2} = \frac{\sigma}{2} \pm \sqrt{\left(\frac{\sigma}{2}\right)^2 + \tau_{max}^2} \quad (6)$$

$$\tau_{12} = \frac{\sigma_1 - \sigma_2}{2} \quad (7)$$

A numerical computing software code was developed to perform the Tsai-Hill methodology calculations. After various geometry combinations, it was possible to find an optimum point for weight and acceptable safety margin. The geometries are represented in Figure 4.

For the determination of materials and their respective properties, a benchmark was conducted focusing on UAVs with similar mission profiles and geometry. Due to market trends and high structural efficiency, carbon fiber reinforced plastic (CFRP) was defined as the sole material to comprise the spar. To determine the properties, the research by Santos [15] and the datasheet from Toray Carbon Fibers Europe [16] were used. The properties utilized are presented in Table 4.

Results and Conclusion

The results obtained allow the selection of cross-sectional configurations that minimize structural weight while maintaining the failure index below 1, respecting operational limits.

By applying the Tsai-Hill method to this geometry, a positive safety margin curve was obtained, with the minimum safety margin equal to 34.49%, located at the wing root semi-span. Using the bending moment equation, it was possible to determine the deflection along the semi-span through direct integration. It was also possible to find the twist angle along the span through double integration of the torsional moment. Therefore, a maximum deflection of 123.66 mm was obtained,

Figure 4. Final geometry of cross-sections.

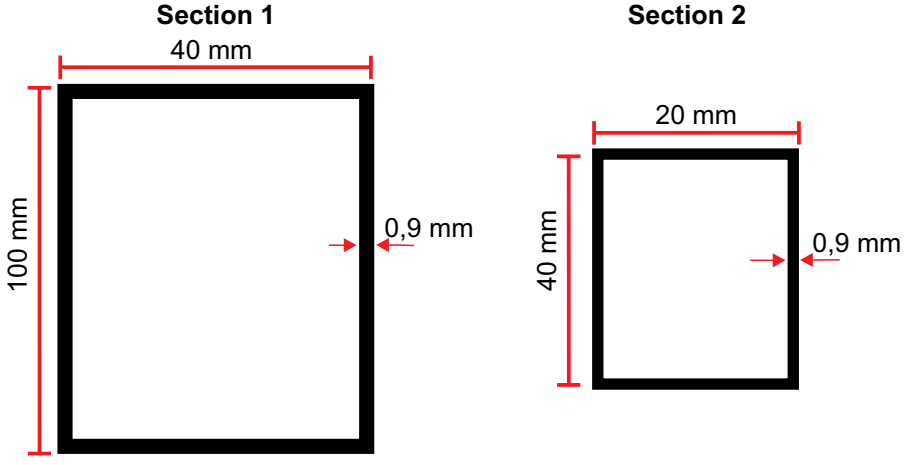

located at the wing tip, and a maximum twist of 12.7°. These values are positive since they represent deformation values that do not considerably alter the aerodynamic properties of the design. The results are presented in Figure 5.

Subsequently, it was possible to calculate the estimated weight of the spar based on the density and volume of carbon fiber used, resulting in 0.982 kg.

The study demonstrates the feasibility of using the Tsai-Hill criterion as a reliable tool in the initial phases of UAV structural design, contributing to the development of lightweight, efficient, and safe aircraft.

Figure 5. Final charts of sizing indicators.

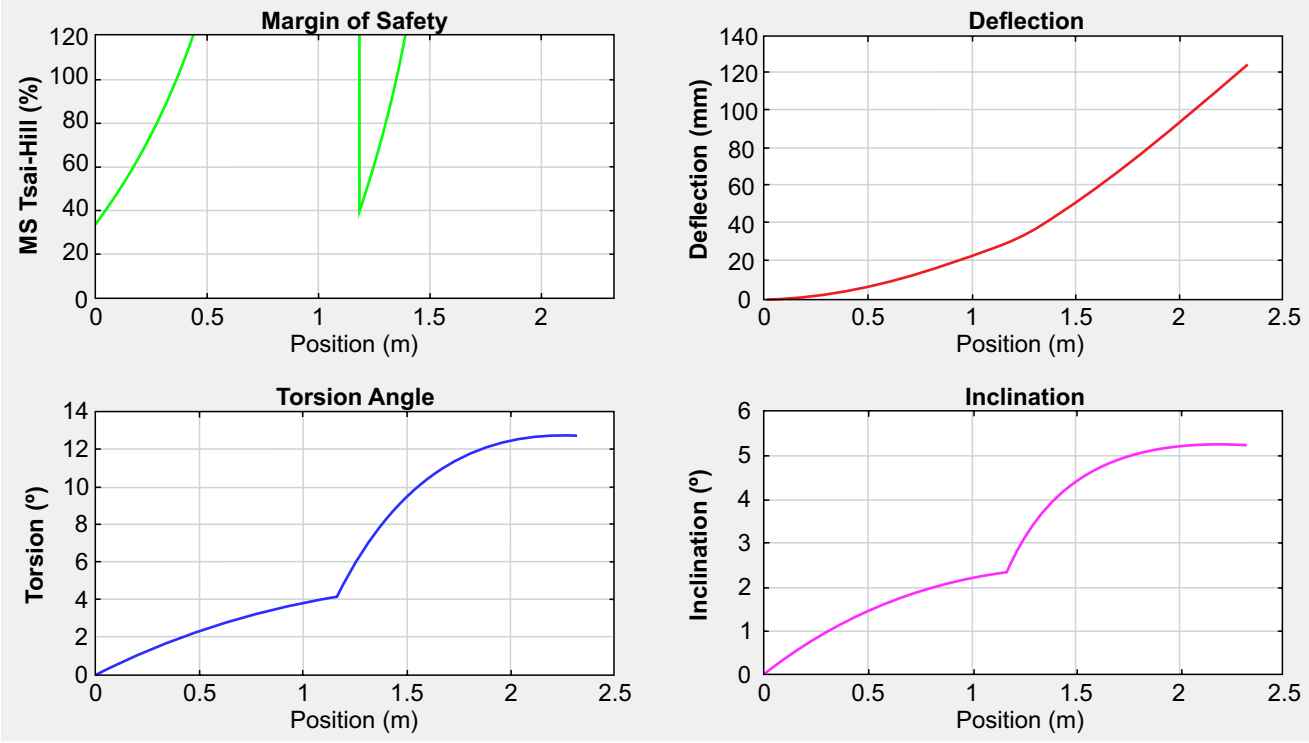

References

1. Raymer DP. Aircraft design: a conceptual approach. 6th ed. Reston: American Institute of Aeronautics and Astronautics; 2018.
2. Barros CP. Introdução ao projeto de aeronaves leves. Belo Horizonte: Centro de Estudos Aeronáuticos (CEA), UFMG; 2001.
3. United States. Federal Aviation Administration (FAA). Title 14 – Aeronautics and Space: Part 23, § 23.333 – Flight envelope. Washington (DC): U.S. Government Publishing Office; 2025.
4. United States. Federal Aviation Administration (FAA). Title 14 – Aeronautics and Space: Part 23, § 23.335 – Design airspeeds. Washington (DC): U.S. Government Publishing Office; 2025.
5. Brazil. Airspace Control Department (DECEA). Instruction of the Air Force Command (ICA) 100-40: Unmanned aircraft and access to Brazilian airspace; 2023.
6. United States. Federal Aviation Administration (FAA). Title 14 – Aeronautics and Space: Part 23, § 23.337 – Limit maneuvering load factors. Washington (DC): U.S. Government Publishing Office; 2025.
7. Rosa E. Introdução ao projeto aeronáutico: uma contribuição à competição SAE AeroDesign. Florianópolis: UFSC/Grante; 2006.
8. United States. Federal Aviation Administration (FAA). Title 14 – Aeronautics and Space: Part 23, § 23.341 – Gust load factors. Washington (DC): U.S. Government Publishing Office; 2025.
9. National Advisory Committee for Aeronautics (NACA). Effective gust structure at low altitudes as determined from the reactions of an airplane. NACA Report No. 692; 1940.

10. United States. Federal Aviation Administration (FAA). Title 14 – Aeronautics and Space: Part 23, § 23.303 – Factor of safety. Washington (DC): U.S. Government Publishing Office; 2025.
11. Tahir NM, Alhaji AU, Abdullahi I. Performance evaluation of unmanned aerial vehicle wing made from Sterculia setigera fiber and Pterocarpus erinaceus wood dust epoxy composite using finite element method Abaqus and structural testing. Res Eng Struct Mater. 2022;8(4):675-694. doi:10.17515/resm2022.378ma0102tn.
12. Talreja R. Assessment of the fundamentals of failure theories for composite materials. Compos Sci Technol. 2014;105:190-201. doi:10.1016/j.compscitech.2014.10.014.
13. Hibbeler RC. Resistência dos materiais. 7th ed. São Paulo: Pearson Prentice Hall; 2009.
14. Timoshenko SP, Gere JM. Theory of elastic stability. 2nd ed. Boston: McGraw-Hill; 1961.
15. Santos CPS, Bichara JRR. Estudo experimental das propriedades mecânicas para compósito em fibra de carbono e matriz epóxi Pipefix (CFRP – Carbon Fiber Reinforced Polymer). Rio de Janeiro: CEFET-RJ; 2015. Available from: https://www.cefetrj.br/attachments/article/2943/Estudo_Experimental_Propriedades_Mec_Comp%C3%B3sitos_Fibra_Carbono_e_Matrix_Ep%C3%B3xi_Pipefix.pdf
16. Toray Carbon Fibers Europe. Torayca M60J: technical data sheet [Internet]. 2025. Available from: https://toray-cfe.com/wp-content/uploads/2025/02/Torayca-M60J-Technical-Data-Sheet.pdf

Process Development Modeling for CubeSats

Camille Grajauskas Gonçalves[1]*, Cristiano Vasconcellos Ferreira[1]*, Xisto Lucas Travassos Junior[1], Eduardo Augusto Bezerra[1], Damylle Cristina Xavier Donati[2], Rodrigo de Oliveira Rodrigues[2], Raquel Viana Pinto Leal[2]
[1]Federal University of Santa Catarina, Department of Mobility Engineering; Joinville, Santa Catarina; [2]SENAI CIMATEC University; Salvador, Bahia, Brazil

CubeSat represents a class of miniature satellites with applications in space and academic research, which stands out for its low cost and simplified manufacturing. This work aims to model the CubeSat development process based on the guidelines proposed by the European Cooperation for Space Standardization, using both the knowledge contained in regulatory documents and the knowledge of those working at the SpaceLab of the Federal University of Santa Catarina. The proposed modeling was implemented on the Draw.io platform, a process automation tool. As a result, a structured and systematic methodology was obtained for the stages involved in the development of CubeSats, which aims to contribute to the standardization and improvement of workflows in small aerospace projects.
Keywords: Cubesat. Modeling. Systems.
Abbreviations: BPMN, Business Process Model and Notation. ECSS, European Cooperation for Space Standardization. WBS, Work Breakdown Structure.

The growing demand for lower-cost and more accessible technological solutions in the aerospace sector has driven the use of miniaturized satellites such as CubeSat. The development of CubeSats by students can begin at different stages, depending on the level of pre-assembly of their subsystems, mission complexity, and theoretical maturity for their development. In any case, the guidelines necessary for their ultimate goal follow the same process modeling pattern as other aerospace products.

Among the recognized guidelines, the niche of Systems Engineering knowledge is identified, which plays a crucial role in ensuring the complete life cycle of a CubeSat. To this end, the European Cooperation for Space Standardization fills this knowledge gap that can be used for the development of CubeSats [1].

Using current literature as the main guide for the construction and launch of satellites in academia, the development process follows a procedure consisting of several stages. However, the search for a visual and systematic way to connect the normative guidelines and supporting documents required at each stage of CubeSat development has been identified. Therefore, it resumes the need for modeling that connects the stages of the guidelines with the stages of the subsystems.

Despite the existence of consolidated guidelines for the development of CubeSats, the practical application of these standards in academic environments are often fragmented and dependent on the practical knowledge of the teams involved. The absence of a structured representation that connects the project phases to the required documents and normative guidelines hinders the replication of processes and the training of new members.

Thus, the contribution of this work lies in modeling a CubeSat development process based on European Cooperation for Space Standardization (ECSS) guidelines and grounded in a real case study, which considers the practices adopted by Senai CIMATEC and SpaceLab.

The proposed model seeks to act as an interface between normative theory and academic practice, promoting structured visualization, standardization, and dissemination of knowledge throughout the CubeSat life cycle.

Received on 17 November 2025; revised 22 January 2026.
Address for correspondence: Camille Grajauskas Gonçalves. Rua Dona Francisca, 8300, Bloco U Zona Industrial, Joinville, Santa Catarina, Brazil. Zipcode: 89.219-600. E-mail: cristiano.v.ferreira@ufsc.br.

J Bioeng. Tech. Health 2026;9(2):91-97

Theoretical Basis

Development Process Modeling

Process modeling is the set of activities to be followed to create one or more models of something for a specific purpose. A model can be defined as "a representation (with varying degrees of formality) of an abstraction of reality expressed in a specific type of formalism" [2].

Amaral defines the modeling method as a structured set of elements and rules used to represent specific aspects of a real process or system [3]. This formalism guarantees the product development process because it influences its effectiveness. Modeling methods that reduce complexity and highlight essential aspects contribute to more effective decisions in product development [4].

Models can differ from reality, as they usually represent only selected aspects of a system relevant to the analysis. Therefore, the model must be chosen according to its intended use [2,5]. This purpose usually involves representation, explanation, specification, analysis, or control of a process or phenomenon [2].

CubeSat Development Models

ECSS

The European Cooperation for Space Standardization [6] is a unified set of standards for European space projects. These standards are derived from a previous standard (Procedures, Specifications and Standards) that was more prescriptive, required extensive documentation, and favored waterfall and incremental development models.

The evolution to ECSS required the industry to learn from experience gained in using common standards, processes, and models. ECSS has become one of the important sets of standards within the space industry [6].

The ECSS standards were developed jointly by the European Space Agency and the European space industry and include four branches: Management (M), Engineering (E), Quality (Q), and Sustainability (S) [7]. Also, to ensure completeness and correctness, ECSS standards require suppliers to perform different types of reviews: Preliminary Design Review, Critical Design Review, Detailed Design Review, and On-Site Acceptance Test, among many others.

CubeSat

CubeSats were initially designed as educational or technology demonstration platforms that could be developed and launched within one to two years [8-10]. However, more advanced missions with CubeSats have recently been developed and proposed, indicating that CubeSats have begun to transition from educational and technology demonstration platforms to actual low-cost missions with high potential in terms of scientific return and commercial revenue [11].

CubeSats considerably reduce the cost and complexity of development and launch compared to more robust traditional satellites, which have redundant subsystems, as evidenced by the significant increase in the number of CubeSat launches over the last decade [12].

CubeSats can be of various sizes, all based on a standard unit called 1U. A 1U CubeSat has a cubic shape, with dimensions of 10 cm × 10 cm × 10 cm and a mass between 1 and 1.33 kg. Since the creation of this standard, larger models have been developed, such as 1.5U, 2U, 3U, 6U, and 12U CubeSats. Figure 1 illustrates examples of CubeSats in 1U (left) and 3U (right) formats, with the 3U model measuring 10 cm × 10 cm × 34 cm [13].

Finally, small satellites have a much lower impact in the event of individual failures, given their relatively low cost and short development time, when compared to larger, more sophisticated satellites, which require budgets in excess of hundreds of millions of dollars [14] and, on average, five to ten years of development [15].

Figure 1. (Color online). 1U CubeSat CP1 (left) and 3U CubeSat CP10 (right) [13].

Development

Case Study: Senai CIMATEC and SpaceLab

The need to implement, in a visual and systematic way, connections between the normative guidelines and the supporting documents required at each stage of the ECSS for the development of CubeSats was identified at Senai CIMATEC University, an educational, research, and innovation institution located in Salvador, Bahia. The mission of CubeSat the project is to retransmit meteorological data between CIMATEC ground stations, involving the development of the nanosatellite and the ground station.

In the case study, Senai CIMATEC received direct guidance from the SpaceLab at the Federal University of Santa Catarina, a laboratory that brings together several research and development groups in space systems in general and has missions such as FloripaSat-1, GOLDS-UFSC, and GOMX-5 [16]. The case study dynamics were established through follow-up meetings and analysis of the total processes and stages carried out for the consolidation of CubeSat in the first half of 2025.

In addition to SpaceLab's guidance, Senai CIMATEC started the project with some CubeSat subsystems already purchased, ready for use, without the need for their raw development. From this initial structure, the Senai CIMATEC team focused on integrating the acquired subsystems and planning the remaining stages of development, following the guidelines established by ECSS standards.

Work Breakdown Structure

Observing Senai CIMATEC's working methods and analyzing the literature on process modeling, the first step is to implement a WBS (Work Breakdown Structure) framework, which is defined by dividing the project into its component elements with the aim of establishing a structure for effective control of the project's scope, schedule, and budget, with the aim of aligning academic and technological practice with European regulations for the development of space systems [17]. The proposed structure consisted of mapping all the stages set out in the ECSS standards, which comprise phases 0 to F, in parallel with the method employed by the Senai CIMATEC project team.

This structure was developed using a spreadsheet that organizes the information into specific columns, facilitating the reading and understanding of the workflow and technical responsibility throughout the project. The columns of the WBS were: (1) Phases (0 to F), (2) Product Design, (3) Project Management (focusing on the role of the systems engineer), (4) Documents/ Gates, (5) Product Design Tools, and (6) Project Management Tools. This segmentation provided a clear view of the relationship between ECSS regulatory requirements and institutional practice, allowing for greater traceability and control of the activities carried out.

In addition, the need for a breakdown by subsystem was identified, since the development of a satellite, even in its CubeSat version, requires an integrated and systemic approach. To this end, the main subsystems present in space missions were considered, namely: Payload, Communication Systems, Power Systems, On-Board Computer (OBC) System, Thermal Control, Propulsion System, Launch System, Attitude and Orbit Control System, in addition to the Structural Design. Each subsystem was assigned the specific tasks required in each phase of the ECSS cycle, considering everything from feasibility studies (phase 0) to operation and disposal (phase F).

The segmentation of each phase into smaller, specific tasks allowed for a more granular understanding of the necessary activities, which directly contributes to the planning, management, and control of the project. The construction of this WBS was based both on practical experience observed at Senai CIMATEC and on official ECSS documents, their appendices, and complementary publications (Tables 1 and 2).

Business Process Model and Notation Modeling

Following validation of the spreadsheet with stakeholders the visual modeling stage of the process began. For this, Draw.io was used, an online diagram modeling tool with direct integration with Google Drive. This choice was made due to the tool's flexibility, accessibility, and adherence to international process modeling standards.

The modeling was performed using the official Business Process Model and Notation (BPMN) notation, which, according to White, is a recognized standard for the graphical representation of business processes. BPMN aims to provide a notation that is understandable to all involved through standardized symbols and a clear visual structure. The main elements of BPMN include Pools, Lanes, Tasks, Gateways (decision points), Events, and Connectors, which together structure the logical flow of a process [18].

In the model, each Pool was used to represent a phase of the ECSS development cycle, functioning as a container for macro-activities conducted at that stage. The pools function as the main divisions of the process and can represent major participants or specific phases, as adapted for this project. Within each pool, tasks corresponding to the macro stages identified in the previously developed WBS spreadsheet were inserted. Each task was represented by an activity block, symbolizing specific actions performed by the team during that phase.

Gateways, represented graphically by diamonds, were inserted to indicate critical decision points in the process. In the context of CubeSat and ECSS standards, these gateways were used to represent mandatory verification moments, such as reports and formal validations required by the standard, for example, the Preliminary Design Review (PDR) and the Critical Design Review (CDR). Thus, each gateway signaled a fork in the process, whose next path would depend on the approval of normative deliverables. Figure 2 represents phase zero of the CubeSat development process to illustrate the process (a visual way of Table 1).

Model Validation

With the modeling completed using the spreadsheet (WBS) and the BPMN diagram in Draw.io, a validation process was conducted with the stakeholders directly involved in the project: SpaceLab/UFSC and Senai CIMATEC. The objective was to assess whether the products developed corresponded to the real needs of the CubeSat development process and whether they contribute to clarity, organization, and alignment with ECSS standards.

During validation, it was identified that both the spreadsheet and the BPMN model offer benefits for understanding and managing the process. Although the proposal is not unprecedented from a methodological point of view—given that there are several ECSS tailoring initiatives applied to CubeSat projects—the combination of visual modeling with the analytical structure, applied to

Table 1. Processes in phase zero for subsystems in the CubeSat Development Process within the WBS structure.

Work Breakdown Structure											
Steps		Systems									
Phases	Product Projects	Payload	Communication System	Energy System	Onboard Computer System	Thermal Control	Propulsion in System	Launch System	Altitude and Orbital Control System	Structural Design
Phase 0: Concept Studies	1 Identify any initial customer requirements or cope of work, which may include: mission, science and top-level system	Identify the general requirements associated with the payload system. Determine the purpose of the payload, such as scientific data collection, remote monitoring, communication, or technological experiments	Identify whether you need telemetry and/or remote control and the type of the antenna. Check whether you need a Ground Station	Analyze the initial forecast for solar panel square footage and battery quantity	Use a percentage value from the project as a reference	Use a percentage value from the project as a reference	Check whether it is necessary or not	Check whether it is necessary or not	Check whether a note is needed (active control) or not. Use a percentage value from the project as a reference (passive control)	Analyze whether the CUBESAT will have 1U, 2U, 3U, or more
	2 Identify and involve users and other stakeholders									
	3 Prepare the project proposal, which include mission justification and objectives, WBS (Work Breakdown Structure) and Technology assesment and maturation strategies									
	4 Satisfy MDR entrance/ sucess criteria									

Table 2. Processes in phase zero for management requirements in the CubeSat Development Process within the WBS framework.

Management			
Project Management	**Gates**	**Product Design Tools**	**Project Management Tools**
Develop preliminary SEMP (System Engineering Management Plan) / Preliminary Project Requirements	MDR - Mission Definition Review Release the mission statement and assess	Needs assessments questionnaire; Standard requirements list; Scenario constraints; Benchmark	Scope management (internal and external), time (time chart), costs (investments and sources), procurement (schedule), risks (technical and managerial), and integration

Figure 4. BPMN for phase zero of the development process made in Draw.io.

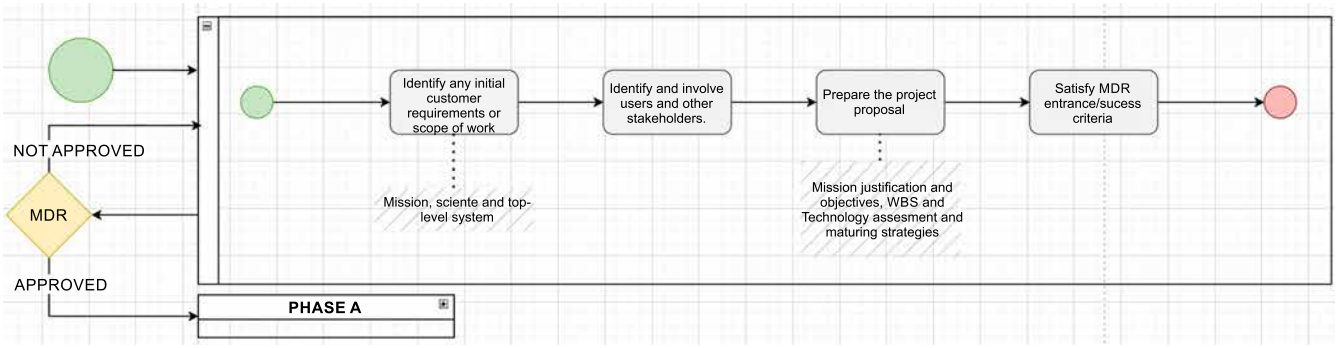

the specific case study of Senai CIMATEC, proves to be effective. The clarity provided by the model allows even teams still in formation or unfamiliar with ECSS to understand what phase they are in, what deliverables are expected, and what critical decisions need to be formally validated.

This structure has also proven useful for SpaceLab, which frequently conducts training and supports other institutions in adopting practices related to space systems engineering. Although SpaceLab already follows ECSS guidelines, it was identified that the absence of a didactic and systematized model hinders the replication and standardized teaching of the process. Thus, the proposed model meets both pedagogical and operational needs, providing a visual and adaptable reference.

From a more technical point of view, the main gain lies in the possibility of more accurately mapping the critical reviews provided for by ECSS (such as PDR, CDR, and QR) with the associated appendices and normative documents, as well as with the subsystems involved in each stage. This makes it clearer, for example, what information from the subsystems should be included in a technical report for approval at a given gate, ensuring greater adherence to the European standard and reducing the risk of documentary omissions.

However, one area for improvement was identified: the BPMN modeling does not cover the development processes of the subsystems listed in the spreadsheet. Although the spreadsheet provides details of the activities per subsystem in each phase of the ECSS cycle, this level of granularity was not incorporated into the Draw.io diagram. This limitation represents an opportunity for future iterations of the model, aiming to integrate the functional perspective of the subsystems with the procedural logic of BPMN, which would further expand the practical application and teaching potential of the proposed model.

Conclusion

The proposal arose from the need to clarify the relationship between the phases of a satellite's life cycle, the mandatory deliverables, and the subsystems involved, especially in environments where practical knowledge was still under development, as in the case of Senai CIMATEC.

Validation with the Senai and SpaceLab teams showed that the model, although not unprecedented on the international scene, was well suited to the reality of the case study. It facilitates understanding of the project stages, helps to locate where the team is in the cycle, and shows more clearly which documents and decisions are required at each phase. It also stood out as a useful tool for training and standardizing future processes.

The main contribution of the model is to serve as a bridge between normative theory and applied practice, allowing for a better visualization of what each ECSS revision requires in terms of subsystems and documentation. As a point for improvement, it should be noted that the subsystem development processes described in the spreadsheet have not yet been modeled in BPMN, which can be explored in future work.

References

1. European Cooperation for Space Standardization. ECSS-S-ST-00C: Description, implementation and general requirements. Noordwijk: ESA-ESTEC, Requirements & Standards Division; 2008.
2. Vernadat F. Enterprise modeling and integration: principles and applications. London: Springer; 1996.
3. Amaral DC. Arquitetura para gerenciamento de conhecimentos explícitos sobre o processo de desenvolvimento de produto [dissertation]. 2002.
4. Browning TR, Ramasesh RV. A survey of activity network-based process models for managing product development projects. Prod Oper Manag. 2007;16(2):217–40.
5. Aguilar-Saven R. Business process modelling: review and framework. Int J Prod Econ. 2004;90(2):129–49.
6. Feldt R, Torstensson N, Hult E, Green LG. Analyzing the cost of complying with ECSS standards for software development. In: Conference on Data Systems in Aerospace (DASIA 2010). ESA SP; 2010. p. 303–7.
7. Balestra L. European Cooperation for Space Standardization (ECSS). In: Trilateral Safety & Mission Assurance Conference; 2008.
8. Cockburn A. Agile software development. Boston: Addison-Wesley Professional; 2002.
9. Puig-Suari J, Turner C, Twiggs RJ. CubeSat: the development and launch support infrastructure for eighteen different satellite customers on one launch. In: AIAA/USU Conference on Small Satellites; 2001.
10. Bouwmeester J, Guo J. Survey of worldwide pico- and nanosatellite missions, distributions and subsystem technology. Acta Astronaut. 2010;67:854–62.
11. Selva D, Krejci D. A survey and assessment of the capabilities of CubeSats for Earth observation. Acta Astronaut. 2012;74:50–68.
12. Buchen E. Small satellite market observations. In: AIAA/USU Conference on Small Satellites; 2015.
13. National Aeronautics and Space Administration (NASA). CubeSat 101: basic concepts and processes for first-time CubeSat developers. Washington (DC): NASA; 2017.
14. Bitten RE, Mahr EM, Kellogg RC. Cost estimating of space science missions. Aerospace Report No.: ATR-2013-00108; 2013.
15. DLA F. How long does it take to develop and launch government satellite systems? Aerospace Report No.: ATR-2015-00535; 2015.
16. SpaceLab UFSC – Space Technology Research Laboratory of Federal University of Santa Catarina. Florianópolis: SpaceLab UFSC; 2023.
17. Devi TR, Reddy VS. Work breakdown structure of the project. Int J Eng Res Appl. 2012;2(2):683–6.
18. White SA. Introduction to BPMN. Boston: BPTrends; 2004 Jul.

Vehicle Gear Ratios Assessment: Study of the Fidelity of a Videogame to Theoretical Vehicle Dynamics

Pedro Augusto Ambrósio Almeida[1]*, Lucas Gusmão Portela Rocha[1], Pedro Bancillon Ventin Muniz[1]
[1]SENAI CIMATEC University, Automotive Department, Salvador, Bahia, Brasil

The modification of certain vehicle dynamics attributes, such as the gear ratios of a transmission system, can generate significant impacts on vehicle behavior under different driving conditions. Such changes influence performance, such as acceleration times, maximum speed, and traction forces. With advancements in simulation technologies featured in electronic games, there has been a growing convergence between simulated dynamic and real-world behavior of theoretical engineering. In this context, modern video games have increasingly established themselves as complementary tools in the educational process, particularly related to automotive engineering, by enabling the customization of technical concepts in a math ambience. However, in-depth analysis is needed to assess whether vehicle input customizations performed in video games follow the expected results when compared to the real world. Thus, the objective of this article is to investigate the impacts caused by gear ratio changes on vehicle drivability in the videogame Forza Horizon 5. The theoretical framework studied, and the tests conducted shows that this game have already being able to simulate, within their parameters, phenomena that are well-documented in real-world studies, which means that games like this can already serve as valuable educational tools.

Keywords: Vehicle Dynamics. Transmission Ratio. Electronic Games.

The gaming market has shown significant growth over the years due to technological advancements. The increase in the player base reached 3.2%, generating revenues of USD 182.7 billion in 2024 [1]. Due to the cloud system on internet, videogames such as Forza Horizon 5 already have over 45 million players [2]. In this video game, players can modify their cars to change dynamics specifications such as suspension geometry, brake balance, down force, engines specifications, and others. Some of these parameters are primarily addressed in automotive engineering through theoretical learning, since practical demonstrations are costly. Given the wide availability of this specific game, the present study focused on the parameters of gear ratio changes, where practical effects could significantly support theoretical comprehension.

Gear ratios can be configured to give different characteristics of acceleration and speed in a vehicle. The higher the gear ratio, the higher the torque transmitted to the wheels, however, wheel speed becomes lower. These settings could affect several vehicle parameters, such as fuel consumption, engine emissions, acceleration, maximum speed, and tractive power.

The tractive power is associated with the resistances encountered while moving the vehicle, considering only a flat track with no elevation. It depends on the friction force acting on the drive wheel, as well as rolling resistance [3]. The power equation is represented as [3]:

$$Pt \cong ½.\rho.C.S.v^3 + a.M.g.v \quad (1)$$

Where: p is the air density, approximately 1.22 kg/m³ at sea level; C is the drag coefficient; S is the frontal area of the vehicle, in square meters; v is the speed, in meters per second; a is the rolling resistance coefficient, 1% of the normal force on the track; M is the mass of the vehicle, in kilograms; g is the gravitational field strength, in meters per second squared.

As an example of the application of this relationship between power and speed, data [3] was collected from different vehicles and divided into three distinct groups: Group 1 for modern

Received on 12 October 2025; revised 20 December 2025.
Address for correspondence: Pedro Augusto Ambrósio Almeida. Rua Manuel dos Santos Correa – Pitangueiras, Lauro de Freitas, Bahia, Brazil. Zipcode: 42701-320. E-mail: pedro.ambrosio@fbter.org.br.

J Bioeng. Tech. Health 2026;9(2):98-103

automobiles, Group 2 for automobiles from the 1960s and 1970s and Group 3, for modern sport utility vehicles (SUVs). Figure 1 shows the relationship between power and speed for all vehicles assessed in the three groups.

The maximum speed increases directly proportional to the increase in power (regardless of the year of the vehicle). According to Equation 1, similar cars (both with equal frontal area, and weight), would be different maximum speed due to their traction power (as long as they are not the same). In this sense, it is possible to customize similar vehicles in terms of gear ratio attributes to verify the differences they encounter at maximum speed. This approach allows for a playful educational simulation for various engineering students who may not have access to simulators or prototype vehicles.

Therefore, this article aims to evaluate whether the gear ratio attribute produces changes in Forza Horizon 5 cars and compare these changes with the expected results.

Materials and Methods

To verify the gear ratio attributes, a racing game was selected, in which the vehicles are similar to those produced commercially worldwide. There are several games in this segment (such as Racer [4]), but the one selected for this study was Forza Horizon 5, developed by Playground Games and published by Microsoft in 2021. This game was chosen due to the combination of its basic simulation parameters and its high accessibility, presenting a wide range of players worldwide [2]. The 2008 BMW Z4 M Coupé vehicle was chosen due to the availability of technical information (engine power curve, shown in Figure 2).

Therefore, a review was conducted to examine the relationship between engine power and vehicle speed presented in the game, and an experimental evaluation was conducted to determine new gear ratio parameters.

Validation was performed in a simulation environment, evaluating the vehicle's response within the game itself.

Figure 1. Relationship between power and speed for the three selected groups.

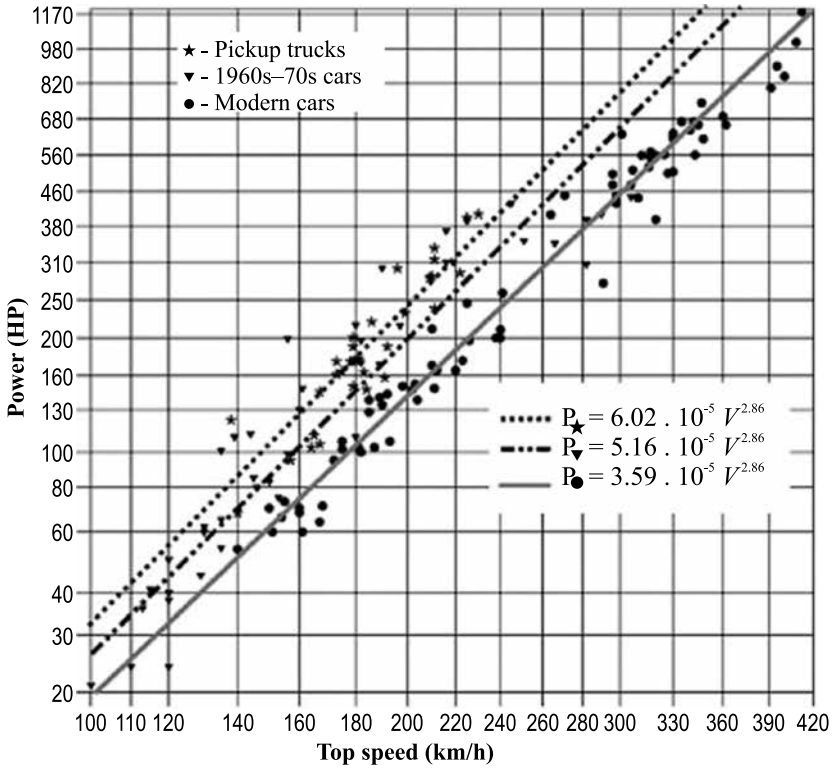

Source: Silveira (2011) [3].

Figure 2. Power and torque curve of the chosen vehicle.

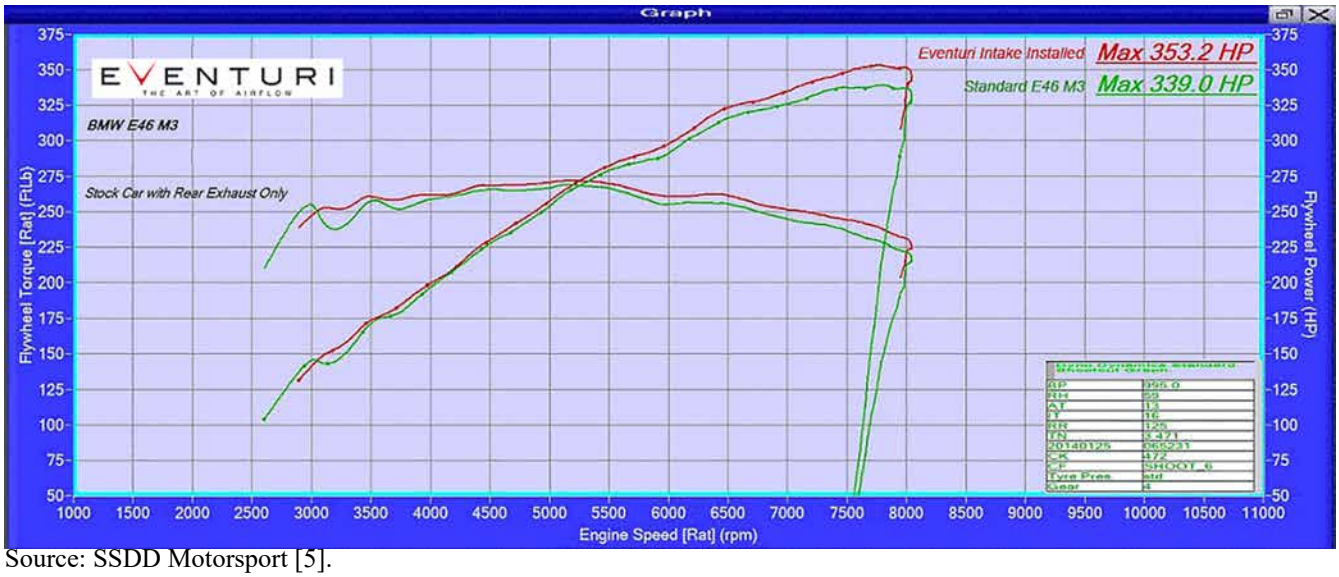

Source: SSDD Motorsport [5].

Two types of tests were conducted with four different car configurations, as follows:

- Maximum speed test: The cars were tested on a 6-kilometer track, starting from the same starting point and ending at the same point, under the same weather conditions in the Forza Horizon 5 simulation environment.
- Acceleration Test: A drag strip was selected to verify the vehicles' starting times.
- The two different car configurations included:
- Standard Car: The car without modifications.
- Custom Car: The car with gear ratios adjusted according to Table 1. The new gear ratios were selected to increase torque to the wheels and serve as a benchmark for student evaluation. This type of gear ratio is common in light vehicles used in cities and urban centers.

Table 1. Gear ratios.

Gear Ratios	Standard Car	Custom Car
Differential	3.62:1	4.40:1
1st gear	4.35:1	4.55:1
2nd gear	2.50:1	2.67:1
3rd gear	1.66:1	1.82:1
4th gear	1.23:1	1.33:1
5th gear	1.00:1	1.00:1
6th gear	0.85:1	0.80:1

Sources: Adapted from Vrum [6].

Both vehicles were subjected to at least three test cycles to verify the results.

A gear diagram was calculated to compare the behavior of the relationship between vehicle speed and engine speed in different gears for the two gear ratio configurations, using Equation 2 [7]:

$$v = \frac{rpm \cdot C \cdot 3{,}6}{r \cdot D \cdot 60} \quad (1)$$

Where: RPM is the engine speed, in revolutions per minute; C is the circumference of the tire used by the car, in meters; R is the selected gear ratio (dimensionless); D is the selected final drive ratio (dimensionless).

Results and Discussion

As seen in Figure 3, the change in gear ratio (for theoretical speed, which considers an environment with no friction, no roll coefficient, and no aerodynamic coefficient) caused differences in the vehicle's speed profile. The customized vehicle had a lower top speed (approximately 300 km/h), as well as a lower maximum speed achieved by each gear.

However, this resulted in greater tractive force at the wheels, which can generate greater

Figure 3. Gear diagram of cars for maximum theoretical speed.

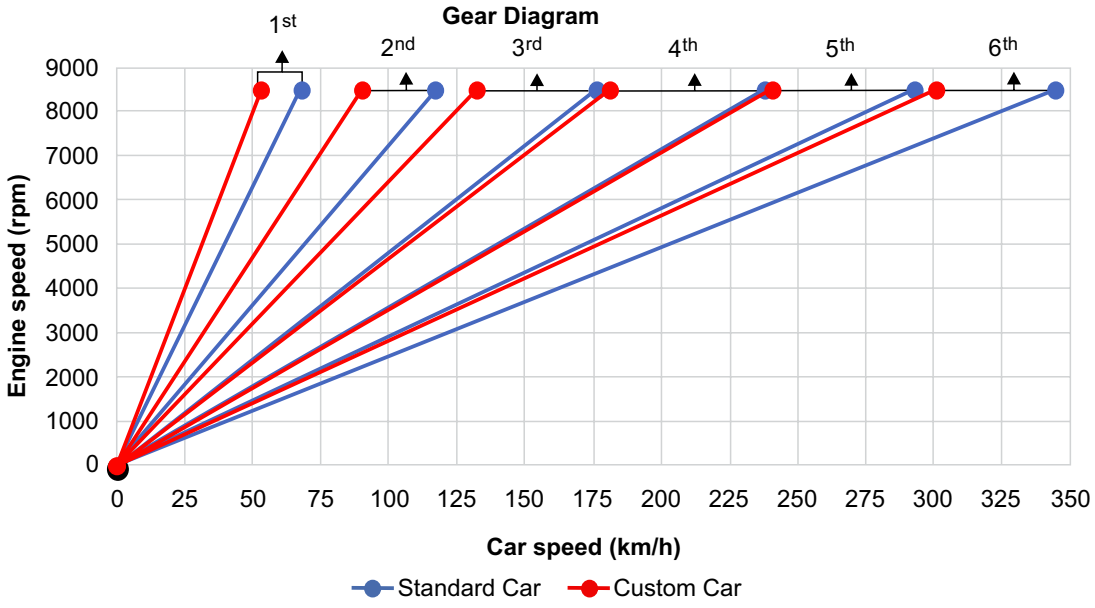

acceleration. Although the engine power curve shows a maximum engine speed of 8000 rpm (Figure 2), the gear ratio diagram used 8500 rpm.

This occurred because the real vehicle (marketed and sold worldwide) has an engine speed limit to minimize potential mechanical lubrication and cooling issues, which were not applied in Forza Horizon 5. Top Speed Test: In the top speed test, the standard car reached 288 km/h, while the custom car reached 291 km/h, as shown in Figures 4 and 5, respectively.

Despite a higher maximum speed than the custom vehicle, the standard vehicle was unable to overcome the maximum speed exhibited by custom car (for the selected track). This could occurred because Forza Horizon 5 uses parameters (which are not disclosed to the user) such as air mass, track inclination, and ambient weather conditions that hindering the vehicle from reaching its maximum theoretical speed (Figure 3). Another aspect is that the customized vehicle had higher tractive force (by increasing the gear ratio, as observed in Table 1), which allowed it to overcome track conditions and, therefore, produce a higher maximum speed in the simulated environment.

Regarding acceleration time (Table 2), the custom vehicle exhibits shorter acceleration times, which explains the maximum speed performance discussed above. Increasing the gear ratio generates higher torque (and higher tractive effort) at the vehicle's wheels, providing lower acceleration time for custom car.

Table 2. Acceleration test times.

Times	Standard car (seconds)	Custom car (seconds)
Time 1	24.42	24.09
Time 2	24.42	24.09
Time 3	24.42	24.09
Average time	24.42	24.09

Furthermore, the gear ratios used in this study were effective, as the custom car were consistently faster. However, if tracks with very long straights were selected, it would be noted that the standard vehicle would outperform the customized vehicle in maximum speed.

Conclusion

This study aimed to evaluate modifications to the gear ratio of a vehicle in a racing game (Forza

Figure 4. Top speed of the standard car.

Figure 5. Top speed of the custom car.

Horizon 5) that could be used as a math simulator for engineering students. The proposed changes to the vehicle's gear ratio, and the tests conducted, indicated that the game was able to reproduce the expected results.

The customized vehicle presented a faster acceleration time, consistent with the modifications designed to increase the gear ratio, contributing to an increase in wheel traction forces. Additionally, the customized vehicle also presented a higher maximum speed (for a 6km track). However, if other, longer tracks were selected, it would be evident that the custom vehicle would have a lower maximum speed than the standard vehicle.

Therefore, for students who do not have access to automotive simulators, Forza Horizon 5 could be a satisfactory tool in engineering classes, as it presents phenomena and vehicles found in the real world.

References

1. Newzoo. How did the global games market reach $182.7B in 2024—and what's next? [Internet]. 2025 [cited 2025 Aug 5]. Available from: https://newzoo.com/resources/blog/global-games-market-update-q2-2025
2. MeuPlayStation. Chegando ao PS5, Forza Horizon 5 bate 45 milhões de players [Internet]. 2025 [cited 2025 Aug 5]. Available from: https://meups.com.br/noticias/forza-horizon-5-45-milhoes/

3. Silveira FLD. Potência de tração de um veículo automotor que se movimenta com velocidade constante. Rev Bras Ensino Fis. 2011;33(1):1–7.
4. Chan MT, Gelowitz CW. Development of a car racing simulator game using artificial intelligence techniques. Int J Comput Games Technol. 2015;2015:1–6.
5. SSDD Motorsport. Eventuri carbon fibre performance intake for BMW E46 M3 01–06 [Internet]. 2023 [cited 2023 May 23]. Available from: https://www.ssdd-motorsport.com/eventuri-carbon-fibre-performance-intake-for-bmw-e46-m3-01-06/
6. Vrum. Ficha técnica Z4 Coupé M 3.2 V6 24V 343cv [Internet]. 2023 [cited 2023 May 23]. Available from: https://www.vrum.com.br/fichatecnica/bmw/z4/2008/009121-9/
7. Ventin P. Sistema de transmissão. Universidade Senai CIMATEC; 2023.

2D Pose Optimization with Genetic Algorithms and Particle Swarm Optimization: A Comparative Analysis for Robotic Localization

Henrique Nunes Teixeira[1]*, Daniel do Carmo Silva Ribeiro[1], Eduardo Furtado de Simas Filho[1], Samara Maria Assunção de Souza[2], Fillipe Valente Braz[2], Tiago Silva e Silva[2]

[1]Federal University of Bahia, DEEC, Salvador, Bahia; [2]Federal University of Recôncavo da Bahia, CETENS; Feira de Santana, Bahia, Brazil

Accurate localization of mobile robots—particularly under conditions of initial uncertainty, known as the Global Localization Problem (GLP)—remains a fundamental challenge in robotics, as it directly impacts autonomous navigation, precise mapping, and safe interaction with the environment. This paper presents a comparative study of two optimization metaheuristics—Genetic Algorithms (GA) and Particle Swarm Optimization (PSO)—applied to the scan-to-map matching problem for 2D localization with LiDAR sensing. A controlled simulation framework was developed, within which 150 independent experiments were conducted on a high-resolution synthetic occupancy map, employing a cost function based on a Euclidean distance field with penalties assigned to invalid poses. The methodology encompassed automated data generation, parameterized execution of the algorithms, and comprehensive statistical evaluation of key performance metrics, including position error, orientation error, computational time, and convergence behavior. The experimental results demonstrate that both algorithms achieve high accuracy in most trials, yet with notable differences. PSO exhibited faster convergence and attained a lower median angular error (0.18° versus 0.45° for GA), though it displayed a greater tendency to converge to local minima, occasionally resulting in substantial localization errors. In contrast, GA, while slower and with a higher median angular error, proved more robust in avoiding large-magnitude failures, thereby yielding more consistent solutions across the simulated scenarios. These findings suggest that the choice between GA and PSO should be dictated by application-specific requirements: PSO is preferable in domains where rapid convergence is essential, whereas GA is advantageous in safety-critical contexts demanding reliability and fault tolerance. Future directions include the design of hybrid approaches that combine the efficiency of PSO with the robustness of GA, as well as validation in real-world robotic systems, extension to 3D localization tasks, and integration with multi-sensor data.

Keywords: Mobile Robot Localization. Scan-to-Map Matching. Particle Swarm Optimization. Genetic Algorithms. Metaheuristics.

Abbreviations: GA, Genetic Algorithms. PSO, Particle Swarm Optimization.

Autonomous and precise localization of mobile robots is a cornerstone of modern robotics, serving as a prerequisite for tasks such as navigation, mapping, and safe interaction with the environment [1]. In many scenarios, localization becomes a critical challenge, particularly when the robot's prior pose is unknown or uncertain—a condition referred to as the Global Localization Problem (GLP). Unlike continuous localization, where the robot has an initial pose estimate that is refined over time, the GLP arises when the robot's initial pose is completely unknown or highly uncertain. This situation may occur, for example, after a system failure, a reset in an arbitrary location, or entry into a completely new environment without prior position information [2].

The challenges inherent to the GLP are multifaceted. First, the initial uncertainty requires the localization algorithm to explore a vast search space, which can be high-dimensional (position and orientation). Moreover, sensor noise (from LiDARs or cameras) and the dynamic nature of environments (with moving objects or structural changes) add further layers of complexity. The phenomenon of perceptual aliasing, where distinct locations in the map present similar sensory characteristics (e.g., long repetitive corridors),

Received on 27 October 2025; revised 20 January 2025.

Address for correspondence: Henrique Nunes Teixeira. R. Prof. Aristídes Novis, 2 - Federação. Salvador, Bahia, Brazil. Zipcode: 40210-630. E-mail: henrique.teixeira@ufba.br.

J Bioeng. Tech. Health 2026;9(2):104-111

can cause the robot to misidentify its location, resulting in significant localization errors [3].

Robust resolution of the GLP is crucial for a wide range of real-world applications. In search-and-rescue operations, robots must localize rapidly in unknown and hazardous environments. Autonomous vehicles, when deployed in unmapped areas or after being transported to new locations, require effective solutions to the GLP before navigation can begin. Planetary exploration rovers, operating in GPS-denied environments, depend on autonomous and reliable methods to determine their absolute position. Failure to solve the GLP robustly can lead to collisions, mission loss, or safety risks [4].

It is important to note that the GLP is intrinsically related to the problem of Simultaneous Localization and Mapping (SLAM). While SLAM builds a map of the environment while simultaneously localizing within it, the resolution of the GLP is often a prerequisite or an essential component for initializing or recovering a SLAM system. A robust SLAM system must therefore be capable of handling the GLP to ensure continuous and reliable operation in challenging scenarios. Recent research continues to explore new approaches to GLP, aiming for higher accuracy and robustness in increasingly complex environments [5].

This work focuses on a central subproblem of localization: scan-to-map matching, which consists of aligning a sensor scan with a pre-existing map. Traditional methods such as Iterative Closest Point (ICP) are widely used, but they can be sensitive to local minima, particularly in environments with ambiguities or lacking distinctive features [6]. To overcome these limitations, metaheuristics such as Genetic Algorithms (GA) and Particle Swarm Optimization (PSO) have emerged as promising alternatives [7,8]. These algorithms are capable of performing global search in the solution space, increasing robustness and the likelihood of finding the correct pose [7].

This paper introduces a computational framework to compare the performance of GA and PSO in solving the scanto-map matching problem for a robot equipped with a 2D LiDAR sensor. Using a controlled simulation environment, we investigate the effectiveness, accuracy, and computational cost of each approach, with the goal of determining which method provides the best trade-off between robustness and efficiency for global localization.

Materials and Methods

The method of this study was designed to systematically evaluate and compare GA and PSO in the task of 2D pose optimization. The process involves constructing a simulated environment, defining a robust cost (fitness) function, and performing controlled executions of the optimization algorithms.

Scan-to-Map Matching Problem

The problem is formalized as the search for the pose $\mathbf{p} = (x, y, \theta)$ that minimizes a cost function, which quantifies the misalignment between a 2D point cloud, $\mathcal{S}$, obtained from a laser sensor, and a pre-existing occupancy map, $\mathcal{M}$. The pose $\mathbf{p}$ consists of a translation (x, y) and a rotation θ. The transformation of a point $\mathbf{s}_i \in \mathcal{S}$ into its map representation, $\mathbf{s'}_i$, is given by:

$$\mathbf{s'}_i = \begin{pmatrix} \cos\theta & -\sin\theta \\ \sin\theta & \cos\theta \end{pmatrix} \mathbf{s}_i + \begin{pmatrix} x \\ y \end{pmatrix} \quad (1)$$

The objective is to find the optimal pose $\mathbf{p}^*$ that aligns all points in $\mathcal{S}$ with the occupied regions of $\mathcal{M}$.

Fitness Function

The evaluation of a candidate pose is carried out through the `scan_to_map_fitness` function, which is minimized. The efficiency and accuracy of this function are critical to the success of the optimization algorithms [9]. To accelerate computation, a Euclidean distance field is precomputed from the occupancy map. This field stores, for each free cell, the distance to the nearest

obstacle, significantly improving performance by avoiding repeated searches.

The error (cost) of a pose $\mathbf{p}$ is computed as the sum of the distances obtained from the distance field for each transformed scan point, $\mathbf{s'}_i$:

$$\text{Cost}(\mathbf{p}) = \frac{1}{N}\sum_{i=1}^{N}\text{DistanceField}(\mathbf{s'}_i) \quad (2)$$

Where N is the number of points in the scan. A penalty is added for points that, after transformation, fall outside the map boundaries, discouraging invalid solutions. This approach is inspired by map-to-scan matching metrics such as Perfect Match.

Optimization Algorithms

Both GA and PSO were implemented to explore the three-dimensional search space (x, y, θ) and find the pose that minimizes the cost function.

Genetic Algorithm (GA)

GA is a metaheuristic based on the principles of natural evolution [1]. The population is composed of individuals, where each chromosome encodes a candidate pose. Evolution proceeds through genetic operators:

- Tournament Selection: Individuals are selected for reproduction based on their fitness value, where a lower error corresponds to a higher probability of selection.
- Crossover: Selected parents exchange genetic information (parts of their pose vectors) to generate offspring.
- Mutation: Small random perturbations are introduced into the offspring to preserve diversity and avoid premature convergence.
- Elitism: The best individuals of each generation are preserved and carried forward, ensuring the retention of the best solutions found.

Particle Swarm Optimization (PSO)

PSO is inspired by the collective behavior of swarms [7]. Each particle in the swarm represents a candidate pose and adjusts its trajectory based on its own best experience (*pBest*) and the best experience of the group (*gBest*). The velocity and position of each particle are updated iteratively according to the following equations:

$$\mathbf{v}_{k+1} = w\mathbf{v}_k + c_1 r_1(\mathbf{pBest}_k - \mathbf{p}_k) + c_2 r_2(\mathbf{gBest}_k - \mathbf{p}_k) \quad (3)$$

$$\mathbf{p}_{k+1} = \mathbf{p}_k + \mathbf{v}_{k+1} \quad (4)$$

Where w is the inertia factor, c_1 and c_2 are the cognitive and social coefficients, and r_1, r_2, are random values. This dynamic allows the swarm to efficiently explore the search space.

Simulation Framework

To ensure reproducibility and a fair comparison, a simulation framework was developed:

1. Map and Data Generation: A synthetic 20×20 meter occupancy map with 0.05 m/pixel resolution was created. Ground-truth poses were generated randomly within free-space regions of the map. For each pose, a 2D LiDAR scan was simulated using the function `simulate_scan_from_pose`, which casts rays from the pose and computes distances to obstacles, adding Gaussian noise of 0.01 m to emulate real sensor imperfections.

2. Execution and Analysis: A total of 150 independent experiments were conducted. In each run, a new ground-truth pose was sampled and a corresponding scan generated. GA and PSO were executed to optimize a randomly initialized pose using the simulated scan. Performance metrics such as position error, angular error, and runtime were recorded for comparative statistical analysis.

Results and Discussion

The performance evaluation of the algorithms was conducted on the simulated map developed in this work (Figure 1). White areas represent

Figura 1. Synthetic occupancy map used in the experiments.

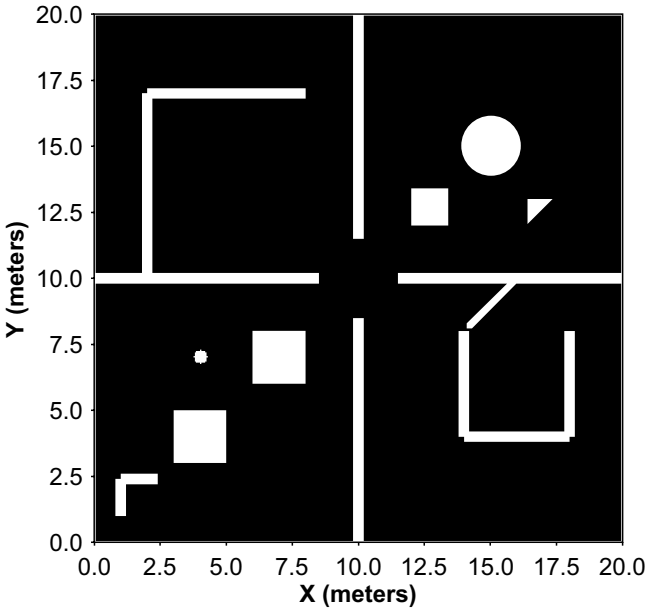

obstacles, while black areas correspond to free navigable space. The map was designed to include a variety of elements, such as obstacles with different geometric shapes (e.g., circles, squares, and angled lines) and structural divisions that segment the environment into distinct regions. This configuration was intended to assess the robustness of the algorithms in scenarios with spatial diversity and moderate complexity.

Statistical Analysis of Position Error

Quantitative analysis of position error reveals similar mean performance between the algorithms. GA achieved a mean position error of 0.4408 ± 0.7329 m, while PSO obtained 0.4664 ± 0.8069 m. The Wilcoxon test confirmed the absence of a statistically significant difference between these distributions $p = 0.1580$.

However, a more detailed analysis based on the median, which is less sensitive to outliers, provides clearer insight: the median position error was only 0.0536 m for GA and 0.0420 m for PSO (Table 1). These values, shown in Figure 2, indicate that both algorithms are capable of achieving high accuracy in most runs. It is also notable that both algorithms exhibit low medians alongside outliers. The high means and standard deviations are therefore largely influenced by a limited number of runs in which the algorithms converged to local minima.The boxplot (Figure 2) also suggests that although the median error of PSO is slightly lower, the spread of its outliers (larger errors) is greater than that of GA, indicating a higher risk of large-magnitude errors.

Statistical Analysis of Orientation Error

For orientation error, the Wilcoxon test indicated a statistically significant difference $p = 0.0187$. Examining the data in Table 1 and Figure 3, we observe that PSO achieved a median angular error of 0.18◦, considerably lower than GA's 0.45◦. This suggests that, in typical scenarios, PSO demonstrated superior capability in correctly aligning the robot's orientation. The statistical significance, combined with a lower median, supports the conclusion that PSO was more accurate in terms of orientation. Similar to

Table 1. Statistical summary of position and angular errors.

Metric	GA		PSO	
	Position (m)	Angle (°)	Position (m)	Angle (°)
Mean	0.4408	23.6882	0.4664	24.3806
Standard Deviation	0.7329	47.9431	0.8069	52.0710
Median	0.0536	0.4476	0.0420	0.1822
Minimum	0.0011	0.0184	0.0127	0.0028
Maximum	2.8100	179.9788	2.8284	179.9386

Figure 2. Distribution of final position error.

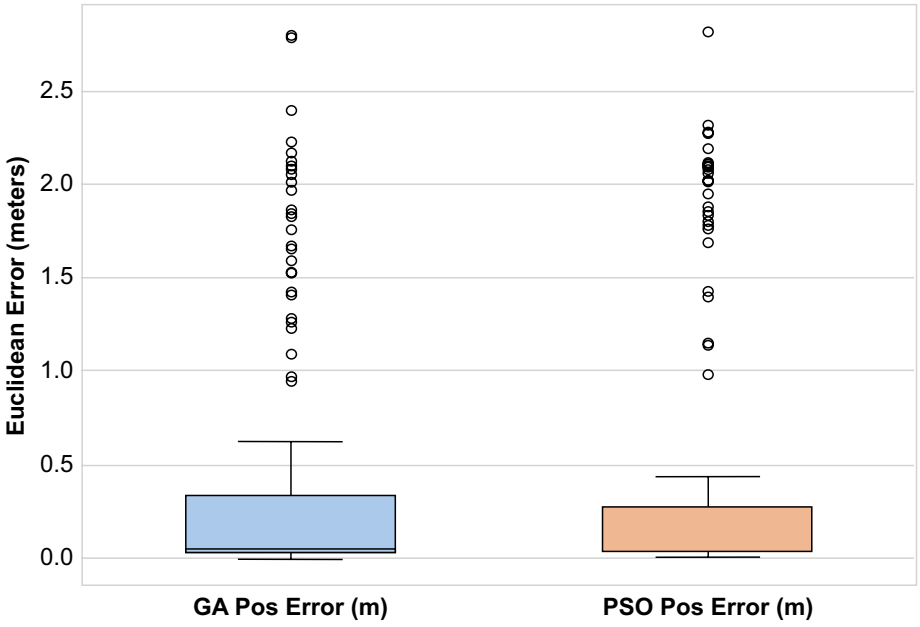

Figure 3. Distribution of final orientation error.

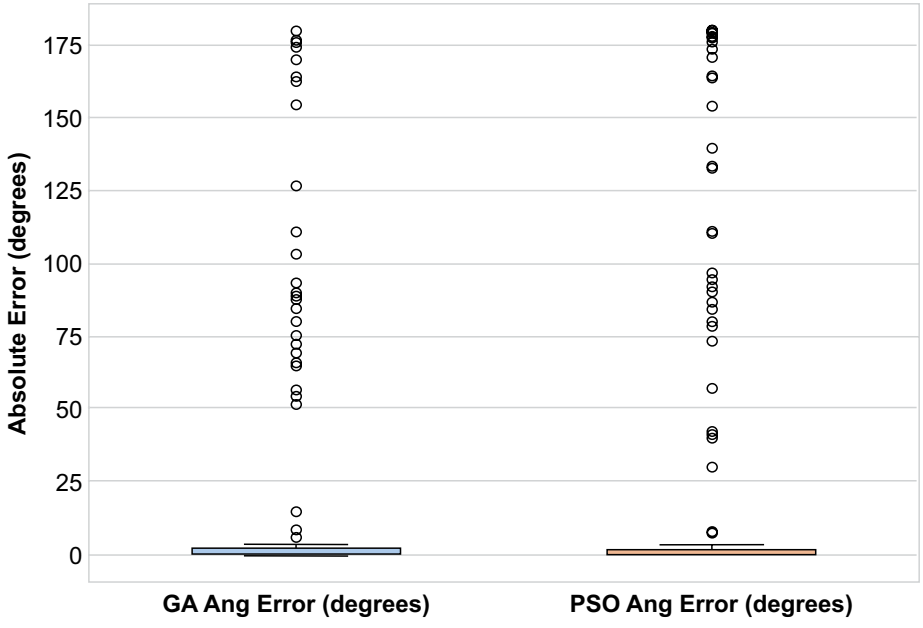

position error, outliers with high angular errors were observed in both algorithms, representing a risk factor to be considered.

Convergence and Computational Cost Analysis

Figure 4 shows that PSO exhibits faster initial convergence, reaching lower fitness values in fewer iterations. GA, in contrast, displays a more gradual convergence, but its mean error curve concludes with smaller variability (standard deviation shadow), suggesting greater stability and consistency across runs in the later generations.

In terms of computational cost, mean execution times were 13.77s for GA and 13.64s for PSO. The absence of a significant difference indicates that,

Figure 4. Average fitness convergence with standard deviation.

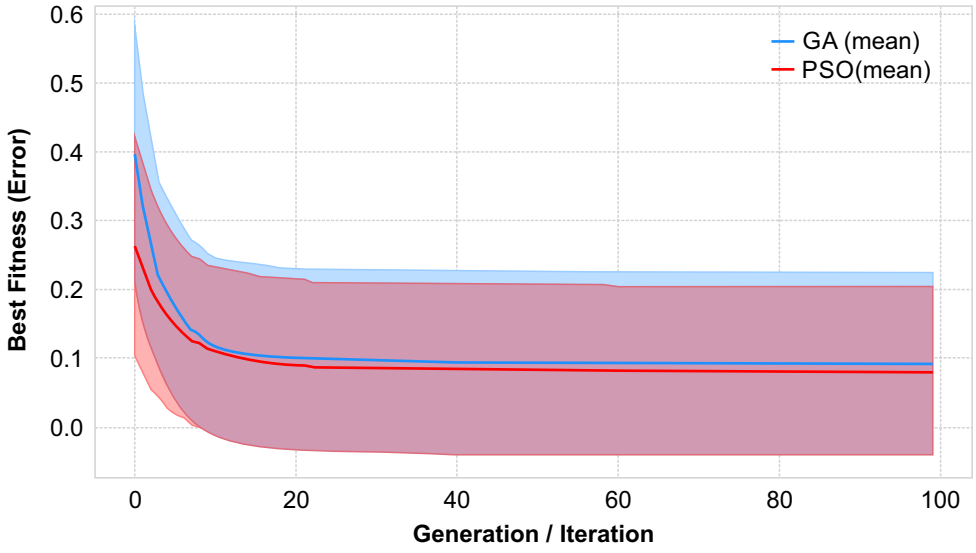

for the parameters used, the choice between the two should not be based on computational efficiency but rather on their accuracy and robustness profiles.

Qualitative Alignment Analysis

Alignment error analysis provides further insight into the robustness of the algorithms. Figure 5 illustrates the bestcase scenario, in which both methods correctly identified the true pose with minimal residual errors, validating their ability to reach the global optimum.

The most revealing scenario, however, is the worst-case outcome (Figure 6). In this experiment, GA maintained an accurate solution (error of 0.054 m), whereas PSO converged to an incorrect local minimum, resulting in an error of 2.83 meters. This finding highlights a fundamental trade-off: PSO's accelerated convergence, which favors speed and lower median angular error, also increases its vulnerability to failures. GA's broader exploration, although slower, proved more robust in avoiding this specific failure mode.

The results indicate that there is no absolute winner, but rather a trade-off—namely, a balance between speed, accuracy, and robustness. PSO stood out for its faster convergence and statistically superior median angular accuracy, making it an attractive choice for applications where computational efficiency is a priority. However, this efficiency comes at the cost of reduced robustness, as PSO demonstrated vulnerability to significant localization errors when converging to incorrect local minima.

In contrast, GA, although slower in its convergence, proved to be more robust, avoiding the large-magnitude errors observed with PSO in the constructed test scenario. This characteristic positions GA as a safer alternative for high-integrity systems, where preventing critical errors takes precedence over optimization speed.

The choice between the algorithms, therefore, depends on the application domain. Systems that can tolerate and recover from occasional failures may benefit from the efficiency of PSO. Conversely, safety-critical systems may require the more cautious and robust exploration provided by GA. Future work could investigate hybrid or adaptive techniques that dynamically adjust the search strategy, aiming to combine the efficiency of PSO with the robustness of GA.

Conclusion

This work presented a comparative analysis of Genetic Algorithms (GA) and Particle Swarm Optimization (PSO) for the scan-to-map matching problem, a fundamental component of mobile robot

Figure 5. Alignment in the best-case scenario.

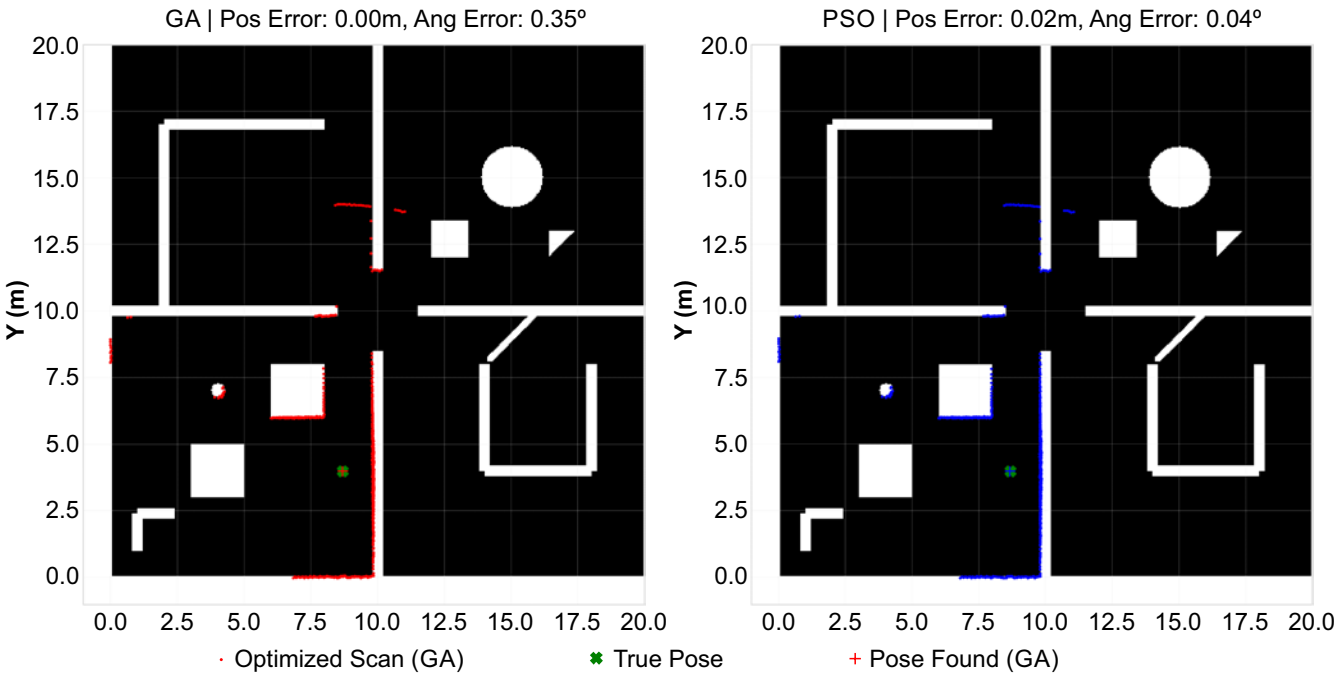

Figure 6. Alignment in the worst-case scenario.

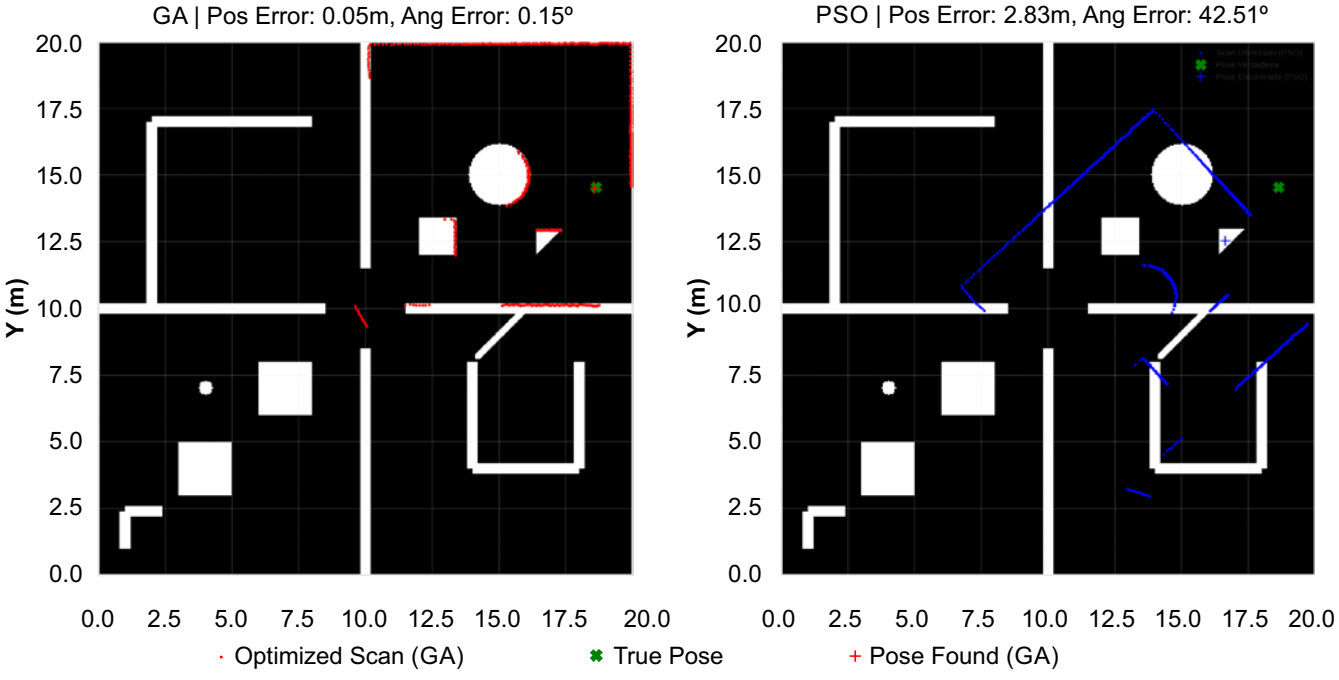

localization. Through a simulation framework, we demonstrated that both metaheuristics are effective tools for 2D pose optimization, overcoming the limitations of local search methods.

The main conclusion of this study is not the absolute superiority of one algorithm over the other, but the identification of a clear trade-off between accuracy, speed, and robustness. PSO distinguished itself by its faster convergence and statistically superior median angular accuracy, making it an attractive option for applications where computational efficiency is paramount. However,

this efficiency comes at the cost of reduced robustness, with PSO showing vulnerability to localization failures when converging to incorrect local minima.

On the other hand, GA, although slower in convergence, proved to be more robust, avoiding the large-magnitude errors observed with PSO in the proposed test scenario. This characteristic positions it as a safer alternative for high-integrity systems, where preventing significant failures outweighs optimization speed.

For future work, the investigation of hybrid approaches that combine the stable exploration of GA with the aggressive convergence of PSO represents a promising direction. Additionally, validating these results with experimental data from robots in real environments and extending the framework to 3D localization are natural next steps in the evolution of this research. Parameter optimization of the algorithms for different types of environments and the incorporation of more sophisticated evaluation metrics also constitute important directions for future contributions.

References

1. Carvalho JLC, Farias PCMA, Simas Filho EF. Global localization of unmanned ground vehicles using swarm intelligence and evolutionary algorithms. J Intell Robot Syst. 2023;107:45.
2. Yin H, Xu X, Lu S, Chen X, Xiong R, Shen S, Li S. A survey on global lidar localization: challenges, advances and open problems. Int J Robot Res. 2024;132:3139–71.
3. Stefanoni M, Sarcevic P, Sárosi J, Odry A. Optimization techniques in the localization problem: a survey on recent advances. Machines. 2024;12(8):569.
4. Campbell S, O'Mahony N, Carvalho A, Krpalkova L, Riordan D, Walsh J. Where am I? Localization techniques for mobile robots: a review. In: Proc 6th Int Conf Mechatronics Robot Eng (ICMRE); 2020. p. 43–7.
5. Chen Y, Wu K, Guo Y, Zhao K, Liu L. Long-distance target localization optimization algorithm based on single robot moving path planning. Sci Rep. 2025;15:25157.
6. Gutmann JS, Schlegel C. AMOS: comparison of scan matching approaches for self-localization in indoor environments. In: Proc EUROBOT '96; 1996.
7. Pinto M, Sobreira H, Moreira AP, Mendonça H, Matos A. Self-localisation of indoor mobile robots using multi-hypotheses and a matching algorithm. Mechatronics. 2013;23(6):727–37.
8. Bouraine S, Bougouffa A, Azouaoui O. Particle swarm optimization for solving a scan-matching problem based on the normal distributions transform. Evol Intell. 2022;15:683–94.
9. Zhang Q, Wang P, Bao P, Chen Z. Mobile robot global localization using particle swarm optimization with a 2D range scan. In: Proc Int Conf Robot Artif Intell; 2017.

Study of the Reuse of Eggshells in the Production of Bioplastics with Soil Enrichment Potential

Giulia Freire Fonseca[1]*, Cecília Araújo Crisóstomo Oliveira[1], Gisele Gonçalves Chagas[1], Ellen Rayane Vitória Santos Costa Brito[1], Beatriz da Paixão Santos[1], Érica Patrícia Lima Pereira[1]

[1]SENAI CIMATEC University, Industrial Microbiology; Salvador, Bahia, Brazil

This comprehensive study investigated the significant potential of eggshell, a readily available calcium-rich bio-waste, as an effective and sustainable additive in bioplastics. This innovative approach aims to substantially improve soil fertility during the material's biodegradation, while concurrently mitigating the environmental impacts associated with conventional limestone mining, the traditional source of calcium, as well as addressing the disposal of fossil-derived plastics. The robust methodology involved preparing plant-based raw materials, developing prototypes with systematic variations in composition and concentration, and comprehensively characterizing the formulated biomaterial. Analyses included precise thickness measurements and rigorous soil biodegradation tests through mass loss coupled with calcium carbonate equivalent ($CaCO_3$) quantification and carbon dioxide (CO_2) emission monitoring. The formulations were systematically studied at concentrations of 0%, 0.25%, 0.5%, and 1% eggshell, with thicknesses ranging from 0.37846 mm to 0.53594 mm. The biomaterials demonstrated promising average soil biodegradation rates of 52.42%, 51.26%, 52.94%, and 57.64% for concentrations of 0%, 0.25%, 0.5%, and 1%, respectively. During the 16 days of biodegradation, the samples released an average of 102.36, 117.55, 128.87, and 138.84 g kg^{-1} of $CaCO_3$. These values disregard the baseline $CaCO_3$ (g kg^{-1}) value found in the soil without the presence of the samples, and it is possible to observe a consistent growing trend in the quantity of this essential nutrient that directly accompanies the increase in eggshell concentration in the formulation. The average aerobic biodegradability rate corresponded to 44.70% within a 14-day interval. Thus, eggshell presented itself as a strong potential additive in bioplastics, enabling formulations that are simultaneously biodegradable and capable of fertilizing the soil.

Keywords: Biodegradation. Bioplastic. Calcium. Eggshell. Fertilizer.

Abbreviations: ADFE, Air-Dried Fine Earth. EF, Eggshell Flour. DABCD, Determination of Aerobic Biodegradability in Soil by Amount of Carbon Dioxide. MLBTS, Mass Loss Biodegradation Test in Soil.

Fossil plastics have revolutionized the industry with the creation of low-cost and multifunctional products. Despite that, since their creation, this polymer has faced contradictions, as highlighted by Conceição and colleagues [1], related to their inadequate disposal in contrast to the dependence of processing companies. However, not only polymers show this growing production and disposal, but also bioproducts such as eggshell.

According to released data by FAOSTAT [2], it is estimated that demand for table eggs will reach 95 million tons. Considering that 10% of the total weight of the egg corresponds to the shell, we will have about 9.5 million tons of a calcium-rich bio-waste, an essential nutrient for animal and plant metabolism. In this sense, the present study is dedicated to exploring the biotechnological potential of eggshell in the development of a bioplastic with full potential to improve soil conditions after disposal. As objectives, we sought to obtain eggshell flour and English potato starch, both raw materials for the biopolymer. Subsequently, to test different bioplastic formulations and evaluate their potential for soil enrichment with calcium during biodegradation through physical/chemical assays. And finally, to systematize with the literature in the field of botany, the importance of calcium for plant development, given the abundance of this nutrient in eggshells [3].

Theoretical Foundation

The eggshell is calcareous layer in which about 96% of the weight corresponds to calcium

Received on 25 October 2025; revised 10 January 2026.

Address for correspondence: Giulia Freire Fonseca. Av. Orlando Gomes, 1845, Piatã, Salvador, Bahia, Brazil. Zipcode: 41650-010. E-mail: giuliafreire39@gmail.com.

J Bioeng. Tech. Health 2026;9(2):112-119

carbonate ($CaCO_3$), while the flour of this byproduct presents 36.9% of bioavailable calcium (Ca) for the organism [4,5]. Thus, it is concluded that eggshell has interesting nutritional values centered on high concentrations of Ca and $CaCO_3$.

In view of this, Matteucci and colleagues [6] points out the waste of this resource, which has high utility for soils. This is because this macroelement favors root growth, intensifies microbial activity, and increases the availability of Molybdenum [7].

The presence of calcium in the soil is not limited to performance, as it is also indispensable for the full development of crops, because as stated by Luo [8] it severely interferes with the maintenance of life in the entire ecosystem.

According to Neto [9], the deficiency of adsorbed metallic cations such as Ca is corrected by the liming technique with limestone, as it results in the accelerated formation of nitrates and sulfites and stimulates nitrogen-fixing bacteria. However, according to Neto & Ramalho [10], limestone extraction causes several environmental impacts, such as erosion, irreversible destruction of fossils, among others. Thus, eggshell becomes a potential fertilizer,given its high concentration of a nutrient demanded by agricultural and forest systems. Therefore, it is pertinent for the biotechnology branch to study the reuse of this material for soil improvement, as an alternative to other degrading sources.

Polymeric materials are among the most used tools currently [11]. However, despite their applicability in long-life products, they have been applied as disposable single-use products [12]. In this sense, the use of biodegradable plastics is a viable alternative because they are produced from renewable sources that have a shorter degradation time.

Starch is the most used raw material for plastic application due to its large-scale availability, biodegradability, and low cost [13]. Originally, it is found in granular form, but it is subject to bond breakage at high temperatures with plasticizers such as glycerol with acetic acid, which provide greater flexibility [14]. The work of Furckel [15] obtained satisfactory results by using agro-industrial residues such as apple flour in starch biopolymers, pointing to the possibility of using other raw materials in starch-based plastic. In this direction, the present work corroborates the concept of circular economy under the conditions of Moreira [12] by conceiving an alternative for a polluting material. The proposal is to use a reused raw material while also attributing a double functionality to it.

Materials and Methods

English Potato Starch Extraction

Following the procedures adopted from Neto & Ramalho [11], the extraction was based on the decantation and drying of the starch from the process of crushing the washed, peeled, and weighed root.

Eggshell Flour (EF)

The chicken eggshells collected by the authors and other collaborators were sanitized, dried, and crushed to form the flour.

Bioplastic Formulation

The bioplastic formulation was grounded on the methodology described by Pereira & Plens [16], with adaptations. Distilled water, starch, acid, glycerin, and eggshell were mixed and heated until reaching a temperature of 90°C. The mixtures were poured into petri dishes and taken to dry in an oven.

Thickness Measurement

Based on Bezerra & Andrade [17], thickness was measured with a micrometer at 5 different points of each polymer to define the overall thickness from a simple average.

Mass Loss Biodegradation Test in Soil (MLBTS)

The experiment was carried out based on the adapted method of Bezerra & Andrade [17]. Each

bioplastic formulation was cut into 3 samples measuring 2cm x 2cm with the aid of a caliper, as shows Figure 1. Subsequently, each one was weighed and buried in different containers with 25g of fertilized topsoil. The mass reduction was monitored by regular weighings and calculated as a percentage.

Quantification of Calcium Carbonate ($CaCO_3$) Equivalent

The method used was adapted from Teixeira and colleagues [18]. Initially, the soil used in each biodegradation was prepared to obtain Air-Dried Fine Earth (ADFE). Subsequently, these samples were heated with 0.5 N hydrochloric acid (HCl), filtered, and diluted. 50 mL of the resulting solution was taken, 3 drops of 1% phenolphthalein indicator were added, and finally, titrated with 0.25 N sodium hydroxide (NaOH) solution. At the end, the 12 samples percentage of $CaCO_3$ were calculated, for each triplicate of concentration.

Figure 1. Sample preparation with a caliper

Determination of Aerobic Biodegradability in Soil by Amount of Carbon Dioxide - CO_2 Emitted (DABCD)

The experimental procedure for the biodegradation test was adapted from the ISO 17556 [19] and Tosin & Pischedda [20]. One bioplastic sample of each concentration, sized 2 cm x 2 cm, were introduced into beakers with 200g of soil, whose pH, humidity, and nutrient levels were previously adjusted. The experimental system also included a negative control (soil only) and a positive control (soil with filter paper measuring 2 cm x 2 cm). Each of these beakers was inserted into a CO_2 capture system, composed of a larger beaker containing a 0.5 N potassium hydroxide (KOH) solution. To ensure isolation, the system was hermetically sealed with plastic film, Parafilm®, plastic bag, and adhesive tape. The quantification of released CO_2 was performed every 2-3 days by titrating the KOH solution with 0.3 N hydrochloric acid (HCl). The KOH solution was completely replaced after each titration.

Results and Discussion

English Potato Starch

The yield of the starch extraction process from the potato was approximately 12.98%. This value is considered low when compared to the results by Neto & Ramalho [11], which acquired 50.14% as the average starch yield for sweet potato, 64.82% for mangarito, and 66.03% for cassava. At the same time, Mendonça [21] obtained 7.89% as the average starch yield for mangarito. Such discrepant differences may be due to differences in the growth and harvesting conditions of the tuber used, given that the procedure followed was similar.

Bioplastic Formulation

Different prototypes were made until the expected final appearance was achieved. In the

first, the heterogeneous granulometry of the EF left a shapeless texture, similar to a dough, making demolding impossible due to its brittle texture.

For the second prototyping, adjustments were made to the flour, repeating the grinding step. From this, bioplastics were produced in triplicate for each EF concentration: 5%, 10%, and 15%. The dough-like texture was repeated, as shown in Figure 2, and this result revealed that such an aspect could be associated with the amount of flour added to the formulation.

For the third prototyping, it was necessary to confirm the viability of the formulation without EF. Thus, 2 different acids were tested, acetic and hydrochloric, and for each, two different starch concentrations. In the end, the most satisfactory formulation had 5% acetic acid and 2.5 g of starch as variable components, illustrated in Figure 3.

In addition, the heating temperature was increased, after observing in Santos and colleagues [14] that the temperature previously used was below the starch breakdown range. Finally, it was possible to demold this prototype with the aid of a spatula. For the last prototyping, the parameters and components defined in the previous one were used, adding EF in lower concentrations than in the previous prototypes, namely: 0%, 0.25%, 0.5%, and 1%. At the end of the process, the expected results for the biopolymer were achieved. Thus, it differs from the best result found by Furckel and colleagues [15], who used 10% of agro-industrial residues in potato starch bioplastic.

Figure 2. Second prototyping, in 5%, 10% and 15% concentrations respectively.

Figure 3. Third prototyping with acetic acid.

Thickness Measurement

The results thickness of each samples used in the MLBTS and DBACD are represented in Tables 1 and 2, respectively.

The average thicknesses of the biopolymers ranged from 0.37846 mm to 0.53594 mm, while the standard deviation values ranged from 0.04568 mm to 0.13042 mm. In a review, Neto & Ramalho [11] obtained average thicknesses between 0.456 mm and 0.6618 mm and standard deviations between 0.032 mm and 0.092 mm. When comparing these results, the bioplastics in this study were less thick, but more shapeless than those in the methodological reference study.

Table 1. Thickness of bioplastics for MLBTS.

Bioplastic	Average Thickness (mm)	Standard Deviation ±
0.00%	0.40132	0.04568
0.25%	0.53594	0.08387
0.50%	0.52705	0.08754
1.00%	0.40132	0.13042

Table 2. Thickness of bioplastics for DBACD.

Bioplastic	Average Thickness (mm)	Standard Deviation ±
0.00%	0.46609	0.05996
0.25%	0.38100	0.09214
0.50%	0.37846	0.02353
1.00%	0.44958	0.09046

Mass Loss Biodegradation Test in Soil (MLBTS)

The weight variation by triplicates average in grams of the polymers during the test can be observed in Figure 4.

Significant mass reductions can be observed in the initial period of the test. This result contrasts with the mass increase between the first and second weighing observed by Neto & Ramalho [11], who associated this gain with soil adherence to the polymer. In the present study, the magnitude of the mass reduction was sufficient to overcome any initial mass gain resulting from soil adhesion, highlighting the expressiveness of the degradation process.

A significant increase was noted on day 7, which can be attributed to higher soil moisture at the time of weighing, which made it impossible to remove excess soil. The Figure 5, presented below, illustrates the results of the averages of the triplicates regarding the mass reduction, in percentage, for each of the eggshell concentrations used.

Over 16 days of degradation in soil, the bioplastics reduced their mass by an average of 52.68%. This result is similar to that of Neto & Ramalho [11], who obtained averages of 57.46% and 58.76% mass reduction during 24 days of degradation.

As evidenced in Figure 5, the sample without EF addition (0%) exhibited a higher degradation rate than the material with 0.25% EF and similar to the bioplastic with 0.5% EF. This observation can be related to the physical characteristics of the material, specifically its thickness and uniformity. The 0% polymer showed less thickness and greater uniformity. In contrast, the 0.25% was the thickest, while the 0.5% exhibited similar thickness to the 0%, but with greater non-uniformity. Interestingly, the prototypes with 1% eggshell, which had an average thickness equal to 0% and the lowest uniformity among all, showed superior degradation. Such results suggest that the presence of eggshell can accelerate the biodegradation process, while increasing the thickness of the material tends to retard it.

Quantification of Calcium Carbonate Equivalent

The Figure 6 illustrates the amount of $CaCO_3$ (g kg^{-1}) released by the biopolymers during the 16-day period. It shows the average of the triplicates for the four eggshell concentrations.

The result demonstrates that the eggshell was efficient in fertilizing the soil with calcium, even when present in low concentrations in the biopolymer.

Determination of Aerobic Biodegradability in Soil by Amount of Carbon Dioxide - CO_2 Emitted

The CO_2 emission and degradation percentage are shown in Figures 7 and 8, respectively.

When summing the biodegradation percentages for the entire period, the total aerobic biodegradability rate was 123.75%, 16.34%, 63.65%, 73.69%, and 25.14% for the positive blank and the materials with 0%, 0.25%, 0.5%, and 1% EF, respectively. Although exceeding the theoretical limit, the positive control result

Figure 4. Weight by triplicates average x Biodegradation time.

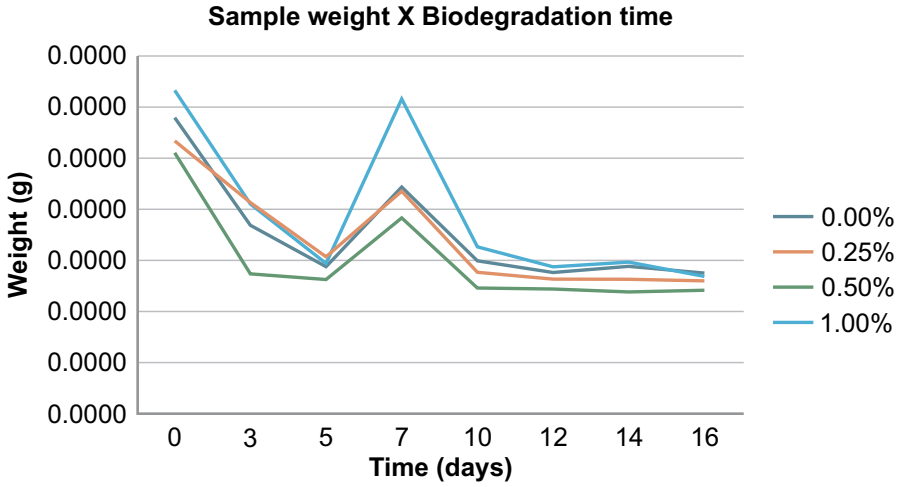

Figure 5. Sample mass reduction by averages of the triplicates.

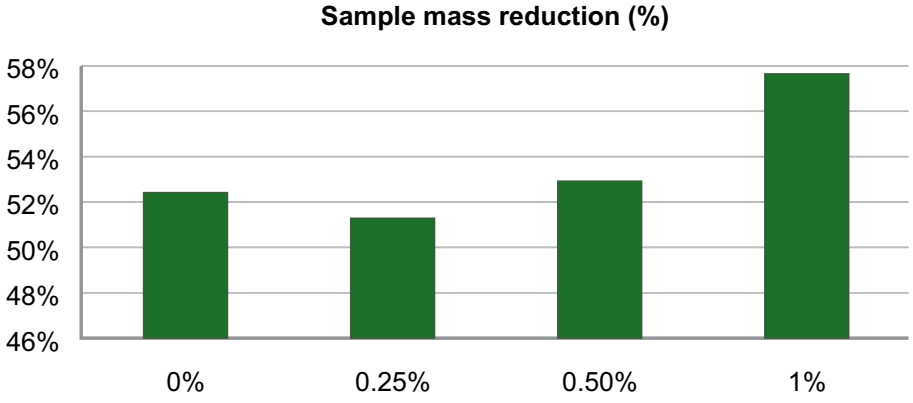

Figure 6. Quantification of $CaCO_3$ equivalent.

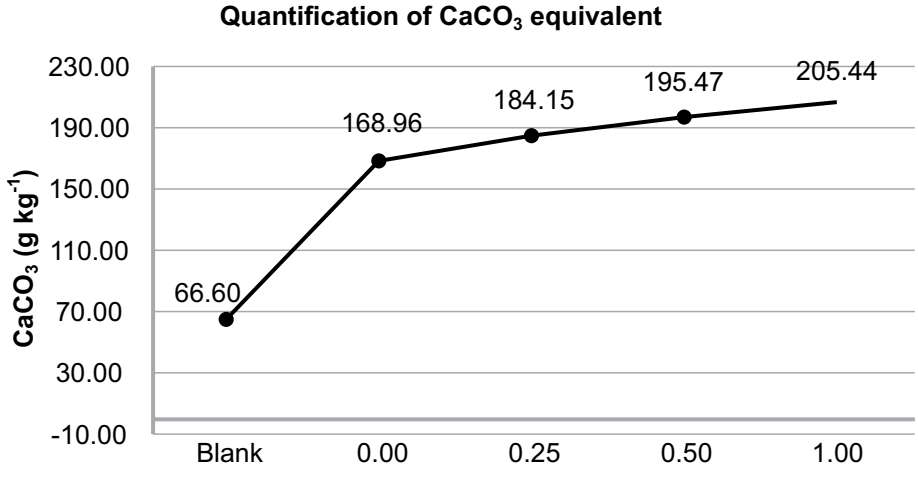

Figure 7. CO_2 emissions in mg.

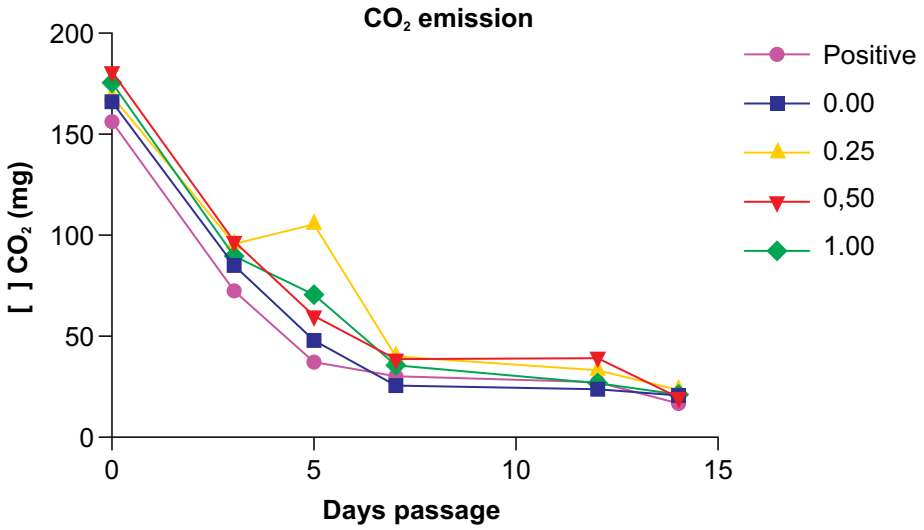

Figure 8. Degradation percentage.

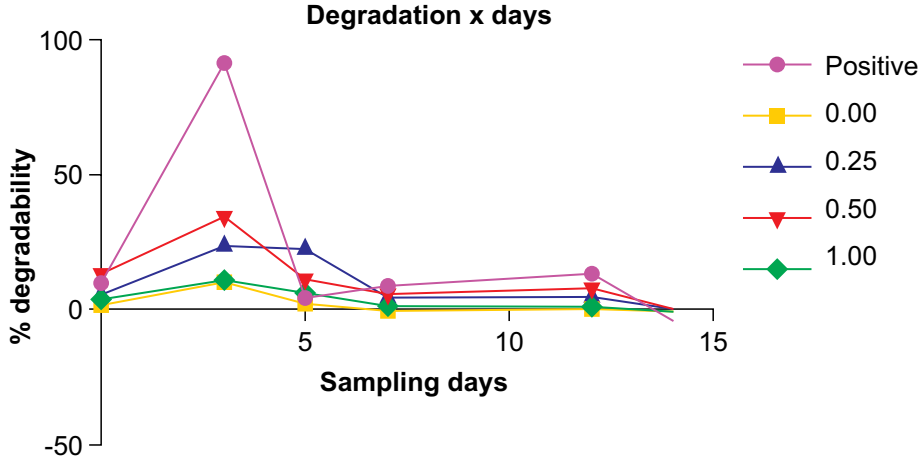

unequivocally confirms that the system conditions (temperature, aeration, and humidity) and the microbial inoculum activity were adequate and robust for the mineralization of a biodegradable polymer. Additionally, cellulose is an easily degradable substrate, especially with the low mass used (0.036g), which can lead to significant percentage deviations. Therefore, the assay is considered valid for the evaluation of the tested biopolymers.

Due to the experiment being conducted for 14 days, and the ideal time for this experiment being 6 months, certain inconsistencies can be attributed to this. Furthermore, this specific experiment was not performed in triplicate for each sample, so the most plausible biodegradation results are from the mass loss assay. Still, the generated data provide an idea of the material's nature, which in future tests can be confirmed by adjusting the parameters mentioned above.

Conclusion

Therefore, the use of eggshell demonstrated success as a functional component in starch-based bioplastics. The results indicate that the additive contributes to soil enrichment by releasing calcium during degradation. This dual functionality represents an innovative solution capable of mitigating the environmental impacts

associated with the disposal of fossil plastics and limestone extraction.

Both biodegradation analyses confirmed the effectiveness of the biopolymer in fertilizing the soil, even at low concentrations of the additive.

Despite the limitations and the short duration of the experiment, especially regarding biodegradation, the data obtained provide a solid basis that validates the concept. Future studies, with adjustments to experimental parameters and longer analysis times, may refine and confirm the potential of this biomaterial as a sustainable and beneficial alternative for agriculture and the environment.

References

1. Conceição MM, Conceição JTP, Dalmas FB, Rosini AM. The plastic as a villain of the environment. Rev Geoc UNG Ser. 2019;18(1). doi:10.33947/1981-7428-v18n1-4024
2. FAOSTAT. Food and agriculture data [Internet]. Rome: FAO; [cited 2024 May 12]. Available from: https://www.fao.org/faostat/en/#data
3. Soares KR, Ximenes LF. Produção de ovos. Caderno Setorial ETENE. 2022;7(214).
4. Neves MA. Alternativas para valorização da casca de ovo como complemento alimentar e em implantes ósseos [dissertation]. Florianópolis: Universidade Federal de Santa Catarina; 1998.
5. Peres AP, Waszczynskyj N. Farinha de casca de ovo: determinação do teor de cálcio biodisponível. Vis Acad. 2020;11(1). doi:10.5380/acd.v11i1.21357
6. Matteucci MBA, Figueiredo RS, Vera R. Comparação de macro e micronutrientes da casca de ovo caipira versus ovo convencional para uso em produção na agricultura familiar. In: Desafios globais, soluções locais: avanços em ciências agrárias e ambientais. Campina Grande: Ed Licuri; 2023. p. 46–51. doi:10.58203/Licuri.21715
7. Sá AAS, Oliveira GH, Silva RP, Assis VCSS, Oliveira CS, Oliveira JA, et al. A importância do cálcio para nutrição de plantas. Sci Elec Arch. 2024;17(2). doi:10.36560/17220241873
8. Luo Y, Sun C, Yang S, Yang L, Zhang S, Zhang C. Characteristics of soil calcium content distribution in Karst dry-hot valley and its influencing factors. Water. 2023;15:1119. doi:10.3390/w15061119
9. Neto SPM. Acidez, alcalinidade e efeitos da calagem no solo. 2009.
10. Neto RLG, Ramalho JS. A evolução do impacto ambiental acarretado pela extração de calcário, tendo como exemplo a mineração Patercal-Partezani no estado de São Paulo. CES Rev. 2010;24.
11. Veloso R. Extração de amido de mandioca, batata doce e mangarito, rendimento e uso na confecção de plástico biodegradável [dissertation]. Brasília: Universidade de Brasília; 2019.
12. Moreira MN. Valorização da casca de ovo como partícula de reforço mecânico e de barreira em filme biodegradável à base de pectina e amido de mandioca [dissertation]. Campinas: Universidade Estadual de Campinas; 2023.
13. Macedo GSA, Castro FS, Pereira MG, Santos AV. Estudo das características físico-químicas e térmicas dos materiais não biodegradáveis e biodegradáveis à base de amido de milho. Braz J Dev. 2020;6(12):99327–47. doi:10.34117/bjdv6n12-431
14. Santos CV, Rodrigues AAL, Meneguzzi Á, Silva RS. Bioplástico desenvolvido a partir da farinha de sabugo de milho (Zea mays L.). In: Ciência e tecnologia de alimentos: pesquisas e avanços. 2024;5:502–13. doi:10.53934/202411.47
15. Furckel M, Souza EL, Soares FASM. Produção e caracterização de biopolímero à base de amido e glicerol com resíduos agroindustriais. In: Seminário de Iniciação Científica e Seminário Integrado de Ensino, Pesquisa e Extensão (SIEPE). Universidade do Oeste de Santa Catarina; 2021.
16. Pereira JMS, Plens ACO. Produção de bioplástico a partir do amido da batata. In: 11º Congresso de Inovação, Ciência e Tecnologia do IFSP. Presidente Epitácio (SP); 2020.
17. Bezerra ES, Andrade PL. Desenvolvimento de bioplásticos à base de casca de bananas e de ovos. In: Ciência e engenharia de materiais: conceitos, fundamentos e aplicação. 2021. p. 217–29. doi:10.37885/210705567
18. Teixeira PC, Donagemma GK, Fontana A, Teixeira WG. Manual de métodos de análise de solo. Brasília (DF): Embrapa; 2017.
19. International Organization for Standardization (ISO). ISO 17556: plastics — determination of the ultimate aerobic biodegradability of plastic materials in soil by measuring the oxygen demand in a respirometer or the amount of carbon dioxide evolved. Geneva: ISO; 2019.
20. Tosin M, Pischedda A, Degli-Innocenti F. Biodegradation kinetics in soil of a multi-constituent biodegradable plastic. Polym Degrad Stab. 2019;166:213–8. doi:10.1016/j.polymdegradstab.2019.05.034
21. Mendonça MM. Caracterização do amido do mangarito [dissertation]. Lavras: Universidade Federal de Lavras; 2019.

Synergy between Innovation, Governance and Accounting in Public Stock Management: Guidelines for Sustainable Practice

Maria de Lourdes Ferraz Heleodoro[1]*, Cristina Conceição Rocha Guedes[1], Saada Lima Chequer Fernandez[1], Aloisio Santos Nascimento Filho[2], Hugo Saba[2,3]

[1]Oswaldo Cruz Foundation - Fiocruz; Rio de Janeiro, Rio de Janeiro; [2]SENAI CIMATEC University; Salvador, Bahia; [3]Bahia State University - UNEB; Salvador, Bahia, Brazil

This study examines the integration between governance practices, accounting information, and public stock management in the context of the COVID-19 pandemic, focusing on sustainable decision-making in a Brazilian public health institution. Efficient stock management in public health is critical for ensuring resource availability, cost control, and service continuity, especially during crises. Conducted as a qualitative descriptive case study at the Oswaldo Cruz Foundation (Fiocruz), the research involved semi-structured interviews with 14 stock management experts. While existing literature explores governance and accounting separately, few studies analyze their intersection with stock management in public health emergencies, leaving a gap this work seeks to address Data analysis, based on content analysis, identified three core dimensions: accounting instruments, knowledge dissemination, and governance perception. The findings reveal significant challenges, including the lack of standardized information systems, limited formal training, and weak interaction between accounting and stock management areas, which hinder the strategic use of accounting information. Despite collaborative practices and adaptive governance during the crisis, the absence of systemic integration undermines operational efficiency and transparency. The study proposes guidelines to strengthen intersectoral cooperation, enhance technical capacity, and implement digital tools, including a managerial dashboard for stock control. By aligning governance, accounting, and stock management, the proposed framework supports innovation, optimizes resources, and promotes sustainable practices in public administration. This research is limited by its single-case design and reliance on expert perceptions, suggesting the need for broader studies in diverse institutional contexts.

Keywords: Sustainability. Governance. Stocks. Accounting.

In January 2020, the World Health Organization (WHO) declared a Public Health Emergency of International Concern due to the spread of the novel coronavirus (SARS-CoV-2) [1]. Shortly thereafter, the Brazilian Ministry of Health declared a public health emergency of national concern, and in March, the WHO officially declared COVID-19 a pandemic. This event triggered an unprecedented health crisis, the impacts of which went beyond the health field, significantly affecting economic, social, and environmental dimensions [2,3].

In this context, public and private institutions were forced to adopt emergency decisions, often under conditions of high uncertainty, reviewing governance mechanisms to ensure more agile, coordinated, and transparent responses. The literature indicates that crisis situations require the adoption of adaptive governance practices, characterized by rapid response capacity, flexibility, and intersectoral cooperation [4,5], to mitigate risks, preserve the continuity of essential services, and reduce the social and economic damage resulting from the emergency. Decision-making based on agile and accurate information has become a strategic element, especially in contexts of digital transformation. In this scenario, the Oswaldo Cruz Foundation/Fiocruz stood out for its leading role in confronting the crisis, being recognized by the WHO as a reference for combating the novel coronavirus in the Americas. With a history of action in health emergencies, the institution mobilized strategic resources and stocks, aligning with guidelines that prioritize the integration of digital systems, data analysis and evidence-based decisions. In the context of the

Received on 10 October 2025; revised 21 January 2026.
Address for correspondence: Maria de Lourdes Ferraz Heleodoro. Oswaldo Cruz Foundation - Fiocruz; Av.Brasil, 4365, Manguinhos/RJ Rio de Janeiro, Brazil, Zipcode: 41650-010. E-mail: ferrazheleodoro@gmail.com.

J Bioeng. Tech. Health 2026;9(2):120-126

pandemic, the pressure for rapid deliveries has heightened the tension between timeliness and the effectiveness of control mechanisms.

Accounting information, recognized as a management support tool, is essential for optimizing inventory control and resource allocation. The integration of management accounting and supply chain management helps reduce risks and improve decision-making [5].

Based on this context, this work presents the results and conclusions of a case study in a public health institution, the governance practices applied to the management of consumer goods inventories during the pandemic, focusing on the use of accounting information by internal managers. Based on this context, this work presents the results and conclusions of a case study in a public health institution, the governance practices applied to the management of consumer goods inventories during the pandemic, focusing on the use of accounting information by internal managers.

Materials and Methods

This is a descriptive, qualitative case study conducted at the Oswaldo Cruz Foundation/ Fiocruz. The objective was to analyze managers' perceptions of knowledge dissemination as a governance tool, focusing on the use of accounting information for sustainable decision-making [6].

The sample included 14 managers specializing in public inventories, intentionally selected for their expertise. Data were collected through semi-structured online interviews, recorded and transcribed, following a script structured around six thematic areas: accounting integration, risk mitigation, accounting practices, interdisciplinary dialogue, training, and equity impact. The evaluation followed the principles of Content Analysis [7], with an inductive approach and supported by Atlas.ti 22 software. Categories were defined based on the interview script, consolidated into three dimensions: (a) accounting instruments; (b) knowledge dissemination; (c) perception of governance.

The project was approved by the Ethics Committee (Opinions No.6,225,917 and 6,301,040), adhering to national and international guidelines for research involving human subjects.

Results and Discussion

Study Category Evaluation

Accounting Instruments Category, Knowledge Diffusion Category and Managers' Perception Category from the perspective of knowledge diffusion as a governance instrument.

The entire study was categorized into three categories, and the interviews culminated in key expressions that indicated the most expressive elements in the interviewees' statements (Figure 1), with information collected by Categories.

The case study demonstrated that asset control in organizations requires agile and accurate information for efficient inventory management, encouraging integration between functional areas and promoting institutional agility [8]. Through interviews with inventory managers, the use of accounting instruments in decision-making was analyzed, highlighting their relevance and benefits, especially in internal environments and challenging external situations, such as during the COVID-19 pandemic [9].

The institution studied has experience in scientific research and is well-equipped to deal with change. However, each moment challenges managers to address new challenges. Organizations seek to improve their performance, and knowledge management emerges as a fundamental strategy to achieve this goal. To this end, it is essential to identify where knowledge exists and is generated within organizations. The use of knowledge auditing, as explained by Daghfous and colleagues [10], guides the organization to manage "what is truly necessary." Discussing knowledge means establishing a dialogue between what is formal and what is informal, between what is available and what is "in the heads of individuals."

Figure 1. Information collected by categories.

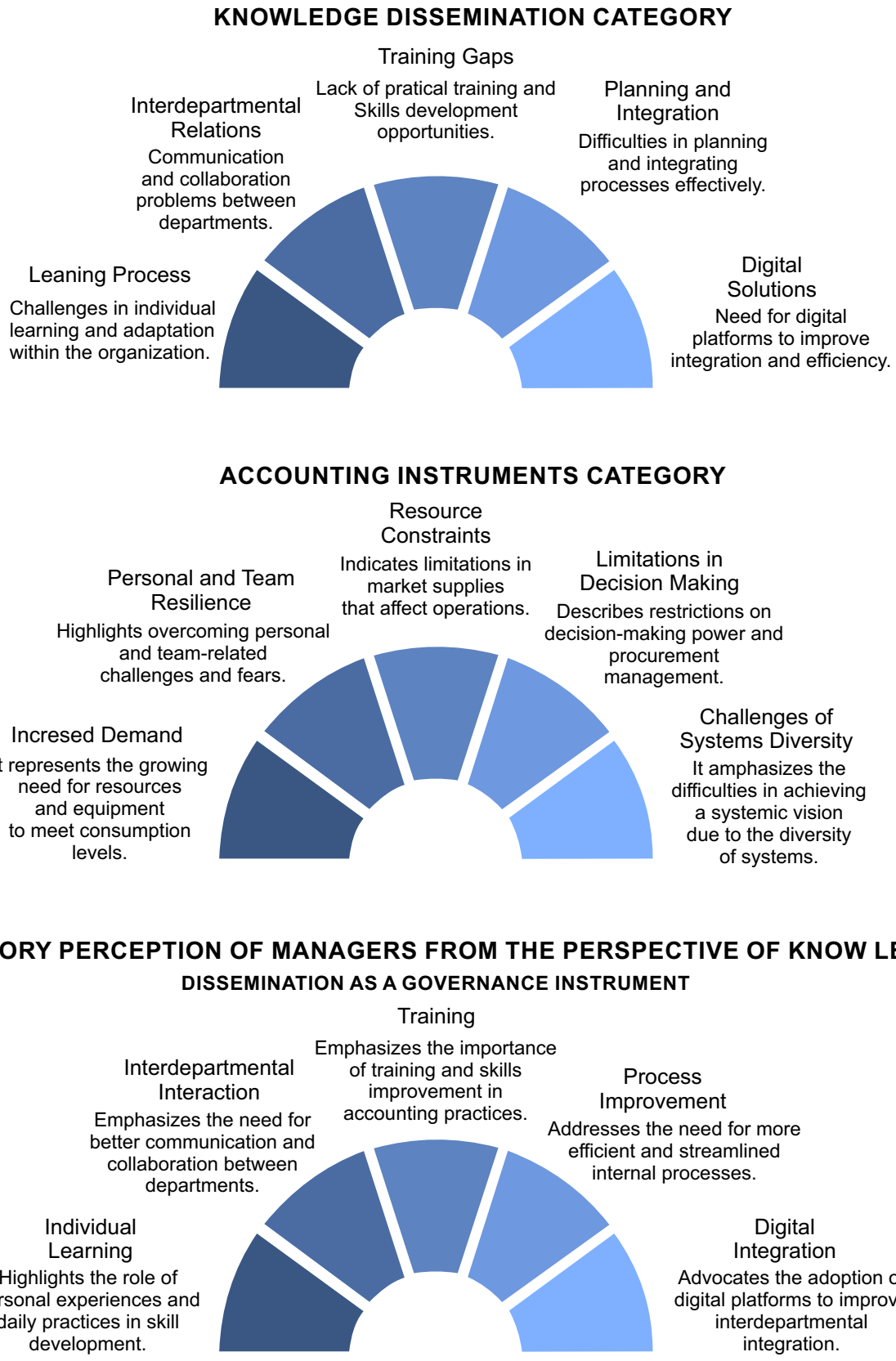

According to Terra (2001) [11], knowledge management can be understood as the ability of organizations to utilize and integrate different sources and types of internal knowledge in order to develop competencies and boost innovation capacity. This process continuously results in the creation of new products, the improvement of processes, the implementation of more efficient management systems, and the consolidation of market leadership.

In the category Perception of Managers from the perspective of knowledge dissemination as a governance instrument, the questions address topics related to control, risks, procedural changes, inter-agency dialogue, recognition of the importance of accounting information, the relevance of training, and the impact of inventory investments. Recording units such as training, controls, risks, learning, systems, and dissemination were captured. The context presented a difficult and challenging internal and external management environment, with the potential for this to occur at any time, present or future, as in the COVID-19 health emergency [9].

According to Oliveira and Malinowski (2016) [12], accounting information systems consist of an integrated set of data whose objective is to organize, measure, report, and analyze information related to the economic events of organizations. They provide their users with the financial information necessary to control their organizations.

The interviews revealed that there is no single information system, which hinders a systemic view of the whole at the time of decision-making. The interviewees' statements did not identify the use of accounting information systems in the decision-making process. However, currently, a vision aligned with business trends is achieved in financial management through the analysis of financial statements, which are considered essential raw material for the preparation of analyses, opinions, and decision-making [13] because "accounting, characterized by recording all of the corporation's transactions, constitutes a large database"[14].

The lack of standardization in the use of computerized systems for warehouse control

Figure 2. Consumable material management dashboard.

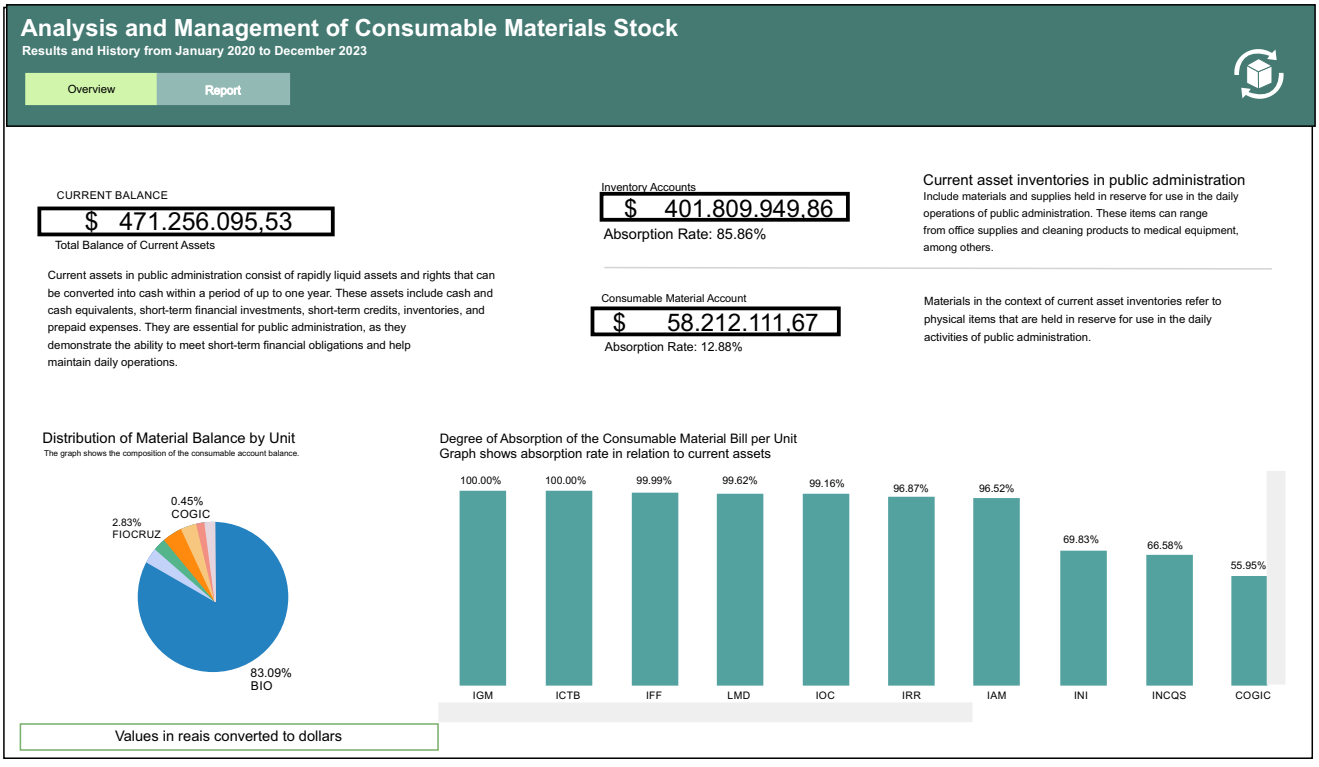

Figure 3. Suggested guidelines.

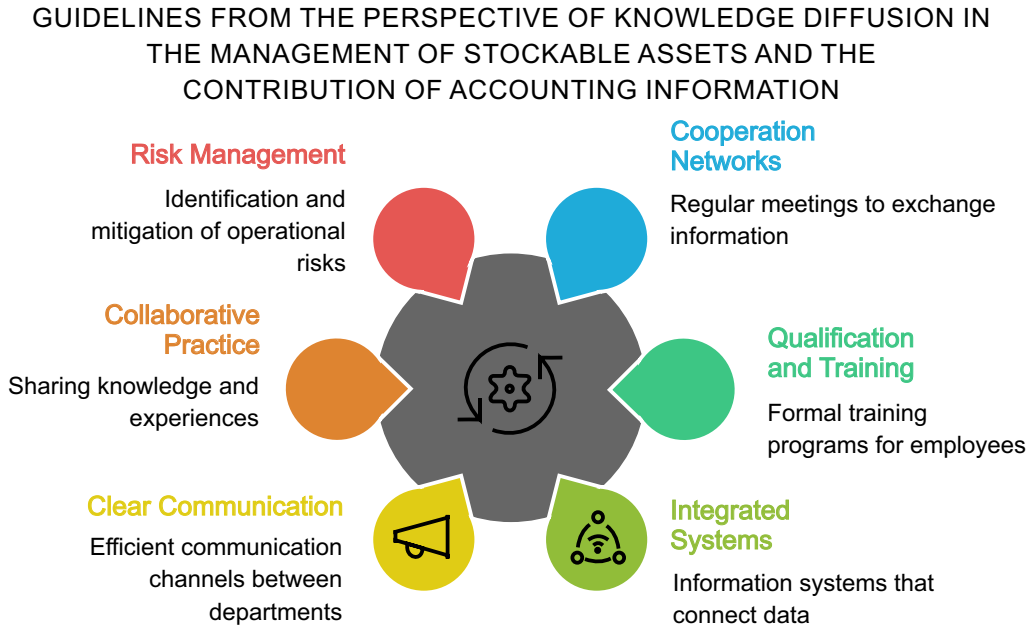

significantly contributes to increased accounting errors, higher storage costs, greater difficulty in identifying operational failures, and limits the effectiveness of decision-making based on reliable data.

According to Taschner and Charifzadeh (2020) [15], the governance structures of each organization or institution vary, with different effects on knowledge sharing, learning, and performance in their supply chains.

Based on the discussions, it was found that decisions are not based on accounting data during the decision-making process. Furthermore, a diversity of internal systems was identified, which makes it difficult to build a systemic view as a whole. Although they do not use accounting information regularly, they identify the absence of a cooperation network between the inventory and accounting areas. The individual learning process is a continuous journey, collaborative practice is also observed in the work environment, the sharing of experiences, in which tacit knowledge is disseminated collaboratively; a lack of training in accounting practice was noted, training was sometimes carried out in daily practice without formal training. There is no clarity regarding the dialogue between the inventory and c Regarding accountability, a dichotomy is noted among the interviewees, while some point out a distance between the inventory management area and the accounting part, while others have a good relationship, highlighting weaknesses in the interaction between the areas. There is no clear dissemination network, which can compromise the challenges faced by the Institution at national and international levels. Therefore, investing in strengthening the various cooperation and interaction networks among the partners that make up the management of storable assets within the Organization will contribute to business success, as the dissemination of knowledge between multidisciplinary areas inspires concern and the need for management attention.

Given the perception of inventory managers, efforts were mobilized to develop an inventory material dashboard (Figure 2).

The analyses conducted highlighted the need to improve integration between the inventory and accounting sectors within public administration. In this regard, guidelines are proposed to foster synergistic action based on intersectoral cooperation, strengthened communication, the

technical qualification of employees, and the strategic use of digital technologies (Figure 3).

Conclusion

The analysis revealed that the lack of effective integration between the inventory and accounting departments compromises the institution's systemic vision and hinders the strategic use of accounting information in decision-making. The lack of standardization in internal systems, the scarcity of formal training, and the absence of clear communication channels reinforce the need for structured actions to promote intersectoral cooperation. Although collaborative practices and examples of resilience exist, especially during the pandemic, weaknesses persist that directly impact operational efficiency and the quality of institutional governance.

The results highlight the importance of investing in the creation and strengthening of permanent collaboration networks, combined with the use of digital technologies for data and process integration. These measures, combined with ongoing professional development, foster transparency, accountability, and innovation in the management of inventories. The proposed implementation of an inventory-focused accounting management dashboard represents a strategic tool to support data-driven decision-making, increase interaction between departments, and consolidate more robust and sustainable governance practices.

In this scenario, the establishment of collaborative networks and the systematization of knowledge not only strengthens public management but also drives academic progress and improves the quality of services provided to society. The implementation of a dashboard, featuring functions such as real-time monitoring of inventory and costs, emerges as a tangible step to overcome communication barriers between sectors. However, it is essential to acknowledge that adopting these measures will face challenges, including the need for technological investments and cultural shifts within teams. Future research could test the applicability of this model in other public administration contexts. By aligning governance, accounting, and inventory management, institutions not only optimize resources but also prepare to respond swiftly to future crises, ensuring sustainability and efficiency in an increasingly complex environment. The work consolidates itself as a practical and analytical reference, paving the way for future studies and the improvement of public management.

Acknowledgement

The authors thank SENAI CIMATEC and its post graduate program on Industrial Management and Technology. His work was performed with the support of Escola Corporativa/Cogepe (Fiocruz) as part of the Management Development Programme (PDG).

References

1. World Health Organization. Statement on the second meeting of the International Health Regulations (2005) emergency committee regarding the outbreak of novel coronavirus (2019-nCoV) [Internet]. Geneva: WHO; 2020 Jan 30 [cited 2026 Feb 19]. Available from: https://www.who.int/news/item/30-01-2020-statement-on-the-second-meeting-of-the-international-health-regulations
2. Faria AF, Araújo CA. Impactos socioeconômicos da pandemia da COVID-19 no Brasil. Rev Adm Publica. 2021;55(4):945-962. doi:10.1590/0034-761220200556
3. Organização das Nações Unidas. Relatório de desenvolvimento humano 2020: a próxima fronteira – desenvolvimento humano e o antropoceno [Internet]. New York: Programa das Nações Unidas para o Desenvolvimento; 2020 [cited 2026 Feb 19]. Available from: https://hdr.undp.org
4. Ansell C, Boin A, Keller A. Managing transboundary crises: identifying the building blocks of an effective response system. J Contingencies Crisis Manag. 2010;18(4):195-207. doi:10.1111/j.1468-5973.2010.00620.x
5. Organisation for Economic Co-operation and Development. The territorial impact of COVID-19: managing the crisis across levels of government [Internet]. Paris: OECD Publishing; 2020. doi:10.1787/0e7460eb-en

6. Heleodoro MLF, Guedes CCR, Reis CACL, Bezerra CS, Nascimento Filho AS, Saba H. Governance in public stock management in synergy with accounting information: towards a sustainable practice. In: Proceedings of SIINTEC 2024. São Paulo: Blucher; 2024. p. 704-711. doi:10.5151/siintec2024-385338
7. Bardin L. Análise de conteúdo. 70ª ed. São Paulo: Edições 70; 2020.
8. Nogalski B, Niewiadomski P, Szpitter A. Agility versus flexibility? The perception of business model maturity in agricultural machinery sector manufacturing companies. Cent Eur Manag J. 2020;28(3):57-97. doi:10.7206/cemj.2658-0845.27
9. Seuring S, Brandenburg M, Sauer PC, Schünemann DS, Warasthe R, Aman S, et al. Comparing regions globally: impacts of COVID-19 on supply chains – a Delphi study. Int J Oper Prod Manag. 2022;42(8):1077-1108. doi:10.1108/IJOPM-10-2021-0675
10. Daghfous A, Zoubi T. An auditing framework for knowledge-enabled supply chain management: implications for sustainability. Sustainability. 2017;9(5):791.
11. Terra JCC. Gestão do conhecimento: o grande desafio empresarial. São Paulo: Biblioteca Terra Forum Consultores; 2001.
12. Oliveira DB, Malinowski CE. A importância da tecnologia da informação na contabilidade gerencial. Rev Adm. 2016;14(25):Art. 25.
13. Silva MP, Couto CHM, Cardoso AAB. Análise das demonstrações contábeis como ferramenta de suporte à gestão financeira. Rev Bras Gest Eng. 2016;7(1):Art. 1.
14. Gomes MLR. A contabilidade como ferramenta de gestão empresarial [Internet]. 2013 Dec 18 [cited 2026 Feb 19]. Available from: https://semanaacademica.org.br/artigo/contabilidade-como-ferramenta-de-gestao-empresarial-0
15. Taschner A, Charifzadeh M. Management accounting in supply chains – what we know and what we teach. J Account Organ Change. 2020;16(3):369-399.

A Multicriteria Decision-Making (MCDA) Method for Decommissioning Offshore Oil and Gas Units in Brazilian Shallow Waters

Antonio José Mendonça Ferreira[1]*, Rodrigo Santiago Coelho[1], Andrea Mendes Costa Mendonça[1]
[1]SENAI CIMATEC University, PPG GETEC; Salvador, Bahia, Brazil

The decommissioning of offshore oil and gas facilities is a critical final stage in the lifecycle of the energy industry. As numerous infrastructures age and production fields mature, Brazil faces a significant increase in decommissioning obligations, particularly in its shallow water regions. Decision-making in this process is notoriously complex, involving a delicate balance of substantial costs, operational risks, environmental impacts, social considerations, and an evolving regulatory framework. This paper proposes a robust methodology to support decision-making in the decommissioning of offshore oil and gas production units in Brazilian shallow waters, aiming to optimize outcomes from a multifaceted perspective. A comprehensive literature review is conducted on international best practices, the Brazilian regulatory scenario, and the inherent challenges of shallow water decommissioning. Multi-Criteria Decision-Making (MCDA) models are explored, with a focus on methods like the Analytic Hierarchy Process (AHP) and compromise ranking solutions such as VIKOR, alongside specialized risk assessment tools like the Hierarchical Analyst Domino Evaluation System (HADES). The proposed methodology integrates technical, economic, environmental, safety, and social criteria into a structured framework designed for managers and regulators. This research is expected to contribute to enhancing the efficiency and sustainability of decommissioning operations in Brazil, minimizing adverse impacts and maximizing stakeholder benefits.

Keywords: Decommissioning. Offshore. Shallow Waters. MCDA. Brazil.

Abbreviations: AHP, Analytic Hierarchy Process. ANP, Agência Nacional do Petróleo, Gás Natural e Biocombustíveis. BPEO, Best Practicable Environmental Option. BSEE, Bureau of Safety and Environmental Enforcement. CA, Comparative Assessment. CIES, Composite Impact Evaluation System. DEAs, Domino Effect Accidents. ECES, Engineering Cost Evaluation System. HADES, Hierarchical Analyst Domino Evaluation System. IRPA, Individual Risk Per Annum. MADM-Q, Multi-Attribute Decision Making-Quantitative. MCDA, Multi-Criteria Decision Analysis. PDI, Programa de Descomissionamento de Instalações. PLL, Potential Loss of Life. QRA, Quantitative Risk Assessment. VIKOR, VIseKriterijumska Optimizacija I Kompromisno Resenje.

The global oil and gas industry is navigating a critical transition as a significant portion of its offshore infrastructure approaches the end of its operational life. In Brazil, this cycle has decisively moved into the decommissioning phase, driven by the aging of assets, the depletion of mature fields, and an evolving regulatory landscape [1]. Decommissioning is not mere demolition; it is a complex, multi-stage process involving the planning, execution, and management of a wide array of activities to safely remove, disable, or repurpose facilities, wells, and pipelines, ensuring both operational safety and environmental protection [2].

This challenge is particularly acute in Brazil's shallow water basins, which hosted many of the nation's pioneering installations. Here, the interactions with sensitive marine ecosystems and other maritime users, such as fishing and navigation, are more intense [3].

The selection of an optimal decommissioning strategy—be it complete removal, partial removal, or repurposing (e.g., Rigs-to-Reefs)—hinges on a multi-criteria analysis that balances technical feasibility, economic viability, environmental stewardship, safety, and social responsibility [4].

Historically, the industry's focus was predominantly on exploration and production, with decommissioning often viewed as a distant, final liability rather than an integral part of the asset lifecycle planning [5]. This paradigm is

Received on 26 October 2025; revised 28 January 2026.
Address for correspondence: Antonio José Mendonça Ferreira. Av. Orlando Gomes, 1845 - Piatã, Salvador – BA – Brazil, Zipcode: 41650-010. E-mail: antonio.mendonca@fieb.org.br.

J Bioeng. Tech. Health 2026;9(2):127-134

shifting. The immense costs, estimated in the hundreds of billions of dollars globally, and growing public and regulatory scrutiny have elevated decommissioning to a strategic priority [6]. The inherent uncertainty in this process, especially concerning subsea infrastructure and well abandonment, further complicates decision-making [7].

This paper addresses the pressing need for a structured and integrated decision-making framework tailored to the Brazilian context. The central research problem is: What decision-making methodology can be developed to optimize the decommissioning of offshore units in Brazilian shallow waters, considering the multiple technical, economic, environmental, safety, and social criteria, alongside the specificities of the national regulatory and operational environment? The absence of such a systematic approach can lead to suboptimal outcomes, including excessive costs, heightened operational risks, unmitigated environmental damage, and social conflicts. This study aims to fill this gap by proposing a robust Multi-Criteria Decision Analysis (MCDA) method. The specific objectives are:

- To analyze the current decommissioning landscape in Brazilian shallow waters, including its regulatory framework and existing practices.
- To review international best practices and MCDA models applied to offshore decommissioning.
- To identify and structure the key criteria and sub-criteria relevant to the Brazilian context.
- To propose a methodological framework incorporating MCDA techniques to evaluate decommissioning alternatives.

Theoretical Framework

The Decommissioning Process

Decommissioning is the final phase of an offshore asset's lifecycle, comprising a sequence of highly specialized engineering tasks. While often described as the reverse of installation, the process is adapted based on technology, safety, and environmental factors [8]. The process is broadly divided into pre-decommissioning, execution, and post-decommissioning stages [9].

The core execution phase typically involves [10]:

- **Well Plugging & Abandonment (P&A):** The most critical step, involving the permanent sealing of wells with cement and mechanical barriers to ensure long-term reservoir isolation and prevent hydrocarbon leakage.
- **Platform and Pipeline Preparation:** Cleaning and purging all systems of residual hydrocarbons and hazardous materials.
- **Conductor Removal:** Severing and extracting the large-diameter pipes that guide drilling equipment.
- **Topsides and Substructure Decommissioning:** Dismantling and removing the upper processing modules (topside) and the supporting structure (jacket or hull). This often requires Heavy Lift Vessels (HLVs) or specialized techniques.
- **Subsea Infrastructure Decommissioning:** Removing or abandoning in-place pipelines, manifolds, and other seabed equipment.
- **Onshore Dismantling and Waste Management:** Transporting removed materials to shore for recycling, reuse, or disposal.
- **Site Clearance:** Verifying that the seabed is clear of operational debris to ensure safety for other marine users.

Decommissioning Alternatives

The strategic choice of a decommissioning alternative is a central decision, with three primary options available, each with distinct trade-offs.

- Complete Removal: This involves removing all man-made structures from the seabed, aiming to restore the site to its original condition. It is the default and often preferred option under international guidelines like the IMO Resolution A.672(16) [11] and regional conventions like OSPAR Decision 98/3 [12], especially in shallower waters. While it offers the highest degree of environmental restoration

and eliminates future liability, it is typically the most expensive and technically challenging option, carrying significant operational risks during heavy lifting and transportation [10].

- **Partial Removal:** In this approach, the topside facilities are removed, but a portion of the substructure (e.g., the jacket below a certain water depth) is left in place. This option can significantly reduce costs and risks compared to complete removal. The remaining structure must not pose a hazard to navigation, typically requiring a clearance of at least 85 feet in U.S. waters [10]. The rationale is often that the submerged structure has already become an established artificial habitat, and its removal would cause more environmental disruption than leaving it.
- **Rigs-to-Reefs (R2R):** This is a specific form of repurposing where the entire platform or its substructure is intentionally left in place or relocated to a designated area to serve as a permanent artificial reef. This practice is widespread in the U.S. Gulf of Mexico, where it has been shown to support significant fish biomass and recreational activities [13]. R2R is often the lowest-cost option for operators and can offer ecological benefits. However, it faces criticism regarding long-term liability, the potential for residual contamination from drilling muds and heavy metals, and the risk of facilitating the spread of invasive species [5].

Regulatory Landscape: Brazil and International Benchmarks

The regulatory framework is a primary driver shaping decommissioning decisions.

- **Brazil:** The Brazilian framework is managed by a triad of agencies. The ANP establishes the core procedures through Resolutions 817/2020 (decommissioning programs) and 854/2021 (financial guarantees) [14]. The IBAMA oversees the environmental licensing process, evaluating impacts on marine biodiversity. The Brazilian navy ensures the safety of navigation through its NORMAM series of regulations [15]. While Brazil's regulations are maturing and aligning with international standards, challenges remain regarding institutional coordination and specific guidelines for complex scenarios like R2R [16]. A significant barrier is the lack of integration of decommissioning activities into the REPETRO tax regime, which imposes heavy import taxes on foreign vessels and services, increasing costs compared to other jurisdictions [17].
- **International Context:** The United Kingdom (North Sea) operates under the strict OSPAR Convention, which mandates complete removal as the default, with limited exceptions for very large structures. Their approach is guided by the principle of Best Practicable Environmental Option (BPEO), determined through a rigorous Comparative Assessment (CA) process. The United States (Gulf of Mexico) has a more flexible framework managed by the BSEE, with a well-established R2R program. However, concerns about regulatory oversight and long-term liability persist [18]. Norway also follows the OSPAR principles, requiring robust financial assurances and detailed decommissioning plans with public consultation [19].

Multi-Criteria Decision Analysis (MCDA) in Decommissioning

Given the complexity and conflicting objectives inherent in decommissioning, MCDA provides a structured and transparent framework for decision support [20]. MCDA models are essential for systematically evaluating alternatives against a comprehensive set of criteria.

Several MCDA methods are relevant to decommissioning. The Analytic Hierarchy Process (AHP) is a powerful technique for structuring the problem and deriving the relative importance (weights) of criteria through pairwise comparisons, effectively capturing expert and stakeholder judgments [21]. Ranking methods like TOPSIS (Technique for Order of Preference by Similarity to Ideal Solution) and VIKOR (a

compromise ranking method) are used to evaluate and order alternatives based on their performance against the weighted criteria [22,23].

More specialized systems have also been developed. The Hierarchical Analyst Domino Evaluation System (HADES) is a quantitative risk assessment (QRA) tool that integrates AHP to model Domino Effect Accidents (DEAs)—cascading failures that traditional static QRAs may underestimate [9]. The Multi-Attribute Decision Making-Quantitative (MADM-Q) system offers an integrated framework combining a bottom-up Engineering Cost Evaluation System (ECES), the HADES risk module, and a Composite Impact Evaluation System (CIES) to provide a holistic quantitative assessment [9]. These tools demonstrate a move towards more data-driven and dynamic decision support systems.

Proposed Method

The proposed methodology is a hybrid MCDA framework designed to be systematic, transparent, and adaptable to the Brazilian shallow water context. It integrates established MCDA techniques with specialized assessment modules for costs and risks.

Methodological Framework

The process follows six main stages:

1. **Problem Structuring:** This initial stage involves defining the specific decommissioning project, identifying key stakeholders (operators, regulators, fishing communities, environmental NGOs), and establishing the set of feasible alternatives (e.g., Complete Removal, Partial Removal, R2R).
2. **Criteria Hierarchy Development:** A comprehensive set of criteria and sub-criteria is structured hierarchically, covering the four primary dimensions: Economic, Environmental, Safety, and Social. This structure, detailed in Table 1, forms the basis for the evaluation.
3. **Criteria Weighting:** The Analytic Hierarchy Process (AHP) is employed to determine the relative weights of each criterion and sub-criterion. This involves structured consultations with a panel of experts and stakeholders who perform pairwise comparisons to reflect their priorities.
4. **Performance Assessment:** Each alternative is scored against each sub-criterion. This is a mixed-methods step:
   - Economic Criteria: Costs are estimated using a bottom-up approach, similar to the ECES model, detailing expenses for each operational phase. Probabilistic modeling is used to address cost uncertainty.
   - Safety Criteria: Risks are quantified using a dynamic QRA approach based on the HADES framework, calculating the Individual Risk Per Annum (IRPA) and Potential Loss of Life (PLL), with a focus on DEAs.
   - Environmental and Social Criteria: These are assessed using a combination of quantitative data (e.g., CO_2 emissions, area of seabed disturbance) and qualitative scores derived from expert judgment and stakeholder input, using a standardized scale (e.g., 1-5).
5. **Aggregation and Ranking:** The VIKOR method is proposed for aggregating the weighted scores. VIKOR is chosen for its ability to provide a compromise solution that is closest to the ideal, which is suitable for decisions where conflicting objectives must be balanced to achieve group utility and minimize individual regret.
6. **Sensitivity Analysis:** The robustness of the final ranking is tested by systematically varying the criteria weights to determine which factors have the most significant influence on the outcome. This step is crucial for understanding the stability of the decision under different priority scenarios.

Criteria and Sub-criteria for Brazilian Shallow Water

Based on a review of international guidelines and the specific challenges in Brazil, using as a reference the set of tools of MCDM to create a

multivariable matrix to cross criterion and sub-criterion that optimizes whole process, to describe the analyses possible under the methodology and it is show on the criteria hierarchy (Table 1).

Case Study Application: Guaricema Field

To try the methodology, a case study was developed based on the decommissioning of the Guaricema field, located in the shallow waters of the Sergipe-Alagoas Basin. This study was conducted based on the documents produced during the PDI – Programa de descomissionamento de instalações, based on the executive report from PETROBRAS, the company that owns the assets. This field, with seven fixed platforms operating since the 1970s, presents a typical scenario for Brazil's aging shallow-water assets.

Scenario and Alternatives

- **Asset:** A representative fixed steel jacket platform in the Guaricema field.
- **Context:** Water depth of ~40 meters, significant marine growth including the invasive coral-sol, proximity to fishing communities, and multiple wells and pipelines.

Alternatives Evaluated

- **A1 (Complete Removal):** Full removal of topside, jacket, and subsea infrastructure for onshore recycling/disposal.
- **A2 (Partial Removal):** Removal of topside, with the jacket cut at a safe depth below the waterline and left in place.
- **A3 [Rigs-to-Reefs (R2R)]:** Conversion of the jacket into a designated artificial reef, following cleaning and preparation.

Application of the Method

Weighting (AHP)

A hypothetical weighting scenario was established reflecting a balanced-responsible approach, giving high importance to Safety and Environmental criteria, followed by Economic and Social criteria. Weights: Safety (30%), Environmental (30%), Economic (20%), Social (20%).

Performance Matrix

Each alternative was scored against the sub-criteria based on data from the literature review and technical reports (Table 2). For instance, A1 received a high score for "Seabed Quality" but a low score for "Direct Costs." A3 scored high on "Habitat Creation" and "Direct Costs" but low on "Residual Contamination Risk."

Results of the Case Study

The aggregated results produced the following ranking:

- Alternative A2: Partial Removal
- Alternative A3: Rigs-to-Reefs
- Alternative A1: Complete Removal

The Partial Removal option emerged as the preferred compromise solution. It offered a significant cost reduction compared to complete removal while mitigating the highest operational risks associated with complex subsea cutting and lifting. Environmentally, it preserved the established artificial habitat of the jacket while removing the primary source of potential pollution (the topside). Socially, it had a mixed impact, reducing conflicts with trawling fisheries (compared to R2R) but still leaving a subsea structure.

The R2R alternative was a close second, highly favored for its low cost and social benefits (recreational fishing, diving). However, it was penalized due to the higher long-term environmental uncertainty associated with residual contamination and the management of the invasive coral-sol.

Complete Removal, despite being the "cleanest" option from a site restoration perspective, was ranked last due to its prohibitive costs and the

Table 1. Proposed hierarchy criterion.

Criterion	Sub-Criterion	Description	Evaluation Type
Economic	Direct costs	Costs for P&A, plattform / pipeline removal, waste management, mobilization / demobilization	Quantitative (M BRL)
	Indirect costs	Long-term monitoring, tax implications	Quantitative (M BRL)
	Economic benefits	Scrap/reuse value, direct job creation	Quantitative (M BRL)
Environmental	Marine biodiversity impact	Habitat loss/creation, invasive species (e.g., coral-sol), impact on proteted species	Qualitative (score 1-5)
	Water & Seabed Quality	Turbidity, noise pollution, risk of residual contamination, seabed disturbance	Semi-Quantitative
	Waste management	Rate of reuse/recycling, final disposal footprint, management of hazardous materials	Quantitative ($)
	Carbon footprint	Energy consumption and GHG emissions from vessels and onshore operations	Quantitative (tCO2e)
Safety	Operational risks	IRPA/PLL from operations (lifting, cutting), structural integrity failures, hydrocarbon releases	Quantitative (HADES)
	Worker Health & Safety	Occupational health risk, accidents	Qualitative (score 1-5)
	Vavigation safety	Interference with shipping routes, risk of collision with residual structures	Qualitative (score 1-5)
Social	Local Employment impact	Loss of operational jobs versus creation of decommissioning jobs	Semi-Quantitative
	Economic diversification	Opportunities for new industries (e.g., renewables, recycling)	Qualitative (score 1-5)
	Conflit with sea users	Impact on artisanal/commercial fishing, tourism, and recreation	Qualitative (score 1-5)
	Public perception	Industry reputation, stakeholder acceptance	Qualitative (score 1-5)

highest operational safety risks, which were heavily weighted in this scenario.

Discussion

The case study demonstrates the methodology's ability to navigate complex trade-offs. The result highlights that the "best" option is not always the most obvious one. While complete removal aligns with a precautionary principle, its high cost and risk can make it impractical. The R2R option, while economically attractive, carries long-term

Table 2. Performance matrix by Ranking (VIKOR).

Sub-Criterion	A1 (Complete Removal)	A2 (Partial Removal)	A3 (Rigs-to-Reefs)
Direct Costs	1	3	5
Habitat Impact	1 (Loss)	4 (Preservation)	5 (Creation)
Residual Contamination	5	3	2
Operational Risks (IRPA)	2	4	5
Local Employment	3	3	4
Fishing Conflicts	5	2	3

ecological and liability questions that must be carefully weighed. The compromise solution of partial removal strikes a balance, though it is not without its own challenges, such as ensuring long-term structural integrity and navigational safety.

The sensitivity analysis revealed that the ranking was most sensitive to the weight assigned to the Environmental criterion. If the risk of residual contamination and invasive species (coral-sol) were weighted even more heavily, the R2R option would become less favorable. Conversely, if Economic criteria were prioritized above all else, R2R would likely become the top-ranked choice. This underscores the critical importance of the weighting phase as a reflection of societal and regulatory priorities.

The method provides a structured rationale for Brazilian regulators and operators to justify their decisions, moving beyond a purely cost-based or a rigid "remove-all" approach towards a case-by-case evaluation that seeks the best practicable outcome.

Conclusion

This paper has proposed a comprehensive MCDA methodology for optimizing the decommissioning of offshore oil and gas facilities in Brazilian shallow waters. The framework successfully integrates economic, environmental, safety, and social criteria, providing a transparent and robust tool for navigating the complex trade-offs inherent in this final lifecycle stage. The case study of the Guaricema field demonstrated the methodology's practical utility, identifying "Partial Removal" as a viable compromise solution that balances cost, risk, and environmental preservation.

The primary contributions of this work are both theoretical and practical. Theoretically, it advances the application of hybrid MCDA models in the emerging field of decommissioning in developing markets. Practically, it provides Brazilian stakeholders with a structured process to make informed, defensible, and sustainable decisions. The research also highlights critical systemic challenges facing Brazil, including the need for enhanced regulatory coordination, the development of onshore recycling infrastructure, and the reform of the tax regime (REPETRO) to create a more favorable environment for decommissioning activities.

The study is limited by its reliance on a simulated case study and illustrative weightings. The availability of detailed, real-world historical data for decommissioning projects in Brazil remains a significant constraint.

Future research should focus on applying this methodology to real, ongoing decommissioning projects in Brazil, incorporating direct input from a diverse panel of stakeholders to refine the criteria weights. Further development of a software-based decision support tool based on this framework would greatly enhance its accessibility and practical application. Finally, in-depth economic feasibility studies on creating a circular economy around decommissioning— including the potential

for domestic recycling yards and the integration with burgeoning industries like offshore wind—would provide invaluable insights for Brazil's transition to a sustainable "Blue Economy."

Acknowledgement

We would like to thank to Professor Rodrigo Santiago Coelho, for his constant and balanced intellectual support, guiding me on the path to overcoming the challenge of the master's degree, We are immensely grateful to the engineer Andrea Mendes Costa Mendonça for her support in the search for technical data, for the emotional and mental support to achieve goals and surpass them when the dare was made.

References

1. ANP. Descomissionamento de instalações. Agência Nacional do Petróleo, Gás Natural e Biocombustíveis; 2023.
2. Hirsh H, Coen MH, Mozer MC, Hasha R, Flanagan JL. Room service, AI-style. IEEE Intelligent Systems. 2002 Jul;14(2):8–19.
3. Li Y, Hu Z. A comparative study of two cost assessment approaches to models for offshore oil and gas platform decommissioning. Applied Energy. 2023;339:120935.
4. Fowler AM, Macreadie PI, Jones DOB, Booth DJ. A multi-criteria decision approach to decommissioning of offshore oil and gas infrastructure. Ocean & Coastal Management. 2014;87:20–29.
5. Camilo A. Rigs-to-reefs: retired oil rigs are becoming artificial reefs, but critics question the tradeoff. Impakter. 2025.
6. OGUK. Decommissioning insight 2018. Oil & Gas UK; 2018.
7. Pereira L. Mature fields decommissioning Brazil. Journal of Energy Law and Resources Symposium. 2019;7(1):1–24.
8. Fam ML, Konovessis D, Ong LS, Tan HK. A review of offshore decommissioning regulations in five countries' strengths and weaknesses. Ocean Engineering. 2018;160:244–263.
9. Li Y, Hu Z. Application of hierarchical analyst domino evaluation system (HADES) in offshore oil and gas facilities' decommissioning: a case study. Ocean Engineering. 2023;272:113741.
10. ICF International. Decommissioning methodology and cost evaluation. 2015. Available from: https://www.bsee.gov/sites/bsee.gov/files/tap-technical-assessment-program/738aa.pdf
11. IMO. Resolution A.672(16): guidelines and standards for the removal of offshore installations and structures on the continental shelf and in the exclusive economic zone. International Maritime Organization; 1989.
12. OSPAR Commission. OSPAR decision 98/3 on the disposal of disused offshore installations. 1998.
13. Pulsipher AG, Daniel WB IV. Onshore disposition of offshore oil and gas platforms: western politics and international standards. Ocean & Coastal Management. 2000;43(12):973–995.
14. ANP. Resolução ANP nº 817, de 2020.
15. ANP. Resolução ANP nº 854, de 2021.
16. Deus ELMC, et al. Offshore decommissioning regulations in Brazil. ResearchGate.
17. ITR World Tax. Decommissioning offshore and onshore installations in Brazilian waters.
18. Ocean Conservancy. Decommissioning: final report. 2024.
19. Norsk Petroleum. Cessation and decommissioning.
20. Greco S, et al. Multiple criteria decision analysis (MCDA). European Journal of Operational Research. 2016;252(1):1–13.
21. Saaty TL. The analytic hierarchy process. European Journal of Operational Research. 1990.
22. Hwang CL, Yoon K. Methods for multiple attribute decision making. In: multiple attribute decision making. Springer; 1981.
23. Al-Barakati AO, et al. A BWM–CRITIC–VIKOR multi-criteria decision evaluation model within a probabilistic linguistic term set framework for oil and gas risk scenarios. Heliyon. 2024;10(10):e11471461.

Physicochemical Characterization of a Clay from Sergipe State and its Potential as an Adsorbent

Aline Santana Prado[1]*, Cleide Mara Faria Soares[1,4], Cochiran Pereira dos Santos[2], Eliane Bezerra Cavalcanti[3,4], Adriana de Jesus Santos[1,4]

[1]Tiradentes University, Food Research Laboratory; [2]Federal University of Sergipe, Physics Department, São Cristóvão; [3]Tiradentes University, Waste and Wastewater Treatment Laboratory; [4]Institute of Technology and Research, Aracaju, Sergipe, Brazil

Water treatment is fundamental to removing industrial dyes, such as methylene blue, and to mitigate their severe environmental impacts. In this context, adsorption stands out as a promising solution due to its efficiency and low cost. The use of clays, especially regional ones, is particularly strategic as it utilizes a local and abundant resource to develop a sustainable, accessible treatment technology that adds value to the region's economy. Thus, this work aims to characterize a regional clay with possible application in the adsorption process. Through the analysis performed, the presence of quartz, calcite, hematite, and feldspar was verified via XRD, in addition to clay minerals such as kaolinite and montmorillonite, which are also part of its composition. The clay minerals are the main components in the adsorption process. From FTIR, it was possible to observe the presence of the 3695 cm^{-1} band, characteristic of kaolinite clays, in addition to confirming the presence of characteristic bands related to the lamellar structure of clays containing tetrahedral and octahedral layers, such as the bands at 984, 914, 796, and 691 cm^{-1}. Through TGA and DTG, the decomposition of kaolinite was noted at temperatures of 480 °C and 680 °C, along with a total mass loss of 1%. With SEM, a low agglomeration of particles was observed due to the low concentration of montmorillonite in its composition; thus, less agglomerated structures tend to have a larger surface area and more free active sites for the adsorption process. And, through BET, it was found that this clay is microporous (Dp = 1.56 nm and Vp= 0.047 cm^3/g) and has a high surface area (S_BET = 36.75 m^2/g), and high inter-pore area, in addition to exhibiting a type IV isotherm with H3 hysteresis, typical of materials with a lamellar structure. Furthermore, preliminary adsorption tests validated this potential, achieving a maximum removal of 89.39% of the dye using a 0.3 g mass.

Keywords: Regional Clay. Characterization. Adsorption. Blue Methylene.

Abbreviations: XRD, X-ray Diffraction. FTIR, Fourier-Transform Infrared Spectroscopy. TGA, Thermogravimetric Analysis. MEV, Scanning Electron Microscopy. BET, Brunauer, Emmett and Teller Method.

Water is an essential element for life, but only 0.01% of the Earth's water is accessible for human needs. This scarcity is worsened by pollution resulting from excessive and uncontrolled human activities in sectors such as transportation, industry, agriculture, and urban development. Industrialization, in particular, has caused environmental degradation, with many factories lacking proper wastewater treatment facilities. Among these pollutants, dyes are some of the most common industrial contaminants.

These highly toxic organic molecules are used in the textile, food processing, paper, and leather industries, with approximately 8,105 tons of synthetic dyes produced each year [1].

Therefore, treating water contaminated with organic dyes like methylene blue is necessary. Among various treatment methods, adsorption has gained popularity for removing organic pollutants because of its simplicity, speed, environmental friendliness, and low-cost adsorbents. It is important to note that the efficiency of this process depends on several factors, including the affinity of the adsorbent surface for the pollutant, pH, temperature, adsorbate concentration, and the specific surface area of the adsorbent [2].

In adsorption, a variety of materials are used to remove pollutants from water, especially dyes. Some of these include layered double hydroxides and minerals found in clays, which are considered promising adsorbents due to their high adsorption

Received on 26 October 2025; revised 17 January 2026.
Address for correspondence: Aline Santana Prado.Avenida Murilo Dantas, N. 300, Farolândia. Aracaju, Sergipe, Brazil. Zipcode: 49032-490. E-mail: aline.prado@souunit.com.br.

J Bioeng. Tech. Health 2026;9(2):135-141

capacity, thermal stability, and surface chemical properties [3]. Clays, such as kaolinite, are naturally abundant, low-cost materials that have controlled porosity and are non-toxic [4].

Kaolinite consists of a tetrahedral silicon layer (SiO_2) and an octahedral aluminum hydroxide layer ($Al_2(OH)_6$). These layers are linked by hydrogen bonds between oxygen atoms and hydroxyl groups, preventing expansion or contraction upon contact with water [5,6]. The isomorphic substitution of Si^{4+} by Al^{3+} in the silica layer of kaolinite creates a negative charge, which serves as an active site for adsorption [4].

Research shows that kaolinite effectively removes dyes like methylene blue (MB), with notable adsorption capacities. This is due to hydrogen interactions between the oxygen in kaolinite and the nitrogen atoms of the MB dye. Therefore, the accessibility of active sites on the clay surface is essential for efficient removal of organic pollutants [4].

Regional development relies on the demand for local products [7], through strategies that highlight a region's resources. For example, Geographical Indication (GI) links product quality to its origin, supporting the local economy [8], and this same idea applies to using regional clays to develop sustainable and affordable technologies.

In this context, finding low-cost materials for water treatment, such as clays, becomes vital, especially for dye removal through adsorption. However, understanding a material's characteristics is necessary before applying it to ensure performance. The main goal of this work is to characterize a regional clay from a municipality in Sergipe to gather the essential information for evaluating, in future studies, the true potential of this clay as an adsorbent for methylene blue dye.

Materials and Methods

Material

The material used in this study was a sample of regional clay from a municipality in the state of Sergipe.

Methods

The regional clay sample was analyzed using X-ray Diffraction (XRD) at the Department of Physics at the Federal University of Sergipe to identify its crystalline phases. The scan range was from 1° to 60°, conducted at a speed of 2°/min.Fourier-Transform Infrared Spectroscopy (FTIR) was employed to identify functional groups within the spectral range of 650 cm^{-1} to 4000 cm^{-1}, using equipment located at the Laboratory of Food Research at the Institute of Technology and Research, Tiradentes University. Thermogravimetric Analysis (TGA) and its derivative (DTG) were performed to assess mass loss as a function of temperature; these tests were carried out under a N2 atmosphere with a flow rate of 50 mL/min, at a heating rate of 10°C/min, over a temperature range of 25 to 900°C. Scanning Electron Microscopy (SEM) was used to examine the morphology at an acceleration voltage of 10 kV and a magnification of 130x.

The TGA and SEM instruments are housed at the Center for Colloidal Systems Studies. N2 adsorption-desorption isotherms (BET method) determined the textural properties, with nitrogen at 77 K (- 196°C). Prior to analysis, samples were pre-treated at 200 °C under vacuum for 2 hours to remove moisture or organic residues. This equipment belongs to the Laboratory of Materials Synthesis and Chromatography at Tiradentes University. Preliminary batch adsorption tests were performed by varying the clay mass (0.1, 0.2, and 0.3 g) in 50 mL of methylene blue solution (initial concentration 5 mg/L) at 25 °C and 175 rpm. The contact time was fixed at 60 minutes, a time longer than the equilibrium time preliminarily determined to be (~20 min), thus ensuring the process reached completion. After filtration, the equilibrium concentrations (Ce) in the filtrate were determined by UV-Vis spectrophotometry (at $\lambda max \approx 664$ nm). The removal efficiency (%R) and the adsorption capacity (qe, mg/g) were also determined.

Results and Discussion

X-ray Diffraction (XRD)

The crystalline phases present in the regional clay were identified according to the Inorganic Crystal Structure Database (ICSD) and are presented in Graphic 1. The analysis revealed the presence of quartz, calcite, feldspar, and hematite, as well as the clay minerals montmorillonite and kaolinite.

Graphic 1. XRD diffractograms for regional clay.

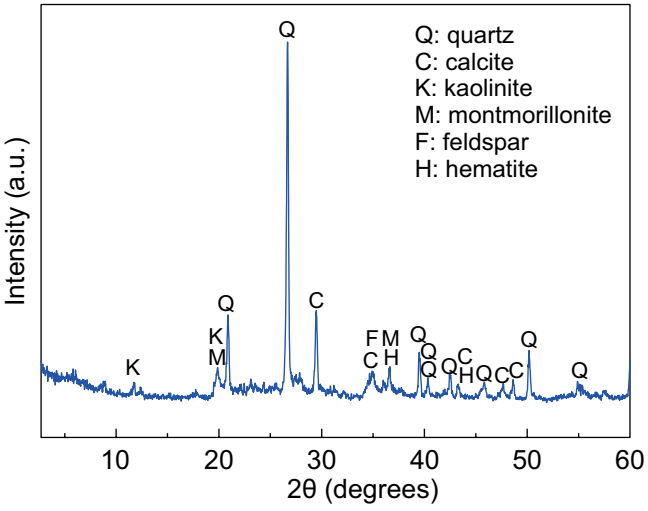

The roles of the identified minerals in adsorption vary: quartz is considered inert due to its stable crystalline structure, while feldspar can release competing alkaline and alkaline-earth cations. In contrast, hematite and calcite provide active sites that enhance adsorption [9,10]. The clay minerals, kaolinite and montmorillonite, are particularly important to the process due to their good ion exchange capacity [10].

Fourier-Transform Infrared Spectroscopy (FTIR)

The FTIR spectrum of the regional clay is shown in Graphic 2.

A band is observed at 3695 cm^{-1}, which is attributed to the stretching vibration of O-H groups present in the composition of kaolinitic clays. The bands at 3622 and 3395 cm^{-1} are related to the

Graphic 2. FTIR spectrum of regional clay.

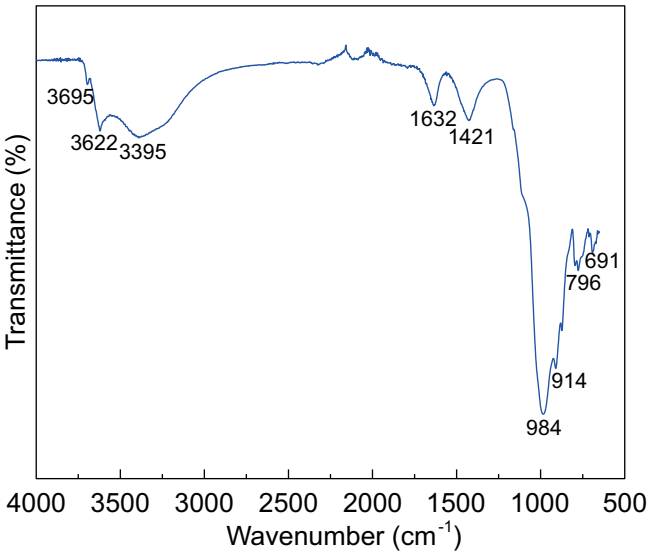

symmetric and asymmetric stretching of hydroxyl functional groups from water present in the clay lamellae [11].

The band at 1632 cm^{-1} is attributed to the typical O-H bending of constitutional water molecules adsorbed on the phyllosilicate surface. The band at 984 cm^{-1} refers to the asymmetric stretching of the internal O-Si-O and O-Al-O tetrahedra. The band at 914 cm^{-1} is attributed to the O-H bending of the carboxylic acid group, and together with the band at 796 cm^{-1}, it refers to the Al-Mg-OH stretching, confirming the presence of quartz. The band at 691 cm^{-1} is related to Si-O stretching [12,13].

In addition to the cited bands, the presence of a band at 1421 cm^{-1} is noted, which is related to the presence of carbonate. It is worth noting that the hydroxyl groups and the negative surface charge of the silicate structures are fundamental for attracting and binding cationic contaminants, thereby enhancing the adsorption process [14].

Thermogravimetric Analysis (TGA)

The curves presented in Graphic 3 are associated with the thermogravimetric analysis (TGA) and its derivative (DTG).

The DTG analysis reveals three main stages of mass loss. The first stage, up to 150 °C, shows

Graphic 3. TGA and DTG curves of regional clay.

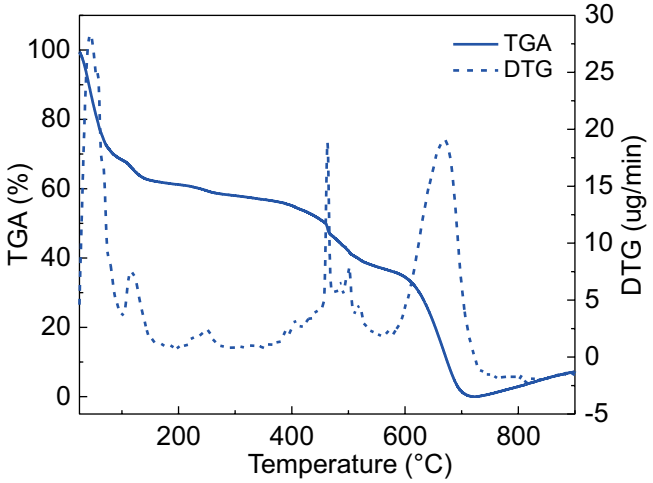

~38% loss attributed to physically absorbed water [15]. The second stage, occurring between 150 °C and 500 °C, corresponds to ~20% mass loss from interlayer water, and includes a distinct endothermic event at 480 °C due to the dehydroxylation of kaolinite into metakaolinite.

A third mass loss of ~41% is observed between
500 °C and 700 °C, which is related to the thermal decomposition of $CaCO_3$ into CaO and CO_2 [16]. Therefore, these results suggest that the sample contains a considerable amount of kaolinite.

Scanning Electron Microscopy (MEV)

Figure 1 shows the particle arrangement of the analyzed regional clay.

Analyzing Figure 1, a low agglomeration of particles can be observed, which correlates with its low concentration of montmorillonite, thus being a characteristic composition of kaolinite-rich clays. This contrasts with montmorillonite clays, where higher particle agglomeration is often associated with high adsorption capacity due to a lamellar structure with swelling properties [17].

The tendency of particles, such as those in montmorillonite, to form stacked agglomerates limits access to their internal surfaces, thereby

Figure 1. SEM micrograph.

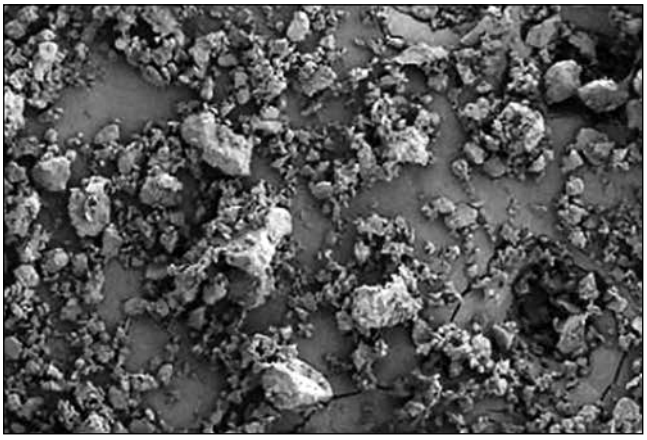

reducing the available surface area — a critical factor for an efficient adsorption process [18].

Brunauer, Emmett and Teller Method (BET)

Graphic 4 shows the adsorption and desorption isotherms for the regional clay. The isotherm is classified as type IV with H3 hysteresis, according to the 1985 IUPAC classification.

This isotherm classification is characteristic of materials with a hysteresis loop, which arises from

Graphic 4. PGraphic 4. N_2 adsorption-desorption isotherm of the regional clay.

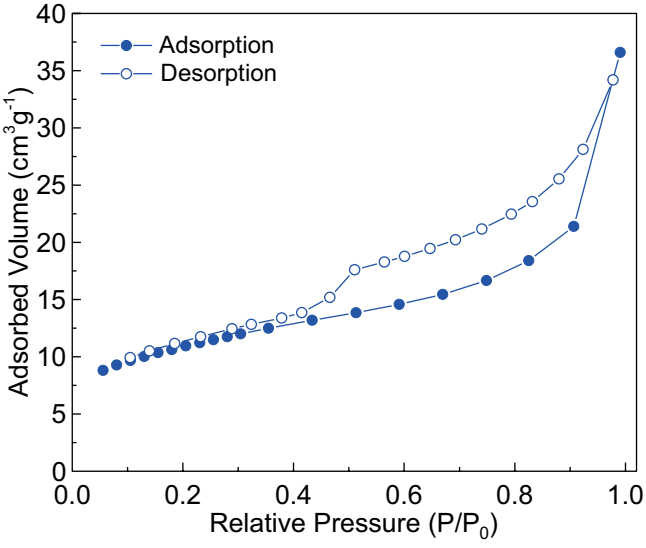

differences between the adsorption and desorption mechanisms. In other words, N_2 molecules remain bound to the adsorbent during desorption. This H3-type hysteresis is also representative of materials with slit-shaped pores (parallel plates), a structure commonly found in clays due to their layered nature [19].

Based on the textural properties, the clay is considered microporous (< 2 nm), with a pore diameter (DP) of 1.59 nm and a pore volume (VP) of 0.047 cm^3/g. In microporous materials, the large internal surface area, combined with overlapping potential energy fields, intensifies the interaction forces between the adsorbent and the adsorbate. This effect, resulting from the small pore size, promotes a superior adsorption capacity, which is particularly effective at low concentrations compared to materials with larger pores [20].

Furthermore, the specific surface area (SBET) was determined to be 36.746 m^2/g. This high surface area suggests that the material has a considerable number of active sites available for the adsorption process [21]. This result is also significantly higher than a value reported in the literature (9.51 m^2/g) [20], which is nearly four times lower than the value obtained in this work.

Preliminary Adsorption Tests

To evaluate the effect of the adsorbent mass, preliminary tests were conducted using 0.1, 0.2, and 0.3 g of clay, all at a fixed contact time of 60 minutes. This duration was adopted to ensure complete equilibrium, as preliminary tests confirmed that the slowest condition (0.1 g) reached its plateau at 45 minutes. Graphic 5 presents the resulting equilibrium adsorption capacity (qe) as a function of the adsorbent mass.

The mass assay results demonstrated the classic opposing trends. The total removal efficiency (%R) rose from 81.41% at 0.1 g to 87.11% at 0.2 g and reached a maximum of 89.39% at 0.3 g, which is attributed to the greater availability of active sites. Conversely, the adsorption capacity decreased from 2.035 mg/g at 0.1 g to 1.089 mg/g at 0.2 g and a minimum of 0.745 mg/g at 0.3 g, indicating lower active site saturation at higher masses.

Graphic 5. Effect of contact time and adsorbent mass on the adsorption of methylene blue.

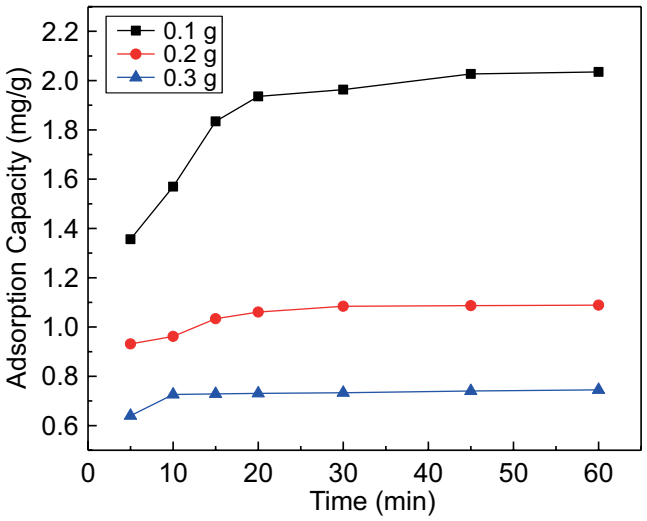

This promising performance in natura (89.39% removal and qe up to 2.035 mg/g) is notably superior to the theoretical maximum adsorption capacity of 0.907 mg/g reported by Shikuku and colleagues 2021 [23] for a natural kaolinite. This difference can be attributed to the Sergipe clay's significantly higher specific surface area (36.75 m^2/g vs. 14.616 m^2/g) and its mixed mineralogy. Furthermore, this cost-effective in natura approach is validated by Del Sordo Filho and colleagues 2021 [24] who concluded that activation did not significantly improve adsorption for Brazilian kaolinite, making the raw material the preferable cost-benefit application.

Conclusion

This work successfully characterized a regional clay from the state of Sergipe, evaluating its potential for application as an adsorbent. XRD and FTIR analyses confirmed a composition rich in clay minerals such as kaolinite and montmorillonite, in addition to accessory minerals.

The presence of hydroxyl groups, fundamental for adsorption, was evidenced. The morphology observed by SEM, with low particle agglomeration,

suggests good accessibility to active sites, which was corroborated by the textural properties obtained from BET analysis. This analysis revealed a considerable specific surface area (36.75 m^2/g) and a microporous structure with a type IV isotherm, typical of lamellar materials, indicating a high adsorptive potential.

This potential was validated by the preliminary adsorption tests, which demonstrated fast kinetics, equilibrium reached at 45 minutes for the limiting condition, and a high removal efficacy, achieving 89.39% of the dye using a 0.3 g mass. Therefore, it is concluded that the studied regional clay possesses promising characteristics for use as an alternative, low-cost adsorbent. For future work, isotherm studies, varying the initial dye concentration, are recommended to determine the material's maximum adsorption capacity, as well as expanding its application to the removal of other priority contaminants, such as heavy metal ions.

Acknowledgement

We thank to Tiradentes University (UNIT) and the Institute of Technology and Research (ITP) for the opportunity and infrastructure that made this work possible. My gratitude is also extended to their laboratories— the Laboratory of Food Research (LPA), the Center for Colloidal Systems Studies (NUESC), and the Laboratory of Materials Synthesis and Chromatography (LSINCROM)— as well as to the Department of Physics at the Federal University of Sergipe (UFS) for carrying out the characterizations. This study was financed in part by Coordenação de Aperfeiçoamento de Pessoal de Nível Superior [CAPES]—Finance Code 001 and Conselho Nacional de Desenvolvimento Científico e Tecnológico [CNPq].

References

1. Khan S, Ajmal S, Hussain T, Rahman MU. Clay-based materials for enhanced water treatment: adsorption mechanisms, challenges, and future directions. J Umm Al-Qura Univ Appl Sci. 2023:1-16.
2. Messaoudi M, Douma M, Tijani N, Dehmani Y, Messaoudi L. Adsorption process of malachite green onto clay: kinetic and thermodynamic studies. Desalin Water Treat. 2021;240:191-202.
3. George G, Ealias AM, Saravanakumar MP. Advancements in textile dye removal: a critical review of layered double hydroxides and clay minerals as efficient adsorbents. Environ Sci Pollut Res. 2024;31(9):12748-12779.
4. Joshi P, Raturi A, Srivastava M, Khatri OP. Graphene oxide, kaolinite clay and PVA-derived nanocomposite aerogel as a regenerative adsorbent for wastewater treatment applications. J Environ Chem Eng. 2022;10(6):108597.
5. Mochiutti E, Sehwarts RLD C, Lima JPO, Carvalho ALS, Neves RDF, Brasil DDSB, et al. Implementação do campo de força CLAYFF no GROMACS: uma aplicação em estrutura de caulinita. Quim Nova. 2020;43(6):804-812.
6. Hnamte M, Pulikkal AK. Clay-polymer nanocomposites for water and wastewater treatment: a comprehensive review. Chemosphere. 2022;307:135869.
7. Oliveira NM. Revisitando algumas teorias do desenvolvimento regional. Informe Gepec. 2021;25(1):203-219.
8. Silva KF, Lima AF, Silva MS. Potentiality of geographical indication of licuri from the Bahia semiarid under the view of the origin-linked quality virtuous circle. Rev Bras Gest Desenvolv Reg. 2022;18(1).
9. Ramos SDO, Dantas GCB, Lira HDL, Pimentel PM, Marciano JEA. Caracterização de argilas de novos jazimentos situados em Parelhas/RN, Brasil, visando aplicação na indústria cerâmica. Matéria (Rio J). 2019;24(2):e12352.
10. Song S, Peng W, Li H. Surface chemistry of mineral adsorbents. In: Adsorption at natural minerals/water interfaces. Cham: Springer; 2020. p. 55-91.
11. Hassaan MA, El Nemr A. Classification and identification of different minerals in Mediterranean sediments using PSA, FTIR, and XRD techniques. Mar Pollut Bull. 2021;173:113070.
12. Marouf R, Dali N, Boudouara N, Ouadjenia F, Zahaf F. Study of adsorption properties of bentonite clay. In: Montmorillonite clay. London: IntechOpen; 2021.
13. Olegario EM, Gili MBZ, Celikin M. Characterization of Philippine natural bentonite. Exp Results. 2021;2:e25.
14. Sellak S, Bensalah J, Ouaddari H, Safi Z, Berisha A, Draoui K, et al. Adsorption of methylene blue dye and analysis of two clays: a study of kinetics, thermodynamics, and modeling with DFT, MD, and MC simulations. ACS Omega. 2024;9(13):15175-15190.
15. Viana AC, Ramos IG, Mascarenhas AJS, Dos Santos EL, Sant'Ana AEG, Goulart HF, et al. Release of

aggregation pheromone rhynchophorol from clay minerals montmorillonite and kaolinite. J Therm Anal Calorim. 2022;147(8):4995-5007.
16. Dos Santos CP, De Jesus Santos A. Estudo do comportamento térmico de materiais argilosos a diferentes taxas de aquecimento. In: Termodinâmica: prática e sem mistérios. Editora Científica Digital; 2021. p. 128-143.
17. Wilkinson N, Metaxas A, Quinney C, Wickramaratne S, Reineke TM, Dutcher CS. pH dependence of bentonite aggregate size and morphology on polymer-clay flocculation. Colloids Surf A Physicochem Eng Asp. 2018;537:281-286.
18. Kaufhold S, Dohrmann R, Klinkenberg M, Siegesmund S, Ufer K. N2-BET specific surface area of bentonites. J Colloid Interface Sci. 2010;349(1):275-282.
19. Thommes M, Kaneko K, Neimark AV, Olivier JP, Rodriguez-Reinoso F, Rouquerol J, et al. Physisorption of gases, with special reference to the evaluation of surface area and pore size distribution (IUPAC Technical Report). Pure Appl Chem. 2015;87(9-10):1051-1069.
20. Alkhaldi H, Alharthi S, Alharthi S, Alghamdi HA, Alzahrani YM, Mahmoud SA, et al. Sustainable polymeric adsorbents for adsorption-based water remediation and pathogen deactivation: a review. RSC Adv. 2024;14(45):33143-33190.
21. Nyairo W, Njewa JB, Shikuku VO. Adsorption of heavy metals onto food wastes: a review. Front Environ Chem. 2025;6:1526366.
22. Kgabi DP, Ambushe AA. Characterization of South African bentonite and kaolin clays. Sustainability. 2023;15(17):12679.
23. Shikuku VO, Mishra T. Adsorption isotherm modeling for methylene blue removal onto magnetic kaolinite clay: a comparison of two-parameter isotherms. Appl Water Sci. 2021;11(6):103.
24. Del Sordo Filho G, Torrecilha JK, Scapin MA, Oliveira SMB, Da Silva PSC. Characterization and adsorption capacity of Brazilian kaolin. J Radioanal Nucl Chem. 2021;329(1):61-70.

Reverse Engineering Applied to a Circuit Breaker Lever: Case Study

Alex Francisco dos Santos Ribeiro Junior[1]*, David Pablo Alves Primo[1]*, Valter Estevão Beal[1], Rodrigo Silveira de Santiago[1], Marcelo Okada Shigueoka[1]

[1]SENAI CIMATEC University, DPI; Salvador, Bahia, Brazil

The obsolescence of components in industrial systems has become a significant and growing challenge for corrective maintenance and operational continuity of complex and high-cost equipment. To address this issue, this work proposes an integrated multidisciplinary approach combining reverse engineering, design for additive manufacturing, structural simulation, and 3D printing technique for recovering and refurbishing obsolete components. As a detailed case study, the functional restoration of a high-power circuit breaker used in a hospital environment was performed, where conventional replacement would involve high costs and prolonged downtime, with direct impact on system safety and reliability. The process involved precise 3D scanning of the original component, followed by parametric modeling with geometric and structural optimization. Computational simulations were conducted to verify mechanical performance under operating conditions. The component was manufactured using an additive manufacturing technique with high-performance engineering resin. The result was a carefully redesigned part showing significant improvements in geometry, strength, and robustness while maintaining full dimensional compatibility and functional interchangeability with the original system. Comprehensive tests demonstrated adequate dimensional accuracy and satisfactory mechanical performance, along with substantial reductions in costs and repair time compared to conventional replacement methods. The developed methodology proved effective as a strategic alternative to address parts' unavailability in the market, providing greater technical autonomy and flexibility in maintaining complex industrial assets, and highlighting the promising potential of integrating digital technologies with reverse engineering as a sustainable and innovative solution for managing obsolescence challenges in electromechanical systems.

Keywords: Reverse Engineering. 3D Scanning. Structural Analysis. Additive Manufacturing.

Maintenance of industrial components is fundamental to ensuring operational continuity and system safety. However, the obsolescence of critical parts, which are often discontinued by manufacturers, poses a significant challenge by hindering direct replacement and increasing maintenance costs and lead times.

In this scenario, reverse engineering emerges as an effective strategy for producing replacement parts. Through advanced three-dimensional scanning technologies such as photogrammetry, stereoscopy, and laser triangulation, and the reconstruction of CAD models, it is possible to replicate complex components, ensuring functional compatibility with the original equipment and avoiding complete system replacement [1-6].

To guarantee the reliability of these replicated parts, the use of computer-aided engineering (CAE) tools becomes essential. Techniques such as the finite element method and meshless methods allow predicting the mechanical behavior of parts, identifying critical points, and validating potential design modifications prior to manufacturing [1].

In parallel, additive manufacturing (AM) arises as a fast and flexible solution for producing these parts, eliminating the need for traditional tooling and enabling the fabrication of complex geometries with high precision. This results in significant reductions in time and cost involved in component replacement [6].

Within this context, Design for Additive Manufacturing (DfAM) complements the process by guiding the redesign of parts to optimize their

Received on 15 October 2025; revised 20 January 2026.

Address for correspondence: Alex Francisco dos Santos Ribeiro Junior and David Pablo Alves Primo. Av. Orlando Gomes, 1845, Piatã, Salvador, Bahia, Brazil. Zipcode: 41650-010. E-mail: leoxon679@gmail.com / davidalves_3@outlook.com.

J Bioeng. Tech. Health 2026;9(2):142-151

functionality, performance, and manufacturability via additive manufacturing. This approach allows incorporating improvements and adaptations not possible with conventional methods.

Several studies demonstrate that the integrated combination of reverse engineering, DfAM, CAE, and additive manufacturing constitutes an effective methodology for replacing obsolete parts, especially in industrial and automotive sectors, bringing benefits such as cost reduction, time savings, and improved component performance [2,5-7].

The present work presents a methodology applied as a case study aimed at cost reduction and the rapid availability of a critical piece of equipment. To this end, it proposes the development of a new lever for circuit breakers by unifying two originally separate components into a single part through the integration of reverse engineering and additive manufacturing. The three-dimensional model will be created from precise measurements and validated by structural simulation using the meshless method, aiming to optimize both functionality and the production process, thus offering an efficient solution for replacing obsolete components in industrial electrical systems.

Circuit Braker

The circuit breaker is a safety device that automatically cuts the electrical power supply to a circuit in case of system overload, protecting the entire system from severe damage [8]. Its operation can also be performed manually through a switch to turn the power supply to the circuit on or off. The damaged part was the lever switch of the equipment made from reinforced polycarbonate with 10% fiberglass. The complete equipment costs R$ 30,000.00.

Materials and Methods

Figure 1 presents the system of the case study process.

Figure 1. Flowchart of the case study process.

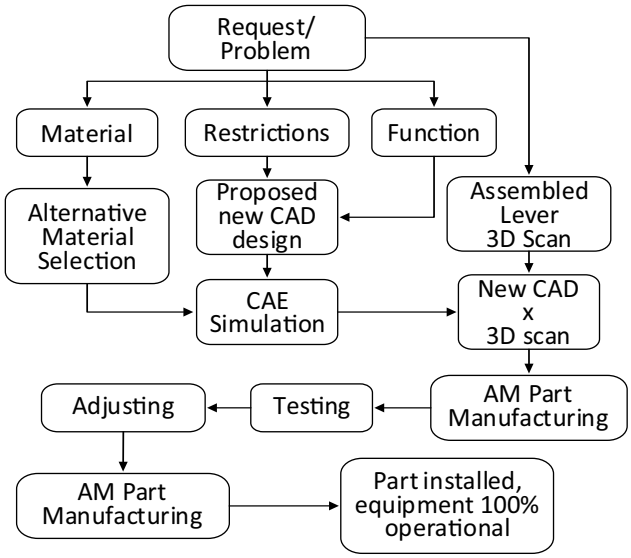

Equipment and Part Evaluation

Figure 2 presents the piece that is the object of study of this work. It can be observed that the switch suffered a fracture in the region of the coupling between the lever (Part 1) and the circuit breaker actuator (Part 2), and the fracture was initiated in the fixing hole location. The component was designed to withstand forces on the order of 30 kgf. The flap is secured in a way that allows it to slide. The movement ofthe part is restricted by an upper stop and a lower stop that lock the movement of the sliding flap, preventing shocks between the lever and the equipment.

Figure 2. Original part.

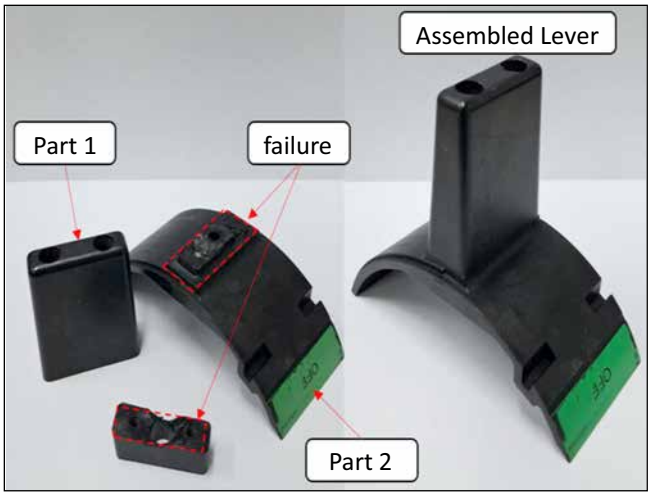

3D Scan Data Acquisition

To obtain the geometry of the damaged part, detailed dimensions were obtained using a Mitutoyo analog caliper model 530-114 with a resolution of 0.05 mm and an accuracy of ±0.05 mm, as well as by scanning the component using the Zeiss 3D scanner model T-SCAN Hawk 2 with a resolution of 0.02 mm and an accuracy of 0.02 mm + 0.015 mm/m, carried out with the assistance of a rotary base using the laser scanning method with reference points positioned on the rotary base, considering a mesh refinement of 0.1 mm. The scanner uses stereo technology with laser triangulation and stereo. Three measurements were taken: left side, right side, and bottom, with the point clouds aligned using the alignment method through Root Mean Square Error (RMSE).

Subsequently, the point clouds were converted into an STL file. The acquisition and processing of the data obtained through the scanner was carried out with the aid of Zeiss GOM INSPECT software. This approach, which combines manual measurements with 3D scanning, is widely recognized as an effective methodology for the accurate reconstruction of parts intended for additive manufacturing [9].

3D CAD modelling and DfAM

For the modeling of the component, the software SOLIDWORKS 2023 was used. The parametric model of the switch was built considering the geometric constraints that require high precision and detailing, as well as the location of the failure, which occurs near the interface of the components, where there is stress concentration. Thus, the All-in-one design was adopted, combining the 2 components into 1, preserving the geometry of the tab required to perform the primary functions of the component and maintaining the main fastening hole, reducing the existing stress concentration, increasing the mechanical strength of the part, and decreasing the number of components for assembly.

Structural CAE

The structural model to verify the performance of the structure after reverse engineering and the change in the manufacturing process was developed using the Altair Simsolid program, which allows for linear or nonlinear structural analyses through the Meshless method. In the structural model, a linear static structural simulation was performed using a material based on ultra-high strength resin manufactured by the company Solidator [10]. Based on the information provided on the manufacturer's website, the process, and the type of resin used, the model was developed considering a linear isotropic elastic material, provided that the maximum deformation is less than 2%, meeting the linear requirement of the material and the numerical model that underpins the Meshless method. For the structural model, three boundary conditions were considered: Force (F) with a magnitude of 350 N applied to the top face of the lever, sliding support (SS) on the rear faces of the circuit breaker actuator, and fixed support (FS) on the faces of the switch mounting hole. Since in the version manufactured by additive manufacturing, the two parts of the original switch were integrated into a single component, contacts or the coupling between the actuator and the lever were not considered.

Additive Manufacturing

The part was designed to be manufactured using the Solidator 8K printer, which allows for production using the SLA technique with the ultra-resistant black resin from the same manufacturer. Table 1 shows the comparison of properties about the original part material and the new part material [10-12].

The equipment operates through a closed solution, so it is not possible to obtain the process parameter information used in the manufacturing of the parts, with only the inclination of the part being modified, positioning it 10 mm above the base of the table and tilted in two planes at 45° to reduce warping effects and distortions of the part (Figure 3).

Table 1. Comparison of properties.

Property	Solidator Ultra-Tough Black Resin	PC+10 GF	Unit
Density	1.19	1.25 –1.28	g/cm³
Modulus of Elasticity	1600	3500	MPa
Tensile Strength	32	60–65	MPa
Elongation at Break	39	5–6	%
Poisson	0.39	0.38	-

Figure 3. Parts hanging on the machine build platform after being manufactured.

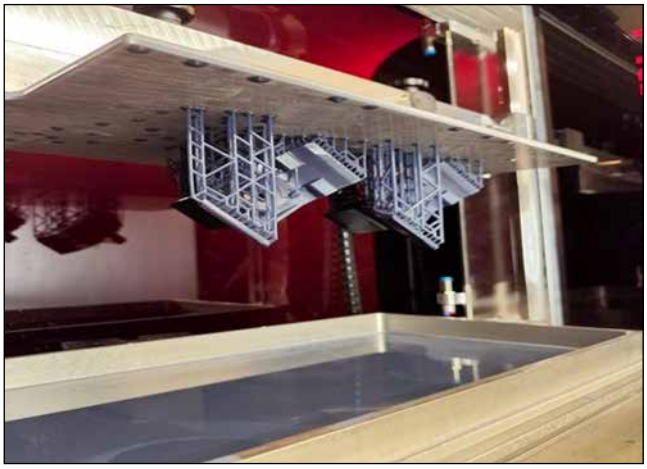

Results

Design Comparison

When comparing the design of the original part with the one made in AM, as shown in Figure 4, the latter stands out for reducing the number of components for assembly and eliminating the weak point that was the interface between the components, removing the need to use screws and presenting a fillet in the fragile area.

Structural Results

Figure 5 shows the equivalent Von Mises stress field in the switch structure. It can be observed that the maximum stress experienced by the switch is 8.72 MPa, at the back part of the piece where it

Figure 4. Design comparison.

Figure 5. Von Mises equivalent stress field.

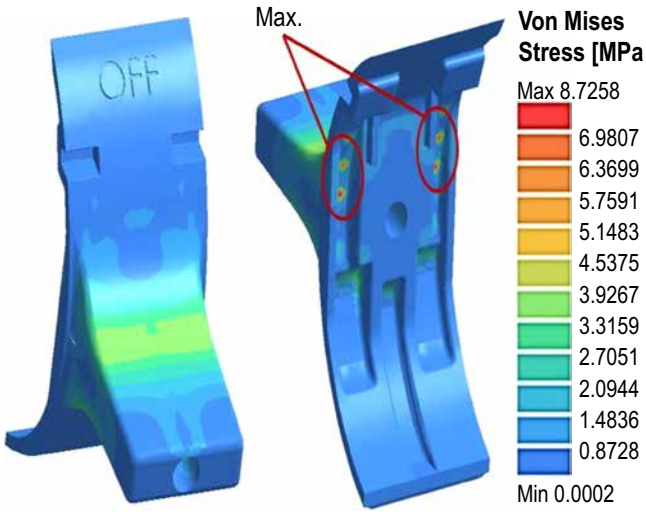

is fixed, the area where the switch contacts the circuit breaker.

In this condition the new part material has a safety factor of 3.67.

Dimensional Evaluation

In this study, measurements were taken using a 3D scanner on the original switch and after the additive manufacturing process, to verify the difference between the original part and the reverse-engineered part. Both measurements on the scanner were performed under the same conditions mentioned earlier. The difference between the original part and the part manufactured by additive manufacturing was assessed using the Cloud Compare program, also employing the RMSE method to compare the average deviation between the two geometries. Graphic 1 shows the comparison between the geometry manufactured by additive manufacturing and the original geometry. The bottom and top parts of the original geometry were fixed to facilitate the scanning process. Subsequently, the same scanning positions were used to evaluate the geometry manufactured through additive manufacturing. It can be observed that the greatest divergences between the original and altered piece occur in the lever region, resulting in an average deviation of - 0.1017 mm.

Graphic 1. Comparison between the manufactured geometry and the original geometry.

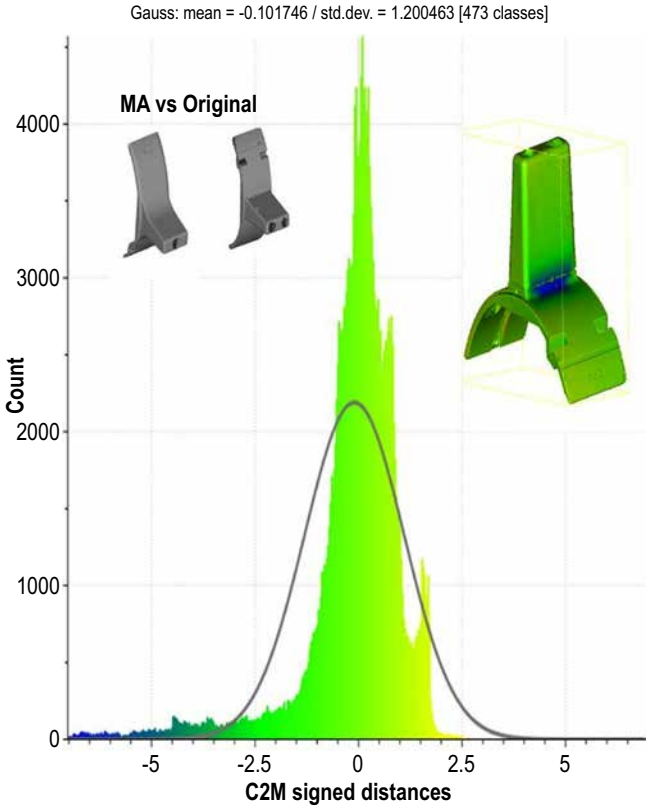

Functionality Evaluation

When trying to use the designed part for the first time, a slight interference was noticed in the main fixing hole, requiring the tolerance of the hole to be adjusted by about 0.1mm to ensure that there was no interference due to contraction during the manufacturing process. The part subsequently withstood the stresses, and its operation after the adjustment was satisfactory (Figure 6).

Figure 6. Manufactured part being used in the circuit breaker.

Cost Analysis

Since the part has no replacement and it is necessary to replace the entire equipment, the usual cost to replace the obsolete part amounts to the full value of new equipment, totaling R$ 30,000.00. However, the budget for the reverse engineering service, geometry validation by scanning, structural simulation, and manufacturing is estimated as shown in Graphic 2. This totals R$ 1,500.00, resulting in a savings of 19 times the original value of the circuit breaker.

Graphic 2. Cost per stage of part development

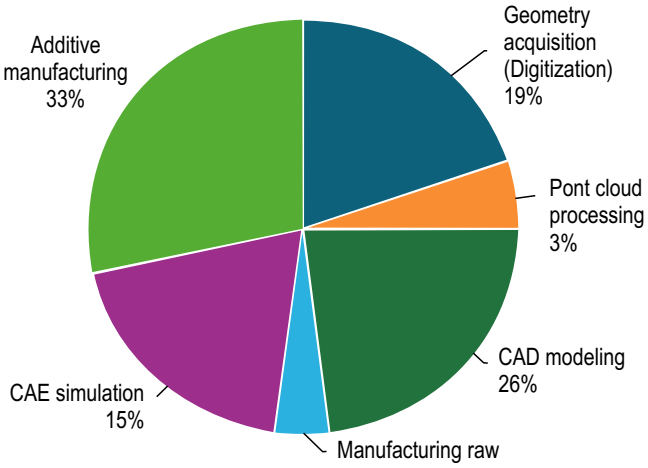

Conclusion

This work demonstrated that the replacement of obsolete components through reverse engineering, combined with structural simulation and additive manufacturing, is a technically and economically viable solution. The circuit breaker lever was redesigned as a single piece while fully maintaining its original functionality. Previous studies have already validated the use of 3D-printed components in industrial contexts (Baladés, 2023 [1]), which reinforces the results obtained. Thus, it is concluded that the proposed objectives were achieved, demonstrating that the adopted methodology is effective for replacing critical parts, promoting operational continuity and cost reduction in industrial systems.

As a proposal for future work, it is suggested to conduct a life cycle analysis of the component produced, comparing its durability to that of the original complete assembly. This investigation would enable a more comprehensive assessment of the technical and economic feasibility of the replacement, considering not only the initial manufacturing costs but also long-term maintenance expenses and replacement frequency over time.

Acknowledgement

The authors would like to thank University SENAI CIMATEC and the “Hospital da Bahia” for the opportunity to work on the case and for the structure to carry out the analyses.

References

1. Eslami AM. Integrating reverse engineering and 3D printing for the manufacturing process. In: ASEE annual conference and exposition, conference proceedings. Washington: American Society for Engineering Education; 2017.
2. Fabian M, Huňady R, Kupec F. Reverse engineering and rapid prototyping in the process of developing prototypes of automotive parts. Manuf Technol. 2022;22(6):669-678.
3. Helle RH, Lemu HG. A case study on use of 3D scanning for reverse engineering and quality control. Mater Today Proc. 2021;45:5255-5262.
4. Milroy MJ, Weir DJ, Bradley C, Vickers GW. Reverse engineering employing a 3D laser scanner: a case study. Int J Adv Manuf Technol. 1996;12:111-121.
5. Pescaru R, Kyratsis P, Oancea G. A case study of reverse engineering integrated in an automated design process. In: IOP conference series: materials science and engineering. 2016;161:012029.
6. Volpato N. Tecnologias e aplicações da manufatura aditiva. São Paulo: Blucher; 2025.
7. Baladés N, Remigio P, Sales DL, Moreno D, López JM, Molina SI. Experimental and simulated study of 3D-printed couplings’ suitability for industrial application. Int J Adv Manuf Technol. 2023;127:665-676.
8. ABB. Circuit breaker basics [Internet]. 2025 [cited 2025 Jul 30]. Available from: https://electrification.us.abb.com/circuit-breaker-basics
9. López J, Vila C. An approach to reverse engineering methodology for part reconstruction with additive manufacturing. In: IOP conference series: materials

science and engineering. 2021;1193:012047.
10. Solidator. Solidator ultra-resistant black resin [Internet]. 2025 [cited 2025 Feb 21]. Available from: https://solidator.com/en/materials/tough-resins/solidator-ultra-tough-black-resin/
11. Kern. Polycarbonate with 10% glass fibre (PC GF 10 V0) [Internet]. 2025 [cited 2025 Jul 30]. Available from: https://www.kern.de/de/technical-datasheet/polycarbonate-pc-gf10-v0?n=2311_2
12. Lookpolymers. EPICHEM Epilon PC GF 10 V0 polycarbonate, 10% glass fiber [Internet]. 2025 [cited 2025 Jul 20]. Available from: https://www.lookpolymers.com/pdf/EPICHEM-Epilon-PC-GF-10-V0-Polycarbonate-10-Glass-Fiber.pdf

Proposal for TRL Adjustment in the Maturation of Agroindustrial Technologies

Cauã de Souza Farias[1]*, Danilo Jefferson Romero[1], Stephanie de Melo Santana[1]
[1]SENAI CIMATEC University, Agroindustria; Salvador, Bahia, Brazil

Technology Readiness Levels (TRL) measure the maturity of technologies and are traditionally applicable to physical products and engineering systems. Although widely adopted by governments and industries, their use presents limitations when applied to areas such as agroindustry, which often rely on descriptive and methodological processes without tangible technological deliverables. In this context, it becomes necessary to adapt TRL to include methods that, although not resulting in a physical product, directly contribute directly to technological development. This study proposes an adaptation of the TRL scale for application in conceptual projects, especially in agroindustry, focusing on the maturation of protocols, planting methodologies, and technical processes. A systematic literature review, with searches carried out in the ScienceDirect and Scopus databases, revealed a lack of approaches that consider processes without a final product in the agricultural sector. As an example, the project at Cimatec Sertão focused on the production of bioethanol from Agave sp., where the TRL scale is used in the maturation of processes and methods involved in Agave cultivation. The adapted proposal redefines TRL levels to include stages such as ideation, scientific validation, proof of concept, and tests at different scales, culminating in commercial application. This new approach provides greater clarity, uniformity, and applicability in agroindustrial projects, ensuring effective communication among researchers and facilitating the evaluation of maturity levels for descriptive technological processes.
Keywords: Readiness Level. Agroindustry. Adaptation.

Developed by NASA in the 1970s, the Technology Readiness Level (TRL) serves as a metric parameter for standardizing technological maturity, facilitating technology development by providing greater technical and operational credibility and reliability, as well as reducing investment risks. It is divided into nine parameters, ranging from 1 to 9, and four phases: Concept, Prototype, Validation, and Production (Figure 1). Lower TRL levels (low technological maturity) carry higher investment risks [1-6].

In 1974, Stan Sadin defined the initial scales containing seven levels of technological maturity, later refined in 1990 to establish two additional levels, totaling nine parameters. The model gained prominence in industry and government and has been widely adopted as the standard framework for technology assessment—supporting everything from scientific investigation for initial technology validation (TRL 1) to the final product stage and market application (TRL 9) [1-6]. TRLs are numbered from 1 to 9 (Figure 1) to measure the readiness of a given technology and track its improvement, maintaining clear, unified, and simple communication so all stakeholders can understand the project [1-6].

The TRL model assumes a linear process of technological development, from laboratory to market. Even with its wide applicability, it presents operational environment limitations, subjective evaluation definitions, and an origin and focus restricted to the aerospace sector, emphasizing well-defined physical products and mechanical systems [1-6]. This situation reveals challenges in applying TRL across various fields—such as healthcare, agroindustry, and chemistry—which have different perspectives that influence project development. Adaptations are therefore necessary, especially for theoretical research and development work [1-6].

In agroindustry, technological development may involve physical products (fertilizers, equipment) but also stems from the production and maturation of processes, such as protocols and methodologies that lead to satisfactory products. This requires

Received on 18 October 2025; revised 15 January 2026.
Address for correspondence: Cauã de Souza Farias. Av. Orlando Gomes, 1845 - Piatã, Salvador – BA – Brazil, Zipcode: 41650-010. E-mail: rosanavieiraalbuquerque@gmail.com.

J Bioeng. Tech. Health 2026;9(2):149-154

Figure 1. Technology Readiness Level scales – TRLs.

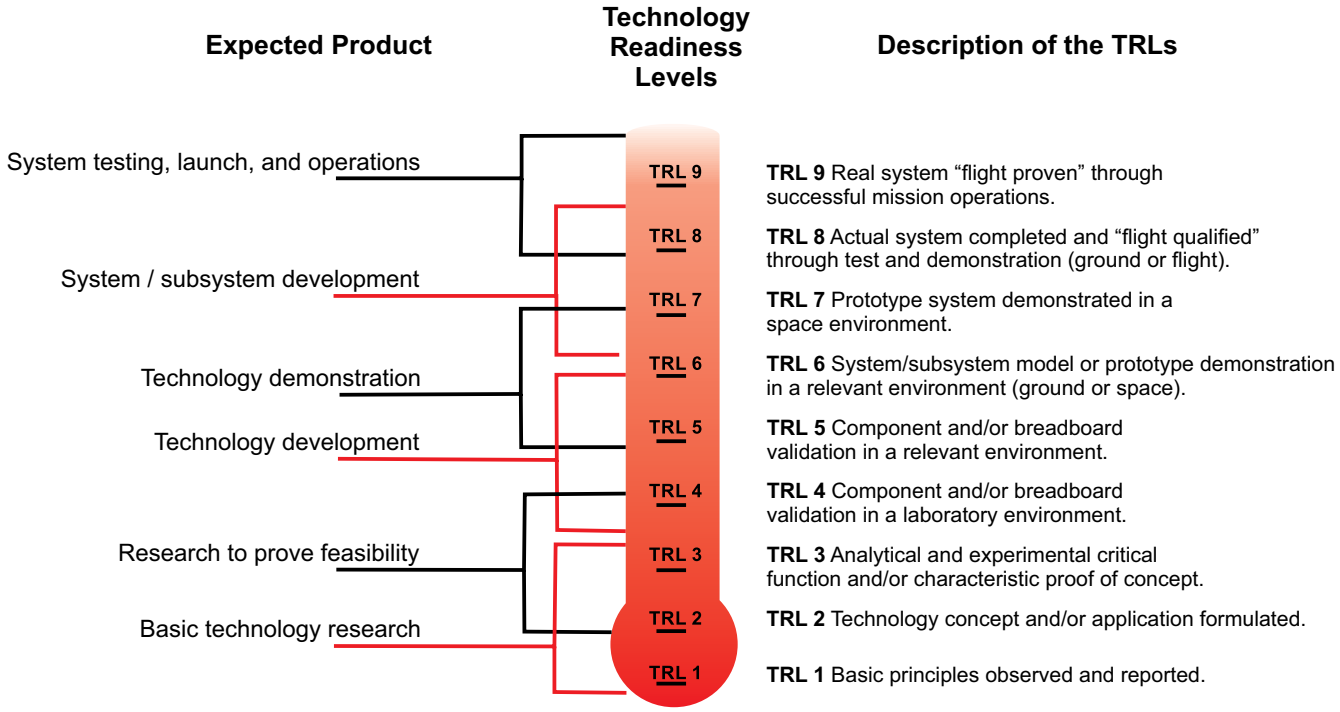

Source: Adapted from NASA (2007) [8].

adaptation to fit within the TRL framework [5]. Literature shows new TRL approaches in different sectors (health, energy, etc.), each with its own adaptations and definitions [1-6].

For example, EPAGRI (2022) adapted TRL to various technological categories in line with its rural and fisheries technology projects. Examples include: A cultivar developed and registered and its respective modifications in the TRL scale: TRL 3 – Pre-breeding stage (collection, exchange, multiplication, and characterization of germplasm in collections or Active Germplasm Banks – AGBs). Carrying out hybridizations or using auxiliary techniques to generate genetic variability, followed by selection based on descriptors; TRL 6 – Evaluation and selection of desired agronomic traits in the material obtained under commercial field conditions (spacing, phytosanitary treatments, others); TRL 9 – Licensed or granted cultivar in use within the production chain, with adoption monitoring [11].

In this context, the United States Department of Defense and Department of Energy have addressed new interpretations and adapted TRL into HRLs (Human Readiness Levels), aiming to understand the relationship between humans and technology, especially in complex systems that can critically affect humans, as well as the models System Readiness Level (SRL) and Manufacturing Readiness Level (MRL), used for the integration of systems and technologies and for product manufacturing, respectively [1-5,12] (Table 1).

The present work aims to present an adaptation proposal that encompasses application in exclusively conceptual projects, particularly in the agroindustrial sector.

Materials and Methods

This literature review followed a systematic review approach to identify, select, and synthesize studies related to the Technology Readiness Level (TRL) in its direct application and respective adaptations to encompass other processes inherent to technology. The research was conducted in the

Table 1. Technology assessment methods.

Model	Approach	Positive Aspects	Negative Aspects
Integration Readiness Levels (IRL)	Integration of components into a complex system	Evaluate component integration	Restricted to technical view
System Readiness Level – SRL	Risk assessment combining TRL with IRL	Combines component readiness with integration	Restricted to technical aspect, excludes obsolescence analysis
System Readiness Level Plus – SRL+	Integrates TRL, IRL, and MRL concepts	Broader technical assessment	Excludes obsolescence analysis
Technology life cycle	Evaluates technology maturity in its lifecycle	Anticipates trends and manufacturing risk	Evaluate manufacturing risk throughout its life cycle. Anticipate emerging trends.
Manufacturing Readiness Level (MRL)	Measures manufacturing maturity of a product, technology, or system	Manufacturing assessment	Assess the manufacturing risk in its life cycle. Seek to anticipate trends.

Source: Adapted from Oliveira A (2014) [9].

ScienceDirect and Scopus databases over a nine-year period (2016 to 2024), using the following descriptors: "technology readiness level"; "technology readiness level" AND "agriculture"; "technology readiness level" AND "TRL"; "technology readiness level" AND "agroindustry," in Portuguese, English, and Spanish. The terms were applied to the title, abstract, and keyword fields to maximize the retrieval of relevant studies on the subject. After data collection, selection criteria were applied to materials without restricted access, assessing the title and abstract, and subsequently classifying them into: 1) Description of TRL; 2) Adaptation of TRL; 3) Presentation of the practical use of the TRL scale.

Results and Discussion

From the survey, more than one thousand articles were found, with the main areas of study being agriculture, aircraft technology, and engineering projects. However, in the environmental sector, and especially in agriculture, no studies were found related to descriptive processes (methodologies, processes) without a final technological product (tangible product). It is therefore necessary to adapt TRL to include ecological, social, and knowledge co- production aspects, as well as non-technological procedures [1-6,8-12]. Technological development in the agroindustrial field is recorded in the literature for technologies that capture and store CO_2, biomass production, and agricultural machinery, among others. However, it is also present in descriptive processes based on cultivation techniques, pesticide application, and plant pathogen identification methodologies [1,7-12]. Therefore, the application of TRL to descriptive methods is unsatisfactory, and an adaptation is needed to encompass these processes while still enabling clear, objective communication and identification of the maturity level [1-6,8-12].

The applicability of TRLs in projects with tangible technology (physical product) is satisfactory; however, this is not the case in projects with theoretical deliverables due to definitional limitations, such as the concept of "prototype" [3-6]. The process of adapting the TRL scale is common in the literature (Table 2), bringing changes and adjustments according to other

aspects that guide technology and that go beyond the standard TRL framework, encompassing new perspectives regarding technology, market parameters, multiple technologies within a complex system, among others [3-6].

From this perspective, an adaptation for applicability in the agroindustrial sector is already reported in the literature; however, it is limited to transgenics/gene editing, marker-assisted selection, bio-control, and tissue culture, all with a technological approach. A new perspective is therefore essential, as the development of diagnostic methods, planting methods, disposal methodologies, among others, is anticipated and would benefit from the use of TRL scales if properly adapted [3-6].

At Senai CIMATEC, with an emphasis on CIMATEC Sertão, projects are carried out based on TRL evolution, where descriptive methodologies (processes and protocols) that generate a final product are presented. In a case study analyzing the projects at CIMATEC Sertão, which bring solutions and innovations to the semi-arid region—such as the production of bioethanol from Agave sp.—planting methods are used, with TRL applied to define the stages and maturity, with the final goal of establishing a planting protocol for agricultural crops such as agave. In this study, TRL evolution is associated with the increased maturity of cultivation techniques, starting from scientific research (TRL 1/2) to nursery trials (TRL 3), plot trials (TRL 4), and finally field planting with TRL 5 and 6 (Figure 2), where the techniques used are validated, scale and environment are increased, and consequently, technological maturity is enhanced. Thus, it was necessary to adapt the scale for use in different areas.

Terms like "prototype," "parts," and "pilot scale" were replaced with agricultural terms such as greenhouse, pots, plots, and experimental fields. Scaling was considered from laboratories to properties over 100 ha (1,000,000 m²), as relevant and operational agricultural environments can be large-scale.

The Brazilian Agricultural Research Corporation (EMBRAPA) and the Agricultural

Table 2. TRL adaptation for the agroindustrial sector at Senai CIMATEC.

Level	TRL Adaptation	Description
1	Ideation – bring the theme and start validating it	Technological and academic research
2	Scientific validation – search scientific databases to validate the idea	Technological and academic research
3	POC – Proof of concept; identify flaws or confirm potential before investment	Laboratory experiments, protected environments
4	Initial testing – in a controlled, small-scale environment	Protected environment, greenhouse, plot experiments
5	Method validation	Field experiments
6	Testingin relevant, medium-scale environment	Relevant field experiments
7	Large-scale test validation	Operational environment experiments
8	Validated procedures	Operational environment experiments
9	Commercial application	Operational environment experiments

Figure 2. TRL evolution in Agave sp. planting.

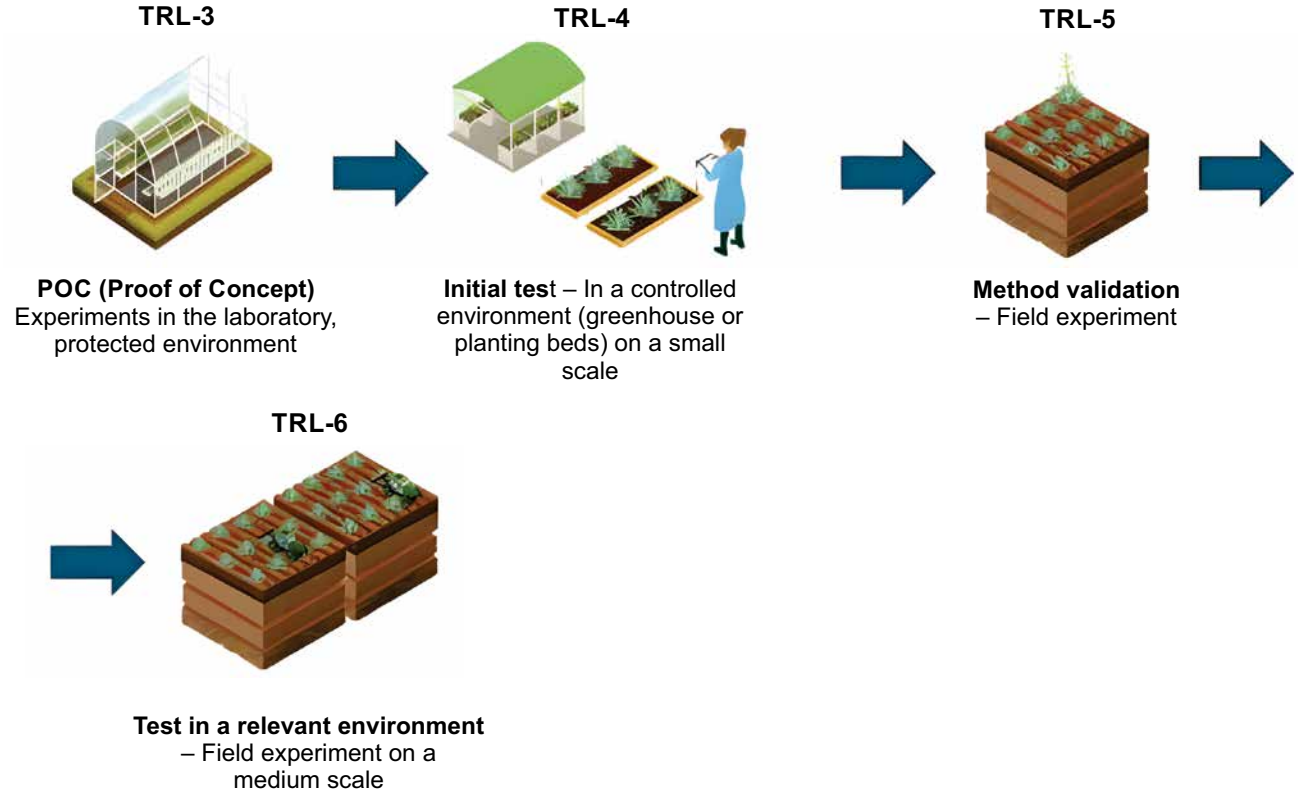

Research and Rural Extension Company of Santa Catarina (Epagri) have agricultural maturity recommendations covering products, methods, and agricultural production [11]. Accordingly, the proposed Technology Readiness Level adaptation (Table 2) replaces physical technology concepts with descriptive procedures that, when properly applied, result in a high-quality final technology.

This adaptation allows agroindustry projects to be carried out with a unified understanding, meeting research projections even when deliverables are limited to lower TRL levels— requiring consistent knowledge of the scale concepts throughout project maturation.

Conclusion

In conclusion, adapting TRL facilitates its use in maturing descriptive processes, such as methodologies and protocols that lead to a physical product, while maintaining a unified, clear, and objective language across the research network.

Acknowledgement

The authors acknowledge Shell Brasil and ANP (Agência Nacional do Petróleo, Gás Natural e Biocombustíveis) for the strategic support provided through regulatory incentives for Research, Development & Innovation. We also acknowledge EMBRAPII and Senai CIMATEC for the encouragement and funding.

References

1. Beims RF, Simonato CL, Wiggers VR. Technology readiness level assessment of pyrolysis of triglyceride biomass to fuels and chemicals. Renew Sustain Energy Rev. 2019;112:521–529. doi:10.1016/j.rser.2019.06.017.
2. Bezerra WRP. Desenvolvimento de aplicativo de suporte à tomada de decisão na gestão da inovação resultante da combinação dos métodos Technology Readiness Level (TRL) e Demand Readiness Level (DRL): o estudo de caso Chesf [dissertação]. Recife: Universidade Federal de Pernambuco; 2021. Disponível em: https://repositorio.ufpe.br/handle/123456789/40184

3. Biesek FL. Modelo para integração das áreas de conhecimento de projeto e manufatura por intermédio do MRL (Manufacturing Readiness Level) e do DFMA (Design for Manufacturing and Assembly) na fase de desenvolvimento de tecnologia de produto [dissertação]. Joinville: Universidade Federal de Santa Catarina; 2018. Disponível em: https://repositorio.ufsc.br/handle/123456789/190065
4. Bukar AM, Asif M. Technology readiness level assessment of carbon capture and storage technologies. Renew Sustain Energy Rev. 2024;200. doi:10.1016/j.rser.2024.114578.
5. Epagri. A escala TRL/MRL: níveis de maturidade tecnológica – o que são e para que servem. Documentos. 2022;(356). Disponível em: https://publicacoes.epagri.sc.gov.br/DOC/article/view/1577
6. Hekmatmehr H, et al. Carbon capture technologies: a review on technology readiness level. Fuel. 2024;363. doi:10.1016/j.fuel.2024.130898.
7. Linhares MVD, Quintella CM. Desenvolvimento de tecnologia (software e hardware) para atuar junto aos fatores de riscos da cadeia produtiva do mel [tese]. 2016. Disponível em: TESE_MARCUS_LINHARES.pdf.
8. National Aeronautics and Space Administration (NASA). NASA systems engineering handbook. NASA/SP-2106-6105. [S.l.]: NASA; s.d.
9. Oliveira AS. Proposta de modelo em redes bayesianas para apoio à tomada de decisão visando produtos sustentáveis [tese]. Salvador: Centro Universitário SENAI CIMATEC; 2021. Disponível em: http://repositorio.universidadesenaicimatec.edu.br/handle/fieb/1185
10. Salazar G, Russi-Vigoya MN. Technology readiness level as the foundation of human readiness level. Syst Eng. 2021;29(4). doi:10.1177/10648046211020527.
11. Veras CAG, Pereira FDES. Escala de maturidade tecnológica (TRL). Brasília: Parque Científico e Tecnológico da Universidade de Brasília (PCTec/UnB); 2022. Disponível em: https://pctec.unb.br/documentos/179-documentos/142-trl
12. White R, Marzano M, Fesenko E, et al. Technology development for the early detection of plant pests: a framework for assessing Technology Readiness Levels (TRLs) in environmental science. J Plant Dis Prot. 2022;129:1249–1261. doi:10.1007/s41348-022-00599-3.

Soil Mixtures with Additions for Expansive Soil Stabilization: A Systematic Literature Review

Anne Pinheiro Garcez[1]*, Marianna Luna Sousa Rivetti[1], Larissa da Silva Paes Cardoso[1], Josiane Dantas Viana[2]
[1]SENAI CIMATEC University, Civil Construction; [2]SENAI CIMATEC University, Management and Industrial Technologies, Salvador, Bahia, Brazil

The volumetric instability of expansive soils poses a significant challenge to civil engineering, particularly affecting pavement works, foundations, and supporting structures. This behavior, associated with the presence of clay minerals such as montmorillonite, results in considerable variations when changes in moisture content occur, triggering expansion and shrinkage processes that compromise the performance and durability of structures. Traditionally, the stabilization of these soils is carried out using cement or lime, however, such methods may increase the stiffness and brittleness of the material, impairing its performance under dynamic loads. In this context, the use of natural or synthetic fibers emerges as a promising alternative, acting as reinforcement to improve strength and crack control. The analysis of rheological properties is crucial for evaluating the feasibility of applying these mixtures in the field. This study presents a systematic literature review, with data extracted from the Scopus database and analyzed in RStudio using the Bibliometrix package, aiming to map the state of the art regarding stabilizing mixtures for expansive soils. The search was guided by keywords such as "soil-cement," "expansive soil," and "lime," followed by the application of filters for subject area, document type, and source type. A total of 105 articles published between 1999 and 2025 were selected. The bibliometric analysis revealed a significant increase in scientific production since 2018, led by countries such as China, India, and Australia, in addition to the concentration of publications in high-impact journals. The results indicate that the integration of fibers, combined with rheological control, has significant potential to mitigate shrinkage and improve the mechanical performance of expansive soils, providing technical support for the development of more durable and environmentally appropriate solutions in geotechnical engineering.
Keywords: Soil-Cement. Expansive Soil. Fiber. Shrinkage. Rheology. Lime.

The volumetric instability of expansive soils represents a significant challenge for civil engineering, especially in paving and foundation works. This behavior is related to the presence of 2:1 clay minerals, such as montmorillonite, which promote significant volume variations when there are changes in moisture content, resulting in expansion and shrinkage processes [1]. In the Brazilian context, among the main known expansive formations are the sedimentary basins of Recôncavo Baiano, Paraná, and Rio Grande do Sul [2].

The shrinkage, present in soil mixtures, is a time-dependent phenomenon that can be defined as the increase in deformation over time, with a reduction in the volume of the concrete element without the action of loads at a constant temperature [3,4]. These deformations also occur when no moisture transfer is allowed with the external environment, being attributed to chemical reactions and internal structural changes [5]. In this sense, such deformations cause the appearance of surface or global cracks, reducing performance and affecting properties in the hardened state.

Traditionally, the methods for stabilizing expansive clay soils involve the use of binding materials such as cement and lime, which are the most common forms of treatment to improve their physical and mechanical properties. Although widely used, these treatments can make the soil excessively rigid and brittle, which is unfavorable under dynamic loading conditions, such as those arising from traffic on pavement systems [6].

Some research has explored more resilient alternatives, among which the use of natural and synthetic fiber reinforcement stands out. The fibers act as reinforcing elements in the soil matrix, promoting a more cohesive internal structure that

Received on 20 October 2025; revised 18 December 2025.
Address for correspondence: Anne Pinheiro Garcez. Av. Orlando Gomes, 1845 - Piatã, Salvador – BA – Brazil, Zipcode: 41650-010. E-mail: annegarcezp2@gmail.com.

J Bioeng. Tech. Health 2026;9(2):155-161

improves the overall strength and stability of the material. This reinforcement contributes to a more uniform distribution of stresses throughout the soil, minimizing localized deformations and reducing excessive pore pressure during loading [7].

In addition, the rheological behavior of the mixtures must also be considered, as properties such as viscosity and yield stress directly influence the feasibility of applying the material in the field [8]. Rheology is also used to evaluate the effects of deformation and material flow, as there are relationships between stress, deformation, deformation rate, and time [9-11].

Thus, it is important to study methods for stabilizing expansive soils, such as using soil mixtures with ideal additions that ensure adequate rheology. In addition, such mixtures should not shrink, making it possible to mitigate problems related to cracking, such as through the use of fibers. Understanding the panorama of research already developed in this area is essential for proposing effective solutions. Therefore, this article aims to present, through a systematic review of the literature based on previously established criteria, the current scenario of scientific investigations involving the analysis of stabilizing mixtures applied to expansive soils for the development of future research in the area.

Materials and Methods

This systematic review was conducted with the aim of mapping the state of the art related to the use of additions for stabilizing expansive soils, focusing on mitigating the volumetric shrinkage of soil-cement mixtures, especially with the use of fibers, in addition to rheological analysis of this mixture. To this end, a structured approach was adopted based on previously established criteria and consisting of the stages of searching, filtering, and analyzing bibliographic data.

Tools and Platform

The data collection was performed in the Scopus database, considered one of the most comprehensive for scientific publications in the fields of engineering, geosciences, and materials sciences. The extracted data were analyzed using R Studio software, using the Bibliometrix package, an open-source statistical tool specialized in bibliometric analysis and scientific mapping.

Bibliometrix allows the processing of large volumes of data, extracted from databases such as Scopus and Web of Science, with a high level of analytical detail. In addition, its application offers rigorous and automated support for the generation of metrics and visualizations that reveal patterns, trends, and the structure of knowledge in a given area. Given its robustness and reliability, Bibliometrix was chosen as the main tool for the analysis stage, providing quantitative support for the systematic review developed and thus enabling a qualitative interpretation of these results.

Search Strategy

The definition of search terms was guided by the main elements addressed in the research, considering the following keywords:

- Soil type and stabilizers: soil-cement, expansive soil, lime;
- Mechanical and physical performance: fiber, shrinkage;
- Application properties: rheology.

Figure 1 shows the main search filter used on the Scopus platform, which combines Boolean operators (AND / OR) to link the different topics of interest. The search field was limited to "Article title, Abstract, Keywords" in order to refine the results to the most relevant publications.

The combination of terms sought to cover experimental studies related to soil-cement and soil-lime mixtures applied to expansive soils, also considering the impact of fibers on shrinkage and rheological properties. This strategy was designed to capture different stabilization approaches and associated properties, as well as studies that relate performance and applicability in the field.

Figure 1. Keywords used to perform data extraction on the Scopus platform.

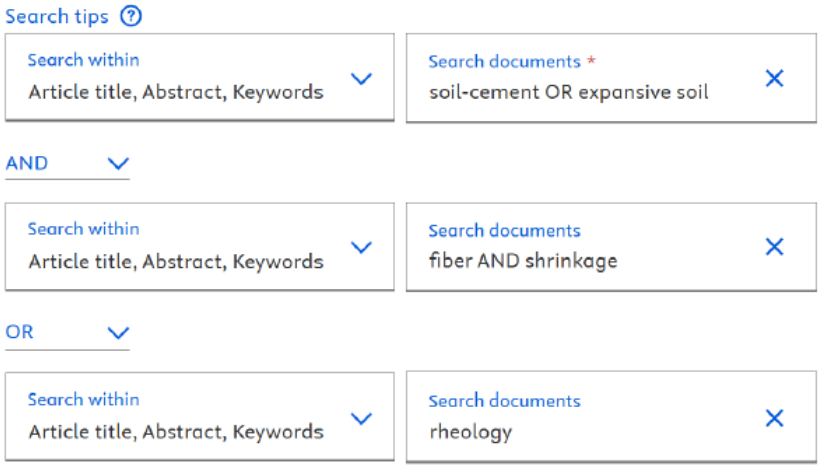

Application of Filters

After the initial search, 194 documents were obtained and then additional filters were applied within the Scopus platform itself to further refine the results and ensure the relevance of the studies collected. The inclusion criteria were:

- Subject Area: Engineering, Materials Science, Earth and Planetary Sciences, Environmental Science;
- Document Type: scientific articles only;
- Source Type: scientific journals only;
- Keyword Filter: Shrinkage, Soils, Soil Cement, Expansive Soil(s), Fibers, Rheology, Lime, Swelling, Soil Stabilization, Cement(s), Soil Reinforcement, Stabilization, Rheological Property, Fiber Reinforced Materials, Fiber Reinforcement, Soil Moisture, Soil-cement.

After applying these filters, the number of documents was reduced to 105 articles, which were exported in .bibtex format, compatible with Bibliometrix. It is worth noting that there were no criteria for excluding articles.

Results

The bibliometric analysis of the 105 selected articles, carried out using the Bibliometrix tool, made it possible to identify relevant patterns in scientific production related to the stabilization of expansive soils with additions (soil-cement, lime, fibers) and the study of rheological and shrinkage properties. The tool generated graphs, tables and relevant indicators on scientific production in the area, such as the most productive authors, most frequent keywords, journals with the highest number of publications, etc. These results are presented and discussed in the following section of this article.

Annual Scientific Production

The database extracted from Scopus covers a period of 26 years, beginning in 1999. In this sense, the period of scientific production analyzed indicates a growth trend over time, with a clearer acceleration since 2018. Although there are annual fluctuations — including a decline observed between 2020 and 2022, probably influenced by the Covid-19 pandemic — the long-term trend is toward an increase in the number of publications, suggesting consolidation and expansion of scientific interest in the topic. This upward trajectory indicates that the area is attracting greater attention, possibly due to the demand for solutions applied to the stabilization of expansive soils and the advancement of experimental and analytical techniques (Graphic 1).

Graphic 1. Annual scientific production.

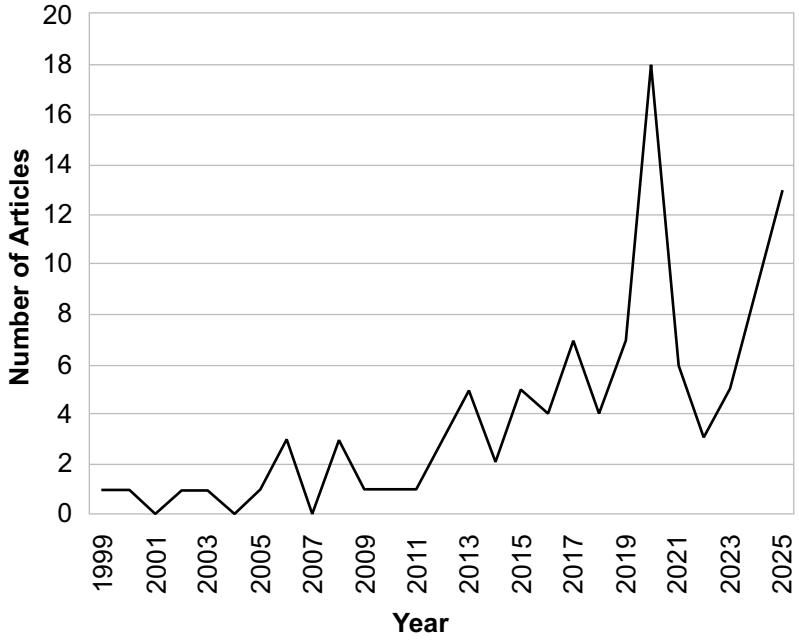

Most Relevant Sources

An analysis of the most relevant sources shows that production is concentrated in specialized journals in the field of study, with emphasis on the source Construction and Building Materials, with eight published documents, followed by the Journal of Materials in Civil Engineering and Yantu Lixue/ Rock and Soil Mechanics, with five documents each, also indicating their thematic importance for the subject. These journals have a high impact factor and are responsible for disseminating a significant portion of the most influential research, which reinforces their role as strategic channels for scientific dissemination. Table 1 provides guidance for future searches, such as choosing journals to submit results to and identifying scientific communities focused on the issues addressed in this article.

Most Relevant Authors

The analysis of the most relevant authors highlights the existence of researchers with recurring production and consolidated impact in the field, who act as hubs for the dissemination of knowledge. Authors

Table 1. Most relevant sources.

Source	No. of Documents
Construction and Building Materials	8
Journal of Materials in Civil Engineering	5
Yantu Lixue/Rock and Soil Machanics	5
Cement and Concrete Composites	4
Geotechnical and Geological Engineering	4
Journal of Building Engineering	4
Journal of Natural Disasters	4
Materials	4
Geomechanics and Engineering	3
Indian Geothechnical Journal	3

such as Wang Y, Xiao H, and Zhang J have a strong influence on the construction of the theoretical body of the references analyzed (Table 2).

Table 2. Most relevant authors.

Author	No. of Documents
Wang Y	6
Xiao H	6
Zhang J	4
Li Z	3
Puppala AJ	3
Xiao G	3
Zhang D	3
Abbaspour M	2
Aflaki E	2
Balan K	2

Corresponding Authors' Countries

Table 3 lists the country corresponding to the author responsible for submitting and corresponding to the paper. This indicator reveals geographical leadership in scientific production, as each article has only one corresponding author, reflecting where research coordination is carried out and where the main groups conducting experimental studies and publications are located. The data show that China leads with 38 articles, followed by India and Australia.

Table 3. Corresponding authors' countries.

Country	No. of Documents
China	38
India	16
Australia	10
USA	5
Brazil	4
Canada	4
Iran	4
France	3
South Korea	3

Countries' Scientific Production

Table 4 considers all articles in which a country appears in the affiliation of at least one author, regardless of whether or not they are the corresponding author. Unlike the previous indicator, the same document can be counted for more than one country, reflecting total participation in publications (including international collaborations and co-authorships), thus providing a broader view. In this scenario, China has a significant presence, with 95 occurrences, followed by India and the United States. Brazil ranks sixth, with seven occurrences. Comparing the two indicators allows us to infer patterns of collaboration: differences in position indicate, for example, countries with a high presence in co-authorships but a lower frequency as the corresponding author's headquarters (and vice versa).

Table 4. Countries' scientific production.

Country	No. of Documents
China	95
India	35
USA	16
Australia	14
France	8
Brazil	7
South Korea	6
Canada	5
Iran	5

Most Global Cited Documents

The documents with the highest number of international citations correspond to reference studies that establish conceptual or methodological foundations for the field. Identifying these documents is essential for the research in question, as it will guide the selection of studies to be read and extracted in terms of

experimental protocols, mixing parameters, and rheological evaluation methods, thus contributing to the definition of the main lines of investigation.

Table 5. Most global cited documents.

Document	Global Citations
Wang Y, 2017, Int. J. Geomech.	238
Khedari J, 2005, Cem. Concr. Compos.	214
Chaduvula U, 2017, Appl. Clay Sci.	182
Ma G, 2020, Constr. Build. Mater.	158
Punthutaecha K, 2006, J. Mater.Civ. Eng.	156
Khattak MJ, 2006, Int. J. Pavement Eng.	153
Puppala AJ, 2000, Transp. Res. Rec.	147
Olgun M, 2013, Geosynth. Int.	145
Lee S, 2017, Geomech. Eng.	136
Soltani A, 2017, Geotech. Geol. Eng.	135

Most Relevant Words

The mapping highlights the most relevant words within the selected article database. It is important to note that these words are derived from the content of the sample articles and represent the thematic emphasis found in the analyzed literature, not always corresponding exactly to the terms originally used in the Scopus search strategy. However, there is still a clear predominance of terms directly associated with the central concepts of the study, such as “shrinkage”, “soil cement”, “rheology”, “fibers”, “expansive soil” and “lime”, revealing an alignment between the research and the issue investigated.

Table 6. Most relevant words.

Keyword	Occurrences
Shrinkage	55
Soils	45
Soil cement	40
Compressive strength	38
Reinforcement	28
Rheology	28
Fibers	25
Soil testing	23
Expansive soil	22
Lime	21

Co-occurrence Network

The co-occurrence network reveals the relational structure between terms and allows us to identify subareas and central nodes that link different topics. In the network, we can see the formation of clusters that bring together concepts such as "soil-cement / lime", "fibers / reinforcement", "shrinkage / clay soil" and "rheology / soil mechanics". These clusters help map predominant lines of research and potential conceptual connections for the project's experimental proposal.

Conclusion

The systematic review carried out made it possible to map the current landscape of research related to the stabilization of expansive soils through mixtures with additions, highlighting the use of soil-cement, lime, and fibers, as well as the relevance of evaluating rheological and shrinkage properties. There has been continuous growth in scientific production in this area, especially since 2018, which shows the increased interest in more effective and sustainable solutions for the treatment of these soils.

The bibliometric analysis identified China, India, and Australia as leaders in scientific production, while high-impact journals, such as

Figure 2. Co-occurrence network.

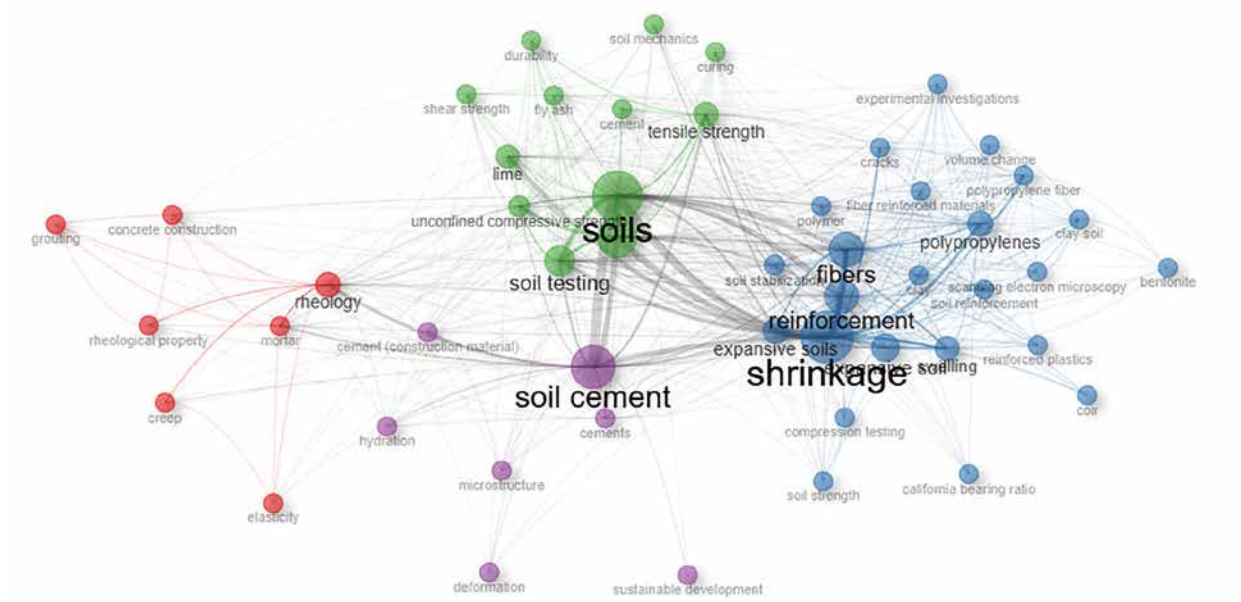

Construction and Building Materials, Journal of Materials in Civil Engineering, and Yantu Lixue/ Rock and Soil Mechanics, concentrate a large part of the most relevant publications. The most recurrent keywords reinforce the centrality of topics such as "shrinkage", "soil cement", "fibers" and "rheology", and co-occurrence networks confirm the convergence of research on issues that combine mechanical performance, shrinkage control, and field application feasibility.

The results obtained demonstrate that fiber reinforcement has significant potential to mitigate problems of volumetric instability and cracking in expansive soils, especially when associated with careful control of rheological properties. In this context, this article provides a solid basis for guiding future experimental studies, assisting in the choice of materials, methodologies and analysis parameters that can contribute to the development of more durable and environmentally appropriate solutions in geotechnical engineering.

References

1. Ferreira SRM, Ferreira MGVX. Volume changes due to variations in water content in a vertisol in the semi-arid region of Pernambuco. Rev Bras Cienc Solo. 2009;33(4):779-791. doi:10.1590/S0100-06832009000400004.
2. Simões PRM. Relevant aspects of the implementation of engineering works in expansive soils and rocks. Research and Development Center – Technical Report. 1987;(26).
3. Al-Saleh SA. Comparison of theoretical and experimental shrinkage in concrete. Constr Build Mater. 2014;72:326-332. doi:10.1016/j.conbuildmat.2014.06.050.
4. Gilbert RI, Ranzi G. Time-dependent behaviour of concrete structures. London: Spon Press; 2011. doi:10.1201/9781482288711.
5. Holt E. Contribution of mixture design to chemical and autogenous shrinkage of concrete at early ages. Cem Concr Res. 2005;35:464-472. doi:10.1016/j.cemconres.2004.05.009.
6. Medina-Martinez CJ, et al. Natural fibers: an alternative for the reinforcement of expansive soils. Sustainability. 2022;14(15):9275. doi:10.3390/su14159275.
7. Reehana S, Muthukumar M. Undrained response of fibre reinforced expansive soil subjected to cyclic loading. Soil Dyn Earthq Eng. 2023;173:108154. doi:10.1016/j.soildyn.2023.108154.
8. Barbosa MP, et al. Determination of rheological parameters of mortars and concrete using alternative techniques. IBRACON Struct Mater J. 2011;4(3):440-480.
9. Banfill PFG. The rheology of fresh cement and concrete – a review. Cem Concr Res. 2003.
10. Reis JFA. Determination of rheological parameters of concrete using the modified cone slump test: case study [dissertation]. São Paulo: UNESP; 2008.
11. Tanner RI. Engineering rheology. 2nd ed. New York: Oxford University Press; 2002. doi:10.1515/arh-2002-0019.

Satellite-Based Quantum Key Distribution: Protocols, Network Architectures, and Continuous-Variable Implementation Challenges

Cássio de Castro Silva[1], Rodrigo Dias Paolillo[1], Antônio Pereira Junior[1], Adriane Martins Alves[1], Yasmin da Silva Bonfim[1], Paulo Monteiro de Carvalho Monson[1], Adler Lima Botelho de Azevedo[1], Luiz Fernando Taboada Gomes Amaral[1], Braian Pinheiro da Silva[1]*, Valéria Loureiro da Silva[1]

[1]QuIIN, SENAI CIMATEC University; Salvador, Bahia, Brazil

Losses and attenuation are the main limitations to implementing secure quantum networks based on fiber or free-space optical links over long distances. A hybrid satellite–ground approach offers an effective solution to overcome these constraints and achieve higher key transmission rates. This article presents a systematic review of publications on satellite quantum communication, providing an overview of quantum key distribution with satellites, the use of satellite networks with emphasis on commonly adopted orbits, and the role of satellites in such architectures. Special attention is given to the implementation of continuous-variable QKD (CV-QKD) in satellite-based channels, highlighting its challenges and potential for integration into future satellite-based quantum networks

Keywords: Quantum Key Distribution. Satellite. Satellite-based QKD. Free-Space Optics. Continuous-Variable QKD.

Abbreviations: QKD, Quantum Key Distribution. DV-QKD, Discrete-Variable Quantum Key Distribution. CV-QKD, Continuous-Variable Quantum Key Distribution. SatQKD, Satellite-based Quantum Key Distribution. FSO, Free-Space Optics. GEO, Geostationary Orbit. LEO, Low Earth Orbit. SNR, Signal-to-Noise Ratio. PATS, Pointing Acquisition and Tracking Subsystem. LO, Local Oscillator. SKR, Secure Key Rate. QPSK, Quadrature Phase-Shift Keying.

Despite the predominance of classical systems in everyday applications such as television, the internet, and GPS, advances in quantum communication are transforming the telecommunications sector, particularly in data security. Quantum Key Distribution (QKD) enables encrypted information exchange with enhanced security and is being tested in projects such as satellite communications to protect data against interception, even by agents with advanced technology.

A systematic review is a research method that analyzes the literature on a topic using explicit criteria for searching and synthesizing information. This approach minimizes bias, consolidates evidence, and identifies gaps in knowledge [1]. The process involves three steps: (1) planning (defining objectives and selection criteria), (2) execution (filtering studies and extracting data), and (3) analysis and synthesis [2]. In rapidly evolving areas such as satellite-based quantum optical communication, where studies are abundant but dispersed, this methodology is essential for mapping the state of the art, guiding future research, and validating scientific results.

Materials and Methods

This study conducted a targeted search on QKD in satellite communications using LENS.org, Web of Science, and IEEE Xplore. The search focused on experimental and space-oriented applications, considering journal and conference articles published between 2015 and 2025. The initial results included 266 records from LENS.org, 116 from Web of Science, and 52 from IEEE Xplore. Python scripts were used to remove duplicates and correct metadata inconsistencies. The query applied was: ("quantum key distribution" OR "QKD" OR "CV-QKD" OR "continuous variable

Received on 26 October 2025; revised 18 January 2026.

Address for correspondence: Braian Pinheiro da Silva. Av. Orlando Gomes, 1845 - Piatã, Salvador – BA – Brazil, Zipcode: 41650-010. E-mail: braian.silva@fieb.org.br

J Bioeng. Tech. Health 2026;9(2):162-168

QKD") AND ("satellite" OR "space-based" OR "space- to-ground" OR "inter-satellite" OR "orbital" OR "LEO" OR "GEO" OR "space link" OR "optical space link" OR "SAT-QKD") AND ("experiment" OR "demonstration" OR "implementation" OR "field trial") NOT ("fiber" OR "terrestrial network" OR "optical fiber").

After automated and manual screening, 245 relevant publications remained. Figure 1 shows the annual distribution of satellite-based QKD research, with a linear trendline confirming steady growth. Most (79.2%) address satellite-based QKD, whereas only 6.8% specifically examine CV-QKD protocols. The remainder cover broader theoretical discussions or less-defined approaches. These results underscore the predominance of satellite-based QKD research, with CV-QKD emerging as a promising subfield. All references in subsequent sections were drawn from this systematic search.

Quantum Key Distribution Protocols

Quantum key distribution protocols are classified into discrete variable (DV-QKD) and continuous variable (CV-QKD) schemes, differing in their implementation requirements and operational principles. DV-QKD protocols encode information in the polarization, phase, or time-bin degree of freedom of single photons, requiring expensive single-photon detectors [3], whereas CV-QKD uses coherent states with quadrature modulation, enabling high-efficiency homodyne or heterodyne detection and leveraging existing telecommunications infrastructure for enhanced scalability [4]. The foundational DV-QKD protocol, BB84, encodes information in the polarization states of photons, allowing communicating parties (Alice and Bob) to detect eavesdropping (Eve) through quantum superposition principles and No-cloning theorem [5, 6]. Enhanced with decoy-state methods, this protocol has demonstrated robust satellite implementations resistant to photon number-splitting attacks [3,7-9].

A critical challenge in satellite-mediated QKD involves establishing trust in the orbital platform, which typically relays signals between ground stations without direct connection [3]. While conventional BB84 requires treating the satellite as a trusted node, measurement-device-independent (MDI) protocols circumvent this limitation by having the satellite (Charlie) perform Bell measurements on quantum states from both parties before broadcasting results [10,11]. This approach enables secure key establishment without relying on Charlie's integrity, although atmospheric turbulence in free-space optics poses implementation challenges [10]. Nevertheless,

Figure 1. Annual distribution of publications from 2015 to 2025 with linear trendline.

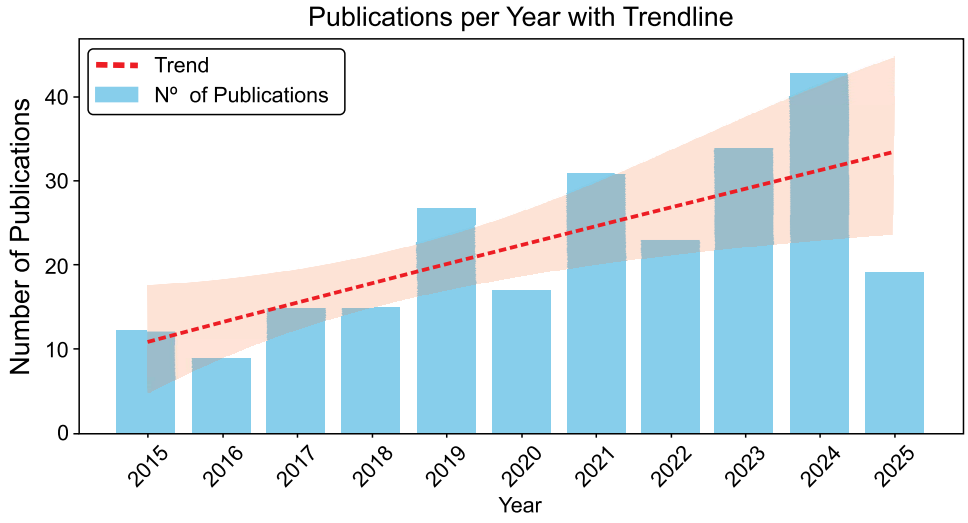

multiple studies have confirmed the feasibility of MDI-QKD [11-13], including satellite-based CV-QKD demonstrations [14].

Entanglement-based protocols represent another significant advancement, with extensive theoretical [15-20] and experimental [21] developments. In these schemes, Charlie distributes entangled photon pairs to Alice and Bob, who perform measurements and basis reconciliation via authenticated channels. The BBM92 protocol extends BB84 by incorporating entanglement measurements, eliminating reliance on Charlie's trustworthiness [16].

Satellite-Based Quantum Key Distribution Networks

With advances in quantum technologies, satellite communication is becoming essential for the realization and scalability of future quantum networks [7]. Although they have their own limitations, especially related to complications involving the link, positioning, and distribution of satellites, functional applications of quantum key distribution are already known in the literature [3,8,14,22].

The use of satellites in QKD depends on factors such as the distance between ground stations, the number of satellites available, and the protocol adopted. The last one is particularly critical, as it influences and adapts to the other parameters.

Hybrid ground-space integration offers a promising solution to mitigate high attenuation in fiber channels and atmospheric losses in free-space optical (FSO) links. China has demonstrated this approach with an integrated quantum network combining fiber and satellite-to-ground links, achieving a 4,600 km range and a key rate of 47.0 kbps in 2021 [3].

A major challenge in such systems is maintaining alignment between moving satellites. Studies from Australia and Singapore indicate that with a residual pointing error of 10 μrad, operation is feasible up to 400 km; however, the Pointing, Acquisition, and Tracking Subsystem (PATS) experiences Signal-to-Noise Ratio (SNR) limitations beyond 150 km due to weak tracking-beacon signals [23].

The successful implementation of satellite-based QKD systems fundamentally depends on the alignment between orbital mechanics and quantum communication requirements. Different orbital configurations present distinct advantages for QKD applications, with altitude, inclination, orbital period, and coverage characteristics directly influencing protocol selection, link performance, and system viability.

These parameters critically determine key distribution efficiency, as quantum communication performance exhibits strong dependence on satellite elevation, access duration, and ground station visibility windows. A systematic evaluation of orbital dynamics reveals how specific orbital regimes optimize different aspects of QKD implementations.

Low Earth Orbit

Low Earth Orbit (LEO) satellites (500-1,200 km altitude) are crucial for quantum communications, as demonstrated by China's Micius satellite [24,25]. However, these systems face significant signal attenuation (20-30 dB downlink, up to 69 dB uplink) [26], with atmospheric turbulence causing transmittance fluctuations that impair protocol efficiency [18,27]. Their Earth proximity offers advantages including reduced diffraction losses [28], relaxed pointing requirements, and simplified adaptive optics needs [29] (Figure 2).

The BB84 protocol remains the preferred PM-DV- QKD choice due to its simplicity and proven security [28], typically implemented in S/C bands where single-photon detectors perform optimally [28]. Operational challenges include intermittent coverage with brief access windows (minutes per day) [3, 30] and demanding tracking requirements due to orbital motion [31]. While finite-size effects impact key rates, their effect is less pronounced in LEO [24].

Figure 2. Schematic diagram of the communication between a constellation of satellites and earth stations.

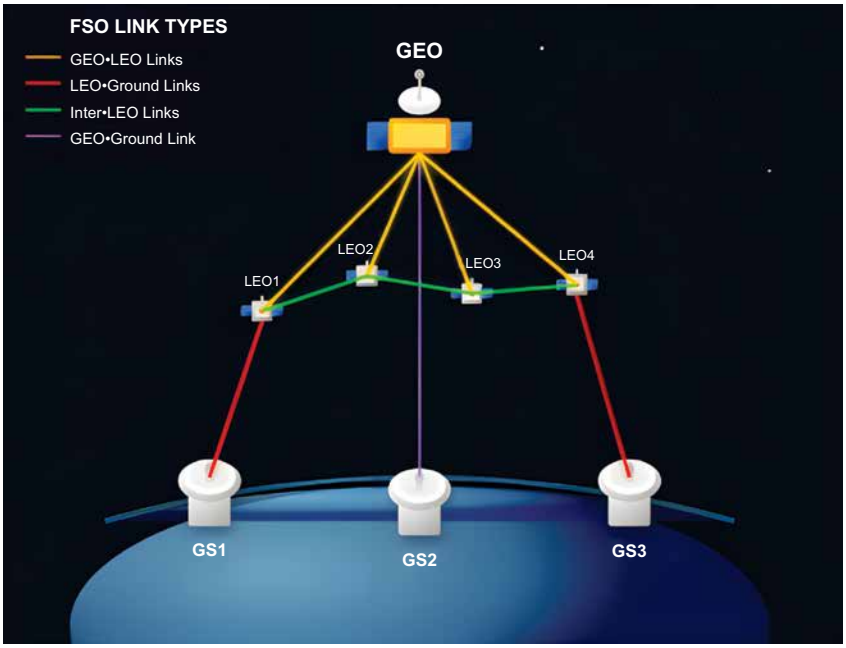

Yellow lines represent optical links between the GEO satellite and LEO CubeSats, which are interconnected by green lines. The red line indicates the link between an LEO and the ground stations (GSs), while the purple line shows the link from the GEO to the GSs.

Geostationary Orbit (GEO)

GEO satellites, located at an altitude of 35,786 km, have complementary characteristics that can be valuable for global quantum networks. This configuration allows permanent connections between the satellite and fixed ground stations, eliminating the complexity of handover between multiple satellites in LEO constellations.

Experiments with Micius have shown that with each handover in LEO, the system requires precise telescope realignment, new negotiation of QKD parameters, and interruption of the quantum key stream [3,25]. With the extended visibility of the GEO orbit, this problem would be mitigated, allowing continuous data accumulation [24], coverage also simplifies network management by reducing tracking complexity.

This operational difference is particularly relevant in CV-QKD, where link stability is crucial for error correction and privacy amplification protocols allowing the implementation of advanced post- processing schemes that require prolonged iterative exchanges between parties [32]. They offer the advantage of maintaining a continuous connection for extended periods, allowing extended QKD operations, and provide 24/7 availability without orbital restrictions [30]. A GEO system can point to a target user on demand in a short time, without the orbital constraints imposed on a LEO system by orbital mechanics [30]. Measurements of quantum-limited signals from a geostationary satellite can show total losses of 69 dB [26].

Satellite-Based CV-QKD: Challenges and Approaches

Satellite-based CV-QKD employs space-qualified optical communication hardware, enabling high- speed operation with IQ modulators and coherent receivers, making it a scalable and cost-effective option for global quantum networks [16,24,27,33,34].

CV-QKD protocols may have a practical advantage in free-space applications, especially in satellite-based channels, because a homodyne detector, in which the signal is coupled to an intense, narrow-band local oscillator (LO) beam, intrinsically filters out background radiation at

non-coincident wavelengths [26], this suggests that CV-QKD can operate in strong stray light conditions and potentially during the day, which for discrete variable protocols would require additional filtering, increasing attenuation and complexity [29].

CV-QKD in FSO and satellite-to-ground links has been investigated theoretically [24], detailed analyses address the feasibility of CV-QKD with Gaussian modulation in uplink scenarios, considering practical factors such as atmospheric turbulence and pointing errors under dynamic and time-varying orbital parameters [32].

Studies also analyze satellite-to-ground CV-QKD in the downlink scenario, which is more favorable for the transmission [33,35], preliminary experiments were carried out on signal transmission in FSO and satellite-to-ground links [24]. More recent proposals include the use of optical phase-shift keying (QPSK) signaling and dual heterodyne/threshold detection receivers to increase the reliability and feasibility of satellite entanglement-based FSO-CV-QKD systems [34].

One of the main challenges of CV-QKD is its lower robustness to transmission losses compared to DV-QKD [32]. With current homodyne detectors, positive secure key rates (SKR) can be achieved only for losses not exceeding 20–25 dB, which is very challenging in satellite-to-ground links [29]. For comparison, positive secure key rates with channel losses exceeding 69 dB (over fiber) have been demonstrated with DV-QKD [29].

Satellite-to-ground links are characterized by strongly variable channel attenuation (fading) [18], atmospheric turbulence induces phenomena such as beam wandering and beam broadening, which increase the average link loss [33] to higher orbits, key generation is affected by finite size effects, due to the limited number of symbols exchanged in a single satellite pass for high-loss channels [26], these can be mitigated by achieving higher transmission rates or considering multiple satellite passes [24].

Although CV-QKD employs standard telecom components, the need for a phase-stabilized local oscillator can raise implementation costs [27]. Atmospheric turbulence is stronger in the uplink, where the signal is affected early in the channel [33], whereas in the downlink most of the path is in vacuum, reducing turbulence effects [7, 35].

Simulations indicate that uplink QKD in the Micius orbit remains highly challenging and is more feasible in lower orbits [32]. To enhance uplink CV-QKD performance, optimization of orbital parameters, beam spot size, receiving aperture, and modulation variance has been proposed [32].

Segmenting the satellite pass and extracting keys from each segment, rather than from the entire pass, improves robustness against channel noise and enables secure key generation even under active collective attacks; this approach also mitigates fading, increasing the secure key rate and enabling communication with higher-altitude satellites [26].

The use of squeezed states extends CV-QKD operation to higher loss and noise levels under given security assumptions, though compression must be optimized for collective-attack scenarios [18]. CV-QKD with discrete modulation offers lower implementation requirements, acceptable key rates, and compatibility with existing infrastructure. In satellite-to-ground links, where payload weight is critical, the homodyne protocol with QPSK shows greater tolerance to excessive noise [33,34].

Conclusion

The coexistence of classical and quantum applications in different satellite orbits demonstrates the potential for faster and more secure global communication. While GEO satellites offer broad coverage for QKD over long distances, LEO satellites stand out for their low latency, essential for real-time applications.

Hybrid integration, as demonstrated by the Micius fiber-optic network, is already a reality and is expected to expand as satellite constellations evolve. The most promising solution for global quantum networks may lie precisely in the

synergistic integration of these two approaches, combining the high transmission rate of LEO satellites with the continuous coverage provided by GEO satellites [32].

This integration will, however, require significant advances on several fronts, including the development of dedicated QKD satellites, more robust protocols for operation in high-attenuation conditions, and the standardization of interfaces between the ground and space segments. The studies analyzed suggest that, with appropriate investment and technological development, satellite-based quantum networks could become an operational reality within the next decade, thus revolutionizing the secure communications landscape on a global scale.

Acknowlegement

This work has been fully/partially funded by the project Implementação do sistema CV-QKD em uma rede quântica real supported by Quantum Industrial Innovation (QuIIN) - EMBRAPII CIMATEC Competence Center in Quantum Technologies, with financial resources from the PPI IoT/Manufatura 4.0 of the MCTI grant number 053/2023, signed with EMBRAPII.

References

1. Rosana Ferreira Sampaio and Marisa Cotta Mancini. Estudos de revisão sistemática: um guia para síntese criteriosa da evidência científica. Brazilian journal of physical therapy, 11:83–89, 2007.
2. Barbara Kitchenham et al. Procedures for performing systematic reviews. Keele, UK, Keele University, 33(2004):1–26, 2004.
3. Yu-Ao Chen, Qiang Zhang, et al. An integrated space-to-ground quantum communication network over 4,600 kilometres. Nature, 589(7841):214–219, 2021.
4. Zhen Qu and Ivan B Djordjevic. High-speed free-space optical continuous-variable quantum key distribution enabled by three-dimensional multiplexing. Optics Express, 25(7):7919–7928, 2017.
5. Wimar Klop, Rudolf Saathof, et al. Qkd optical ground terminal developments. In International Conference on Space Optics—ICSO 2020, volume 11852, pages 388–403. SPIE, 2021.
6. Murali Krishna Pasupuleti. Quantum key distribution protocols: Security analysis and real-world implementations. International Journal of Academic and Industrial Research Innovations(IJAIRI), 05:267–278, 06 2025.
7. Sheng-Kai Liao, Wen-Qi Cai, et al. Satellite-to-ground quantum key distribution. Nature, 549(7670):43–47, 2017.
8. Sheng-Kai Liao, Hai-Lin Yong, et al. Long-distance free-space quantum key distribution in daylight towards inter-satellite communication. Nature Photonics, 11(8):509–513, 2017.
9. Giulia Guarda, Domenico Ribezzo, et al. Bb84 decoystate qkd protocol over long-distance optical fiber. In 2023 23rd International Conference on Transparent Optical Networks (ICTON), pages 1–4. IEEE, 2023.
10. Yuan Cao, Yu-Huai Li, et al. Long-distance free-space measurement-device-independent quantum key distribution. Physical Review Letters, 125(26):260503, 2020.
11. Xingyu Wang, Chen Dong, et al. Feasibility of space-based measurement-device-independent quantum key distribution. New Journal of Physics, 23(4):045001, 2021.
12. Dong Chen, Zhao Shang-Hong, et al. Measurement-device-independent quantum key distribution with q-plate. Quantum Information Processing, 14(12):4575– 4584, 2015.
13. Hoi-Kwong Lo, Marcos Curty, et al. Measurement-device-independent quantum key distribution. Physical review letters, 108(13):130503, 2012.
14. Qingquan Peng, Ying Guo, et al. Satellite-to-submarine quantum communication based on measurement-device-independent continuous-variable quantum key distribution. Quantum Information Processing, 21(2):61, 2022.
15. Dong Chen, Shang-Hong Zhao, et al. Measurement-device-independent quantum key distribution with pairs of vector vortex beams. Physical Review A, 93(3):032320, 2016.
16. Minh Q Vu, Hoang D Le, et al. Entanglement-based satellite fso/qkd system using dual-threshold/direct detection. In ICC 2022-IEEE International Conference on Communications, pages 3245–3250. IEEE, 2022.
17. Xinliang Wei, Lei Fan, et al. Optimizing satellite-based entanglement distribution in quantum networks via quantum-assisted approaches. In 2024 International Conference on Quantum Communications, Networking, and Computing (QCNC), pages 280–287. IEEE, 2024.
18. Nedasadat Hosseinidehaj and Robert Malaney. Cv-qkd with gaussian and non-gaussian entangled states over satellite-based channels. In 2016 IEEE Global Communications Conference (GLOBECOM), pages 1–7. IEEE, 2016.

19. Johannes Pseiner, Lukas Achatz, et al. Experimental wavelength-multiplexed entanglement-based quantum cryptography. Quantum Science and Technology, 6(3):035013, 2021.
20. Xiaoyu Ai, Robert Malaney, et al. Short codes and entanglement-based quantum key distribution via satellite. In 2017 Sensor Signal Processing for Defence Conference (SSPD), pages 1–5. IEEE, 2017.
21. Sebastian Ecker, Johannes Pseiner, et al. Advances in entanglement-based qkd for space applications. In International Conference on Space Optics—ICSO 2022, volume 12777, pages 925–945. SPIE, 2023.
22. Sheng-Kai Liao, Jin Lin, et al. Space-to-ground quantum key distribution using a small-sized payload on tiangong-2 space lab. Chinese Physics Letters, 34(9):090302, 2017.
23. Denis Naughton, Robert Bedington, et al. Design considerations for an optical link supporting intersatellite quantum key distribution. Optical Engineering, 58(1):016106–016106, 2019.
24. Daniele Dequal, Luis Trigo Vidarte, et al. Feasibility of satellite-to-ground continuous-variable quantum key distribution. npj Quantum Information, 7(1):3, 2021.
25. Aleksandr Khmelev, Alexey Duplinsky, et al. Eurasian-scale experimental satellite-based quantum key distribution with detector efficiency mismatch analysis. Optics Express, 32(7):11964–11978, 2024.
26. Ivan Derkach and Vladyslav C Usenko. Applicability of squeezed-and coherent-state continuous-variable quantum key distribution over satellite links. Entropy, 23(1):55, 2020.
27. Guoqi Huang, Ziang Song, et al. Enhanced performance of measurement-device-independent quantum key distribution over turbulent channels through adaptive optics: G. huang et al. Quantum Information Processing, 23(3):68, 2024.
28. Satya Ranjan Behera and Urbasi Sinha. Estimating the link budget of satellite-based quantum key distribution (qkd) for uplink transmission through the atmosphere. EPJ Quantum Technology, 11(1):66, 2024.
29. Davide Orsucci, Philipp Kleinpaß, et al. Assessment of practical satellite quantum key distribution architectures for current and near-future missions. International Journal of Satellite Communications and Networking, 43(3):164–192, 2025.
30. Angel Alvaro, Luis Pascual, et al. Caramuel: The future of space quantum key distribution in geo. In 2022 IEEE International Conference on Space Optical Systems and Applications (ICSOS), pages 57–65. IEEE, 2022.
31. Peide Zhang, Jaya Sagar, et al. End-to-end demonstration for cubesatellite quantum key distribution. IET Quantum Communication, 5(3):291–302, 2024.
32. Jin Cheng, Yujie Chen, et al. Feasibility and parameter optimization of ground-to-satellite uplink continuous-variable quantum key distribution. New Journal of Physics, 27(2):023011, 2025.
33. Jinyi Li, Jian Zhou, et al. Discrete modulation continuous variable quantum key distribution under fast fading channel. Physica Scripta, 99(11):115118, 2024.
34. Thang V Nguyen, Hoa T Le, et al. Enhancing design and performance analysis of satellite entanglement-based cv-qkd/fso systems. IEEE Access, 11:112097–112107, 2023.
35. Yichen Gao, Guanqun Song, and Ting Zhu. Optimizing global quantum communication via satellite constellations. arXiv preprint arXiv:2501.00280, 2024.

International Overview of Quantum Security: Mapping Organizations, Technologies, and Use Cases in PQC and QKD

Mabel Diz Marques Mota[1]*, João Carlos Passos[1], Alexandre de Santa Bárbara[1], Guilherme João Musse Neto[1], Gabrielly da Silva Roman[1], João Marcelo Silva Souza[1]

[1]SENAI CIMATEC University, Center of EMBRAPII CIMATEC in Quantic Technologies; Salvador, Bahia, Brazil

The article presents an international overview of the quantum security ecosystem, focusing on Post-Quantum Cryptography (PQC) and Quantum Key Distribution (QKD). The methodology involved a systematic mapping of 85 active organizations, revealing the predominance of the private sector (84.7%), with the highest concentration in the United States (30.59%) and China (14.12%). The data indicate a strong presence in the development of hybrid solutions (65.88%), which can be attributed to the pursuit of greater implementation flexibility, particularly in contexts of technological transition. These solutions are directly associated with strategic sectors such as telecommunications (31 organizations), cloud computing (17), and finance/government (16). Use cases demonstrate applications in IoT, 5G networks, blockchain, and digital identity, with notable contributions from companies such as Infineon, Toshiba, ID Quantique, CryptoNext, Microsoft, and DigiCert. Additionally, the results suggest increasing maturity, commercial expansion, and the relevance of PQC and QKD for technological resilience and sovereignty, establishing these technologies as pillars of secure digital infrastructures in the era of quantum computing.

Keywords: Quantum Communication. Post-Quantum Cryptography. Quantum Key Distribution. PQC. QKD.

The advancement of quantum computing threatens to compromise the main public-key algorithms currently in use, such as RSA (based on integer factorization) and ECC (elliptic curves), whose security relies on mathematical problems that quantum algorithms, such as Shor's, can solve in polynomial time [1]. In this context, two approaches are being explored: Post-Quantum Cryptography (PQC), which employs algorithms resistant to quantum attacks on classical systems [2], and Quantum Key Distribution (QKD), which ensures secure key generation and distribution based on physical principles, such as no-cloning and entanglement [3].

PQC is undergoing standardization by the National Institute of Standards and Technology (NIST) [2], while QKD already has commercial applications in optical networks and satellite-based systems [4]. Both are being adopted complementarily in sectors such as telecommunications, cloud computing, and financial services [5]. However, there is still a lack of studies that systematically analyze how these technologies are being applied globally, considering the nature of organizations, the sectors served, and implementation models.

This article presents a mapping of international initiatives in PQC and QKD, identifying their geographical distribution, implementation approaches, and use cases. The study is structured as follows: Section 2, theoretical foundations of PQC and QKD; Section 3, methodological aspects; Section 4, analysis of results; and Section 5, final considerations.

Theoretical Framework

A Quantum Key Distribution (QKD) protocol enables two spatially separated parties (Alice and Bob) to share and generate random, secure sequences—secret keys [8]. Unconditional security is guaranteed by the laws of quantum mechanics, making it impossible for an eavesdropper (Eve) to interfere with the communication without being detected. A protocol can be divided into two main stages: the distribution of quantum states and post-

Received on 20 October 2025; revised 22 January 2026.
Address for correspondence: Mabel Diz Marques Mota. Av. Orlando Gomes, 1845 - Piatã, Salvador – BA – Brazil, Zipcode: 41650-010. E-mail: mabel.mota@fieb.org.br / mabeldizmarques@gmail.com.

J Bioeng. Tech. Health 2025;9(2):169-172

processing. Modern communication revolves around the Internet as a fundamental building block for interactions between parties, requiring data protection and privacy. QKD enables the construction of secure communication networks using infrastructures compatible with existing optical networks [8].

Post-Quantum Cryptography (PQC) is based on identifying mathematical problems that are difficult to solve even by fully operational quantum computers [5]. The security of these algorithms lies in the intrinsic difficulty of these problems, not in the computational limitations of classical computers. PQC emerges as a promising solution to protect future computer networks and machines in the era of quantum computing. Unlike QKD, which relies on quantum mechanical properties for symmetric key distribution, PQC encompasses a family of asymmetric key schemes (public-key cryptography) that are secure against both classical and quantum attacks. As an example, Amazon has introduced a hybrid KYBER mode for its AWS Key Management Service [9], demonstrating the adoption of PQC in cloud environments for key security.

Critical Infrastructures (CI) and Industrial Control Systems (ICS) are highly vulnerable to cyberattacks, with the potential for massive economic and social losses [5]. The transition to post-quantum cryptography in these environments is crucial [5].

The implementation of post-quantum cryptography (PQC) and quantum key distribution (QKD) is essential to secure future communications against the threat of fault-tolerant quantum computers [5]. Both technologies are considered the most promising for future quantum-secure cryptography [5].

Materials and Methods

This study conducted systematic mapping, with manual collection of secondary data between May and July 2025. The data sources included the Quantum Insider platform, technical reports, institutional websites, and public documents from companies, research centers, and governmental initiatives.

A sample was prospected, consisting of organizations with identified activities in technologies based on PQC and/or QKD. The selection was based on public evidence of development, products, or technological applications. The variables considered for analysis were: country of origin, type of organization, adopted technology, implementation approach (software, hardware, or both), application sector, and use cases.

The data were organized and tabulated in a Microsoft Excel spreadsheet and subjected to descriptive analysis using relative frequency, with the aim of characterizing the global quantum security ecosystem.

Results and Discussion

The data collection and analysis enabled the identification of 85 active initiatives involving technologies based on PQC and/or QKD. Figure 1 presents the geographical distribution of the mapped organizations.

The United States leads with 26 organizations (30.59%), followed by China with 12 (14.12%), forming a technological polarization axis that

Figure 1. Geographical distribution.

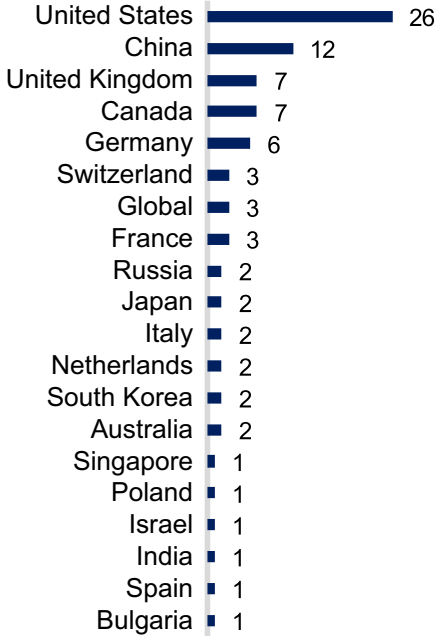

reflects the centrality of quantum security in digital sovereignty and industrial competitiveness agendas. The distributed presence in other countries demonstrates that, while concentrated, the technological race is already expanding to various markets and economic blocs.

The predominance of the private sector is highlighted in Figure 2. Fifty-four established companies and 18 startups account for 84.7% of the initiatives. This corporate leadership is complemented by 9 research centers, 3 cooperative initiatives, and 1 governmental body, forming a network that combines corporate innovation, academic research, and collaborative efforts.

This hybrid structure is typical of emerging technological fields [6,7], where knowledge transfer occurs through continuous interactions among universities, companies, governments, and society, enabling rapid translation of research into commercial applications.

Figure 3 indicates that 65.88% of solutions adopt hybrid hardware and software approaches, followed by 31.76% exclusively in software and 2.35% solely in hardware. The predominance of hybrid models signals a pursuit of flexibility, scalability, and robustness—essential attributes for integration into complex digital environments and for ensuring security against multiple attack vectors.

The sectoral analysis (Figure 4) shows that telecommunications concentrate the highest number of initiatives (31 organizations), followed by cloud computing (17), finance and government (16), IoT/automation (8), blockchain/fintech (7), and digital identity (6). This distribution highlights the prioritization of sectors critical to digital infrastructure and services.

Figure 3. Type of technological implementation.

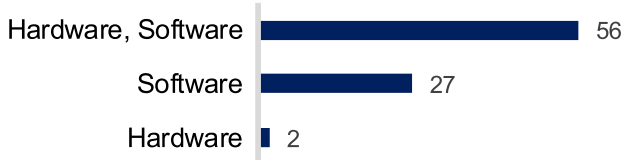

The use cases underscore the maturity and strategic relevance of these technologies:

(i) IoT and Automation: Infineon integrates PQC into chips to secure data in smart factories, autonomous vehicles, and connected homes, ensuring resilience even in resource-constrained devices.

(ii) Telecommunications Networks: Toshiba, in partnership with BT, operates an urban quantum network in London, protecting financial, governmental, and healthcare communications, including satellite-based transmissions.

(iii) Finance and Government: ID Quantique secures transactions and governmental communi--cations on Orange's fiber network (France), complying with regulations such as GDPR.

(iv) Blockchain and Fintech: CryptoNext applies PQC to strengthen smart contracts and digital wallets, preventing quantum attacks and enhancing trust in decentralized platforms.

Figure 2. Organizational profile.

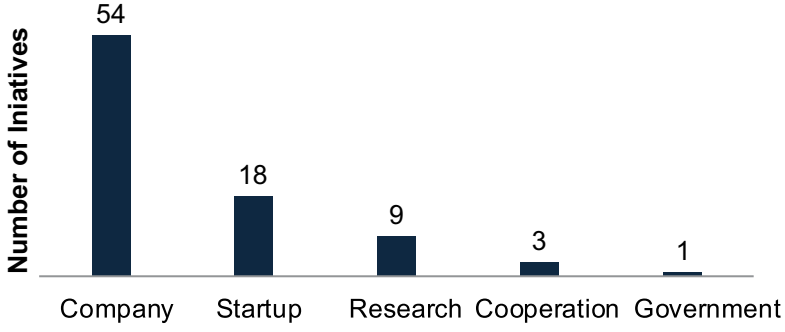

Figure 4. Sectoral applications.

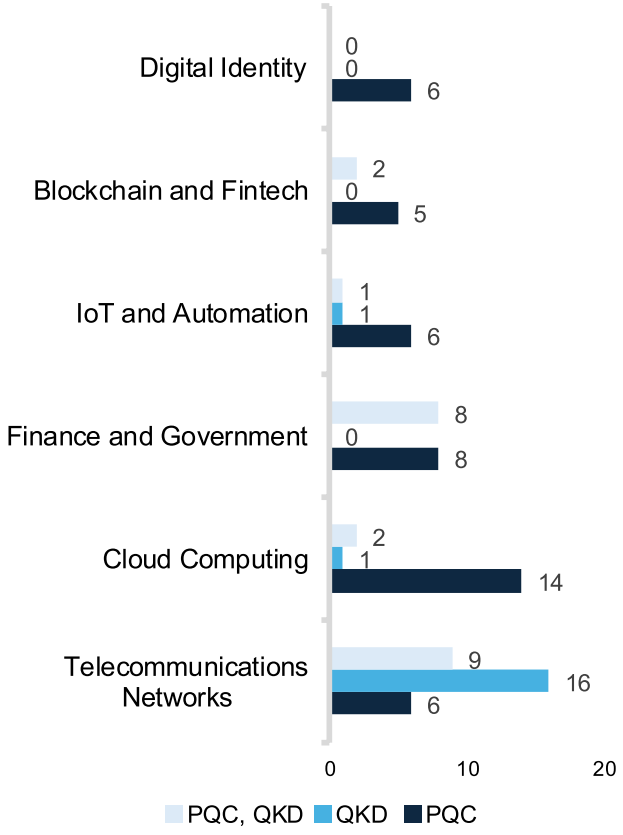

(v) Cloud Computing: Microsoft incorporates PQC into Azure with Post-Quantum TLS and researches QKD for secure networks, protecting sensitive data in scalable environments.

(vi) Digital Identity: DigiCert provides quantum-resistant certificates, used by Panasonic in India, and combats deepfakes with signed metadata for secure authentication.

In this context, the results reveal a global ecosystem concentrated in strategic hubs, with corporate leadership and hybrid solutions targeting critical sectors. PQC and QKD are advancing toward commercial maturity, becoming essential for secure communication and digital sovereignty.

Conclusion

This study revealed the maturity and strategic impact of PQC/QKD within a dynamic global ecosystem, with 85 mapped organizations, led by technological hubs such as the United States (30.59%) and China (14.12%). The predominance of hybrid solutions (65.88%) and the strong presence of the private sector (72 organizations) highlight the pursuit of flexibility and innovation in response to the threats posed by quantum computing. Additionally, they demonstrate maturity in critical sectors, with practical applications led by companies such as Infineon, Toshiba, ID Quantique, CryptoNext, Microsoft, and DigiCert, addressing specific demands in areas such as 5G network protection, cloud security, digital authentication, and decentralized financial transactions. These advancements reinforce quantum security as a cornerstone for resilient digital infrastructures, aligned with regulatory requirements and technological sovereignty.

References

1. P. W. Shor, "Algorithms for quantum computation: discrete logarithms and factoring," Proceedings 35th Annual Symposium on Foundations of Computer Science, 1994.
2. NIST, “Post-Quantum Cryptography Standardization,” [Online]. Available: https://csrc.nist.gov/projects/post-quantum- cryptography
3. V. Scarani et al., “The security of practical quantum key distribution,” Rev. Mod. Phys., vol. 81, no. 3, pp. 1301–1350, 2009.
4. Y. Zhang et al., “Continuous-variable quantum key distribution system: past, present, and future,” arXiv preprint arXiv:2310.04831, 2023.
5. Del Moral JO et al. Cybersecurity in critica l infrastructures: A post-quantum cryptography perspective. IEEE Internet of Things Journal, v. 11, n. 18, p. 30217-30244, 2024.
6. Cai Y et al. Triple helix or quadruple helix: which model of innovation to choose for empirical studies?. Minerva, v. 60, n. 2, p. 257-280, 2022.
7. Roman M, Fellnhofer K. Facilitating the participation of civil society in regional planning: Implementing quadruple helix model in Finnish regions. Land use policy, v. 112, p. 105864, 2022.
8. Dias MA et al. Distribuição quântica de chaves com modulação não gaussiana: protocolos, desempenho e segurança. 2023.
9. BAavdekar R et al. Post quantum cryptography: Techniques, challenges, standardization, and directions for future research. arXiv preprint arXiv:2202.02826, 2022.

Exploring Unmanned Aerial Vehicles Communication in Maritime Environments: Challenges and Perspectives

Aldalice Rodrigues Dias[1]*, Miguel Oliveira do Amaral[1], Amanda Andrade Alves Barreto[1], Arthur Ribeiro de Cerqueira[1], Leonardo Ferreira Daltro[1]

[1]National Industrial Service - Integrated Manufacturing and Technology Center, Drone Competence Center; Salvador, Bahia, Brazil

With the continuous advancement of embedded technologies and the growing demand for remote and autonomous operations, Unmanned Aerial Vehicles (UAVs) have been increasingly employed in a variety of maritime applications, including platform inspections, cargo transport, search and rescue missions, environmental monitoring, and open-sea surveillance. However, maintaining reliable, high- performance communication between UAVs and control stations remains one of the main operational challenges, primarily due to the lack of fixed infrastructure, the long distance from shore, and adverse and highly variable environmental conditions. This work presents an exploratory literature review, categorizing the key factors that influence communication performance: latency, data transfer rate, frequency bands (VHF, L, C, Ku, Ka), and phenomena such as signal refraction and multipath propagation over the sea. The limitations of traditional maritime communication systems, such as VHF and L-band, and their impacts when adapted to aerial missions are analyzed in detail. Emerging technologies, including Low Earth Orbit (LEO) satellite constellations, High-Altitude Platform Stations (HAPS), and hybrid architectures that integrate aerial, maritime, and satellite links, show strong potential to expand coverage and reduce latency in challenging oceanic environments. In addition, prospects for sixth-generation (6G) networks are discussed, highlighting their potential to enable ultra-responsive control, enhanced link resilience, and massive data transmissions in remote areas. Selecting the most suitable communication architecture must account for mission type, data volume, and operational context. Despite recent advances, significant gaps remain, underscoring the need for continued research and innovation to develop resilient, mission-tailored communication architectures for UAVs operating in maritime domains.

Keywords: Unmanned Aerial Vehicles. Maritime Communication. Satellite Communication Systems. Maritime Environments.

With the advancement of embedded technologies and the growing demand for autonomous solutions, Unmanned Aerial Vehicles (UAVs) have expanded their applications beyond terrestrial environments, reaching challenging maritime scenarios [1,2]. In open-sea operations, UAVs are increasingly employed for equipment transport, platform inspection, navigation support, search and rescue, monitoring, and surveillance of remote areas, establishing themselves as strategic tools [3,4].

However, the effectiveness of these operations relies heavily on communication reliability, particularly in missions requiring real-time data transmission, such as high-resolution video streaming and advanced telemetry [4,5]. While terrestrial networks (4G, 5G) can deliver high speeds and low latency in coastal areas, the maritime environment lacks fixed infrastructure, leading to a dependence on technologies such as VHF radio, microwave links, and satellite communications [2]. Moreover, environmental factors including climate variability, atmospheric attenuation, and sea-surface reflection affect signal propagation, making it difficult to maintain stable links [1,6].

Given these challenges and the limited maturity of UAV applications in open-sea operations, this work examines the technical constraints imposed by the maritime environment, with a focus on communication systems. It presents existing solutions and discusses potential approaches to enhance reliability and performance in maritime UAV operations, particularly in those requiring real-time connectivity.

Received on 22 October 2025; revised 19 January 2026.
Address for correspondence: Aldalice Rodrigues Dias. Av. Orlando Gomes, 1845 - Piatã, Salvador – BA – Brazil, Zipcode: 41650-010. E-mail: aldalice.rd@gmail.com.

J Bioeng. Tech. Health 2026;9(2):173-178

Materials and Methods

This study adopts a qualitative, exploratory approach based on a technical literature review conducted using the IEEE Xplore, Scopus, and Google Scholar databases. Initially, the search focused on articles published within the last 10 years, with an emphasis on the application of UAVs in maritime and offshore operations. The search strategy followed a Boolean logic approach, using combinations such as: "UAV AND maritime communication AND satellite links" OR "UAV AND offshore communication" NOT "terrestrial".

Priority was given to publications directly addressing communication between UAVs and their ground control stations, considering technologies such as VHF/UHF radio links and satellite communications. During the analysis, it was observed that a significant portion of the publications focused on scenarios beyond the original scope, such as UAV-to-UAV mesh networks, mobile buoys powered by UAVs, and other forms of hybrid architectures. Although these did not strictly meet the initial selection criteria, some of these works were incorporated for providing relevant insights, including coastal applications, adapted naval technologies, and recent innovations in the field. The inclusion of these studies aimed to support the comparison between typical challenges of maritime communication and those encountered when adapting these solutions to UAVs operating in the same environment.

Data analysis was conducted through thematic categorization, grouping the main technical challenges and communication strategies identified in the literature. This approach enabled a reflection on current technological gaps and the identification of potential pathways for developing solutions better aligned with the demands of the maritime context.

Literature Review

This section analyzes the limitations and challenges of communication technologies employed in maritime environments, as well as their adaptation to UAV operations. The analysis covers: latency, which is essential for real-time control; data transfer rate, a key factor for video streaming, telemetry, and sensor data transmission; frequency bands (VHF, L, C, Ku, and Ka) and their suitability for maritime use; (3.4) environmental conditions, such as signal refraction and multipath propagation; and the current landscape of applications, highlighting limitations and gaps in long-range and open-sea missions.

Latency

Latency is one of the most critical factors in long-range maritime operations, where communication must ensure that command transmission and data reception, such as images, videos, or telemetry, occur with minimal delay [2].

In high-criticality missions, even small delays can compromise UAV control and, in extreme cases, lead to aircraft loss [7,8]. In operations such as search and rescue or real-time inspections, the literature recommends values close to 10 ms at the 99.9th percentile in controlled LTE environments [7-9]. Outside areas covered by terrestrial networks, performance degrades significantly. GEO satellites typically present 550–700 ms RTT [10], whereas LEO constellations can reduce this to 20–50 ms [4,6,10]. Emerging technologies such as High-Altitude Platform Stations (HAPS) [11] can achieve latencies below 10 ms, and hybrid architectures in which UAVs act as relay nodes combined with LEO satellite backhaul are emerging as promising solutions to mitigate critical delays in open-sea operations [12,16].

Data Transfer Rate

The data transfer rate is a determining factor for advanced UAV applications in maritime environments, such as high-definition video streaming, high-frequency telemetry, and integration with high-sampling-rate sensors [4] [13]. While vessels typically require only voice or

text communications, UAVs demand significantly higher throughput. Long-range and low-power technologies such as Long Range (LoRa) and Long Range Wide Area Network (LoRaWAN) provide good coverage for intermittent data but, with typical throughput below 50 kbps, are unsuitable for continuous video transmission [13] [4]. In coastal regions, 4th Generation (4G) and 5th Generation (5G) networks can exceed 100 Mbps with latencies below 20 ms, provided there is nearby coverage [14,15].

Within the horizon of emerging technologies, communication architectures oriented toward 6th Generation (6G) are integrating Artificial Intelligence (AI) and Machine Learning (ML) capabilities to optimize dynamic link selection, predictive routing, and adaptive spectrum allocation in maritime operations [16]. Techniques such as Massive Multiple-Input Multiple-Output (Massive MIMO), Federated Learning, and Over-the-Air Computation (AirComp) show potential to enhance the resilience and efficiency of UAV communications even under energy and line-of-sight constraints [16,17].

Frequency Bands

The frequency band used in communication systems is a determining factor for transmission performance, as it directly influences range, data rate, and latency in UAV–maritime communications [4,18]. In general, lower frequencies provide greater range at lower data rates, while higher frequencies allow higher throughput but with limited range and increased susceptibility to interference and obstacles [18,19].

Very High Frequency (VHF)

Covering 30–300 MHz, with predominant maritime use between 156–174 MHz, VHF is widely employed for voice communications between vessels and coastal stations, and between 118–137 MHz in aviation [4,9,19]. It is characterized by equipment simplicity, line- of-sight reliability, and resistance to atmospheric interference. However, its limited bandwidth makes it unsuitable for high-rate data or video transmissions, restricting its use to commands and simple messages [4,19].

L-Band Communication

Operating between 1–2 GHz, the L-Band is used in mobile services, aeronautical communications, GPS, and satellite telephony [20]. It features low attenuation in rain and fog, good signal penetration, and global coverage through LEO satellites. However, its limited bandwidth restricts its application for large data volumes [20].

C-Band Communication

Operating from 4–8 GHz, the C-Band is stable and weather-resistant, widely used in satellite television broadcasting and fixed-platform communications, including Very Small Aperture Terminal (VSAT) systems [21,22]. The C Band offers good signal stability and lower susceptibility to rain attenuation compared to higher frequency ranges such as Ku or Ka bands. This makes it suitable for robust communications in open-sea environments, where adverse weather conditions are frequent [22].

Ku-Band Communication

Operating in the 12–18 GHz range, the Ku Band stands out for its higher bandwidth, enabling the transmission of larger volumes of data. It is widely used in satellite internet services and high-definition digital broadcasting, including on ships and commercial aircraft [22]. However, it is more susceptible to rain fade. Studies indicate that such effects can be mitigated through techniques such as adaptive modulation and link redundancy, although these measures may increase latency and operational costs [18,23].

Ka-Band Communication

Operating between 26.5–40 GHz, the Ka-Band offers higher speeds than the previous bands and is adopted by modern constellations such as OneWeb and Starlink [24][25]. It requires highly directional antennas and sophisticated tracking systems, increasing cost, power consumption, and complexity, especially on mobile platforms [25,26].

Environmental Conditions

The maritime environment imposes additional challenges on UAV communications, not only due to the absence of terrestrial infrastructure but also because of physical and atmospheric phenomena that degrade signal quality [14,18,19]. Conditions such as storms, fog, high humidity, and abrupt temperature variations increase attenuation and reduce link stability [18].

In addition, the sea surface promotes multipath fading caused by the reflection of electromagnetic waves, resulting in delay spread, phase distortions, and packet loss [18,19]. These effects are more critical at higher frequencies and are amplified by the altitude and speed dynamics of UAVs. Strategies such as antenna diversity, adaptive modulation, and error correction coding are recommended to mitigate these impacts [13,16].

Applications Overview: UAV Operational Scenario

The deployment of UAVs in open-sea environments remains relatively uncommon, with operations predominantly concentrated in coastal areas or near offshore platforms equipped with supporting infrastructure [4,6,14]. In these regions, the most frequent applications include environmental monitoring, offshore structure inspection, navigation assistance, search and rescue, border surveillance, and light cargo delivery [24]. Despite gradual expansion, long-endurance missions and fully autonomous operations in open-sea contexts are largely confined to military or experimental domains. This limitation is primarily attributed to challenges in connectivity, energy autonomy, and link resilience [4,6].The principal technical challenges identified in the literature include: (i) the absence of fixed communication infrastructure, (ii) severe bandwidth limitations for real-time data transmission, (iii) susceptibility to link failures caused by adverse environmental conditions, and (iv) the complexity of integration with existing naval systems [2,5].

Results and Discussion

Literature indicates that no single communication solution guarantees robust connectivity for UAVs in maritime environments, as each scenario presents distinct constraints related to range, data demand, energy availability, and environmental conditions.

As discussed by Pan and colleagues, Yu and colleagues, and Gorczak and colleagues in their studies presented that latency is a limiting factor for time-sensitive missions, particularly in search and rescue operations and real-time inspections [7-9]. Nomikos and colleagues, Ghazaliand colleagues, Wei and colleagues, and Paladin and colleagues highlight that data rate directly constrains continuous video streaming and the integration of complex sensors [4,13-15].

Regarding frequency bands [9,19,20], lower bands such as VHF and L offer robustness under adverse conditions and long-range coverage, but lack sufficient throughput for high-demand applications. In contrast, Ku and Ka-bands support high data rates and multiple video streams, although they are more susceptible to atmospheric attenuation and require high- precision tracking systems, which increase cost and complexity, especially in small UAV platforms. Section 3.4 further emphasizes that multipath fading, delay spread, and rain attenuation can significantly degrade link quality, particularly at higher frequencies [18,19,22].

In practical applications, selecting an appropriate communication architecture involves

balancing range, robustness, and throughput capacity. For instance, low-latency critical missions, such as search and rescue or real-time offshore inspections, can benefit from LEO satellite links (e.g., Starlink, OneWeb), which offer data rates between 50 and 200 Mbps with latencies below 50 milliseconds. However, these systems require precise tracking mechanisms and a reliable power source. Periodic data collection missions, including environmental and meteorological monitoring, may utilize GEO satellites or VHF/UHF bands, which provide lower data rates but are sufficient for intermittent transmissions, ensuring wide coverage and reduced power consumption. Coastal operations can leverage LTE/5G networks, achieving data rates above 100 Mbps and latencies below 20 milliseconds, although these depend on proximity to terrestrial infrastructure. For open-ocean scenarios, hybrid architectures, such as combinations of LEO satellites with HAPS, or integration with Unmanned Surface Vehicles and buoy-based repeaters, can extend coverage while maintaining moderate latency and high throughput.

Hybrid integration stands out as the most promising approach. Recent solutions incorporate UAVs as relay nodes, HAPS platforms, and multi-hop links, forming collaborative surface–air–satellite networks. These architectures offer a balance between performance and cost, while adapting to diverse mission profiles. Future integration with 6G networks may enable terabit-per-second data rates and sub-millisecond latencies, supporting ultra-responsive control and multiple simultaneous high-definition video streams, even in remote regions.

Beyond raw transmission capacity, link resilience is essential. As noted in the Section "Environmental Conditions", environmental phenomena can cause abrupt channel degradation. Therefore, robust architectures must incorporate channel redundancy, failover protocols, and fallback operational modes. The application of AI and ML, already proposed in 6G frameworks, could facilitate automatic switching between radio frequency (RF), Free-Space Optics (FSO), and satellite links, as well as predictive routing to avoid congestion and low-coverage areas.

Nevertheless, significant gaps remain in the literature. Most studies emphasize technical performance, with limited consideration of economic and logistical feasibility, particularly regarding the implementation of hybrid architectures in small and medium UAV platforms. There is also a lack of comprehensive research on integration with existing naval systems and the development of unified communication protocols that ensure full interoperability among aerial, maritime, and space-based assets.

In summary, the future of UAV connectivity in maritime environments will be shaped by the convergence of multiple technologies, supported by intelligent network management. Progress depends not only on advancing communication links, but critically on the ability to integrate heterogeneous systems adaptively, ensuring coverage, performance, and reliability under extreme conditions.

Conclusion

The analysis conducted demonstrates that, while the deployment of UAVs in maritime scenarios is technically feasible and holds significant potential, communication remains one of the primary bottlenecks for large-scale adoption. Optimal communication architecture must be treated as a core element of system design rather than an isolated decision.

The findings indicate that most technologies traditionally employed in the maritime sector, although robust, are unsuitable for continuous high-rate data missions. The architectures reviewed present viable alternatives to mitigate these limitations, yet still face challenges such as atmospheric attenuation, tracking complexity, and bandwidth constraints within specific frequency bands.

Emerging developments point toward intelligent hybrid architectures that combine satellite, radio, and HAPS links, supported by adaptive protocols and AI-driven coordination. Technologies such as Massive MIMO, dynamic beamforming, and integration with 6G networks have the potential to significantly transform airborne communication,

extending coverage while reducing latency. Economic feasibility, maintenance logistics, and regulatory compliance will be decisive for transitioning these solutions from prototypes to operational deployment.

Given the existing technological gap, UAV connectivity in open-sea environments emerges not only as a promising research frontier but also as a strategic enabler for more reliable, responsive, and adaptive aero-maritime operations. This evolution is expected to directly impact safety, operational efficiency, and the expansion of autonomous capabilities within the maritime domain.

References

1. Xiang TZ, Xia GS, Zhang L. Mini-unmanned aerial vehicle-based remote sensing: techniques, applications, and prospects. IEEE Geosci Remote Sens Mag. 2019;7(3):29-63.
2. Akhtar MW, Saeed N. UAVs-enabled maritime communications: opportunities and challenges. IEEE Syst Man Cybern Mag. 2023;9(3):2-8. Available from: https://ieeexplore.ieee.org/document/10123456
3. Duan GJ, Zhang PF. Research on application of UAV for maritime supervision. J Shipp Ocean Eng. 2014;4:322-326. Available from: http://www.davidpublisher.org/Public/uploads/Contribute/55c9c3c7f2f9e.pdf
4. Nomikos N, Tsiropoulou E, Pappas N, et al. A survey on UAV-aided maritime communications: deployment considerations, applications, and future challenges. IEEE Open J Commun Soc. 2022;4:56-78.
5. Niknami N, Saeed N, Akhtar MW, et al. Maritime communications—current state and future potential with SDN and SDR. Network. 2023;3(4):563-584. Available from: https://www.mdpi.com/2673-8732/3/4/34
6. Zeng Y, Zhang R, Lim TJ. Wireless communications with unmanned aerial vehicles: opportunities and challenges. IEEE Commun Mag. 2016;54(5):36-42.
7. Pan G, et al. Introduction to UAV communications. In: UAV communications: modeling and analyses. Singapore: Springer Nature; 2024. p. 1-21.
8. Yu Z, et al. Fault-tolerant cooperative control of unmanned aerial vehicles. Singapore: Springer; 2024.
9. Gorczak P, et al. Robust cellular communications for unmanned aerial vehicles in maritime search and rescue. In: 2019 IEEE Int Symp Safety Security Rescue Robotics (SSRR); 2019. p. 229-234.
10. Frąckiewicz M. Mobile & portable satellite internet in 2025: the ultimate guide to Starlink Roam, HughesNet, Inmarsat, Viasat & more [Internet]. TS2 Space; 2025. Available from: https://ts2.tech/en/2025-satellite-internet-showdown-starlink-vs-viasat-vs-hughesnet-vs-oneweb-more/
11. Carter CM, et al. High-altitude platforms (HAPS)—a promise not reached. In: Unmanned aircraft systems in the cyber domain; 2019.
12. Dang KD, Le HD, Nguyen CT, Pham AT. Cooperative HARQ-aided multiple UAVs in optical aerospace backhaul networks. IEEE Access. 2023;11:138247-138260.
13. Ghazali MH, Teoh K, Rahiman W. A systematic review of real-time deployments of UAV-based LoRa communication network. IEEE Access. 2021;9:124817-124830.
14. Wei T, et al. Hybrid satellite-terrestrial communication networks for the maritime Internet of Things: key technologies, opportunities, and challenges. IEEE Internet Things J. 2021;8(11):8910-8930.
15. Paladin Z, et al. The 5G-supported unmanned aerial vehicles for emergency cases response. In: MIPRO; 2023.
16. Nomikos N, et al. Improving connectivity in 6G maritime communication networks with UAV swarms. IEEE Access. 2024;12:18739-18751.
17. Zhao H, et al. Space-air-ground-sea integrated network with federated learning. Remote Sens. 2024;16(9):1640.
18. Barclay LW. Propagation of radiowaves. Vol. 502. London: IET; 2003.
19. Lázaro F, et al. VHF data exchange system (VDES): an enabling technology for maritime communications. CEAS Space J. 2019;11(1):55-63.
20. Liu J. Overview of low earth orbit satellite communication systems. Appl Comput Eng. 2025;145(1):1-6.
21. Raj A, Jha BM, Sharma AK. Design of compact hybrid profiled corrugated feed horn for SATCOM C band. Int J Syst Assur Eng Manag. 2023;14(5):1841-1846.
22. Singh H, et al. Proposed model for radio wave attenuation due to rain (RWAR). Wirel Pers Commun. 2020;115(1):791-807.
23. Foschini GJ, Gans MJ. On limits of wireless communications in a fading environment when using multiple antennas. Wirel Pers Commun. 1998;6(3):311-335.
24. Del Portillo I, Cameron BG, Crawley EF. A technical comparison of three low earth orbit satellite constellation systems to provide global broadband. Acta Astronaut. 2019;159:123-135.
25. Zhao J, et al. Beam tracking for UAV-mounted SatCom on-the-move with massive antenna array. IEEE J Sel Areas Commun. 2018;36(2):363-375.
26. IEEE Communications Society. Starlink LEO network goes live [Internet]. New York: IEEE ComSoc; cited 2025 Aug 9. Available from: https://www.comsoc.org/node/19101.

A Review of Central Pattern Generator-Based Approaches for Quadruped Robot Locomotion

João Pedro Almeida Miranda Silva[1], Felipe Mohr Santos[1]*
[1]SENAI CIMATEC, Robotics Department, Salvador, Bahia, Brazil

This paper reviews locomotion control approaches for quadruped robots, with a specific focus on methods based on Central Pattern Generators (CPGs). CPGs are bio-inspired neural circuits that generate rhythmic motor commands, offering a computationally efficient solution for controlling complex robotic movements. The study explores fundamental concepts of quadruped locomotion, including gait types and parameters and details the application of CPGs, highlighting the use of different oscillators, such as Hopf and Van der Pol, and their integration with Inverse Kinematics. The review emphasizes the potential of hybrid control techniques, which combine CPGs with learning-based methods to enhance the robot's adaptability and robustness on various terrains. The paper concludes that CPGs, especially when combined with hybrid control strategies, present a promising and efficient solution for achieving stable and adaptive locomotion in quadruped robots.
Keywords: Quadruped Robot. Locomotion Control. Bioinspired Control. Central Pattern Generator.
Abbreviations: CPG, Central Pattern Generator. RL, Reinforcement Learning. ZMP, Zero Moment Point. MPC, Model Predictive Control. WBC, Whole-Body Control. VMC, Virtual Model Control. SLIP, Spring-Loaded Inverted Pendulum.

Quadruped robotics has gained increasing prominence due to its versatility in various applications, such as inspections in confined and hard-to-reach places, exploration of uneven terrain, and activities that require climbing [1-3].

This versatility is mainly due to the articulated structure of its legs, which gives it versatile mobility to ensure stability, optimizing locomotion in different environments [1,4].

Several methods for controlling the locomotion of quadrupedal robots have emerged over the past few years, whether model-based or learning-based methods. Among them, the Central Pattern Generator (CPG) is an approach that combines utility and convenience since it can control the robot's locomotion using little computational power [5].

This paper aims to explore the main concepts related to quadruped robot locomotion, with an emphasis on control techniques based on Central Pattern Generators and their applications. The methodology for this review involved a systematic search of scientific databases, including IEEE Xplore, Scopus, and Google Scholar. The search was conducted using keywords such as "quadruped robot," "locomotion control," "Central Pattern Generator," and "bio-inspired control."

The selection criteria prioritized review articles and research papers with robust simulation or experimental results, with a focus on publications from the last decade to ensure the inclusion of state-of-the-art techniques. We also present the fundamental concepts of quadruped locomotion, from the concepts of gait to a brief presentation of other control techniques used, and the Central Pattern Generators as a technique for controlling the locomotion of quadruped robots, presenting the different oscillators used and different applications. Nevertheless, we finally present final considerations on the use of CPGs for the purpose of quadruped robot locomotion.

Quadruped Robots Locomotion

The locomotion of a quadruped robot can be defined as a coordinated set of movements of its four legs, giving the robot the ability to move around the environment [6]. This coordinated movement of the quadruped's legs is defined by external parameters and a specific type of gait,

Received on 28 October 2025; revised 10 January 2026.
Address for correspondence: Felipe Mohr Santos. Av. Orlando Gomes, 1845 - Piatã, Salvador – BA – Brazil, Zipcode: 41650-010. E-mail: felipe.barreto@fieb.org.br.

J Bioeng. Tech. Health 2026;9(2):179-184

which will determine the sequence and contact time of each leg with the ground. The type of gait adopted directly impacts the robot's performance, influencing not only its stability, but also its agility and speed of locomotion [4].

Characteristics of Gait in Quadrupedal Robots

Usually, the gait cycle is divided into two subsequent phases: the support phase, in which the foot is in contact with the ground, propelling the robot in the direction of movement, and the swing phase, in which the foot is executing a trajectory in the air until the next point of support [7].

The type of gait adopted will define when each leg will be in the stance or swing phase. In static gaits, such as walking and crawling, the robot always keeps at least three legs in contact with the ground, which ensures greater stability at the expense of slower movement [1]. On the other hand, dynamic gaits, such as trot, pace, and gallop, have phases in which only one or two legs are in contact with the ground, enabling higher speeds of locomotion and requiring more sophisticated control to maintain balance and stability.

The robot's locomotion speed can be calculated according to the gait parameters, such that the speed v is given by:

$$v = \beta \frac{d_{step}}{T} \quad (1)$$

Where T is the period of a complete cycle of the foot movement, given by the sum of the stance phase period (Tst) and the swing phase period (T_{sw}), $T = T_{st} + T_{sw}$ [8], β represents the duty cycle of gait, that is, the ratio between the support time and the total cycle time, $\beta = T_{st}/T$ (values greater than 0.5 suggest greater stability), and finally dstep represents the step width. In addition to these parameters, the maximum elevation of the foot during the swing phase, or ground clearance (g_c), and the maximum penetration into the ground during the stance phase, or ground penetration (g_p), are other important parameters that influence the robot's ability to overcome obstacles [8].

Locomotion Control Methods

In order for the quadruped to be able to follow a certain gait while maintaining body balance, control methods must be applied to ensure precise movements and stability [1,4]. Such methodologies are categorized as model-based control (whether bio-inspired or not) and learning-based control [4].

Among the model-based methods, Model Predictive Control (MPC) stands out, which anticipates and optimizes actions considering constraints and plant reaction forces [4], and Whole-Body Control (WBC) [9], which determines ideal torques to minimize tracking errors. The Zero Moment Point (ZMP) criterion [10] is widely used to ensure stability by keeping the center of mass projection within the support polygon formed by the feet in contact with the ground. There are also approaches that explore analogies to physical or biological systems for generating movements, such as Virtual Model Control (VMC) [11] and the Spring-Loaded Inverted Pendulum (SLIP) model [12].

Learning-based controllers enable the robot to develop control policies through environmental interaction. Reinforcement learning (RL), a prominent approach, enables the robot to learn to maximize cumulative rewards using algorithms such as Proximal Policy Optimization (PPO) and Soft Actor-Critic (SAC) in continuous and high- dimensional environments [4]. The main advantage of RL lies in its adaptive learning capability, allowing it to generalize to complex and unseen terrains via Domain Randomization, as well as offering resilience to disturbances and optimizing energy efficiency [4,13,14].

A summary and comparison of these control methods are presented in Table 1.

Central Pattern Generators for Quadruped Robotics

Central Pattern Generators, in biology and neuroscience, represent a set of neuronal cells present in the spinal cord of vertebrates, responsible for generating rhythmic motor movements [5].

Table 1. Comparison of different locomotion control methods for quadruped robots, highlighting their main advantages, disadvantages, and notable applications.

Control Methods	Main Advantages	Main Disadvantages	References
Pure CPG (Hopf, VDP)	Computational simplicity, natural motion generation.	Open-loop, low adaptability to unexpected terrain	[15,16]
CPG + Inverse Kinematics	Precise foot position control, facilitates obstacles avoidance	Higher complexity can generate unfeasible joint solutions	[8,18]
Hybrid CPG (with RL)	High adaptabilidy and robustness, learns to handle different terrains and speeds.	Requires trainning (often time-consuming), can exhibit unexpected ("black-box") behavior	[8,20-23]
Model Predictive Control (MPC)	Optimizes future trajectory, good for dynamic and aggressive locomotion.	High computational cost	[4]
Whole-Body Control (WBC)	Controls the entire ronot's body, considering all forces and torques.	Complex model, difficult to implement	[9]

Unlike the other control methods presented, using CPGs it is possible to directly control the joints of the quadruped [15], or even control each of its legs [8] in a synchronized manner without the need for complex trajectory planners, state machines, or optimizers.

Oscillators for CPG

The application of CPGs to quadruped robotics represents a bioinspired control technique that consists of mathematically representing the rhythmic signals generated by CPGs through oscillatory, nonlinear, and coupled dynamic systems, which allow the generation of rhythmic movement control signals even when the control and sensory systems are isolated [1].

Although all oscillators usually share the same structure, the phase shift and coupling between them allow the creation of varied locomotion patterns, or different types of gait [5] (Figure 1).

The Hopf oscillator, represented by Equation 2, is one of the most widely used due to its mathematical simplicity and maturity [15]:

Where x and y represent the state variables. The term $r^2 = x^2 + y^2$ represents the squared radial

Figure 1. Coupling diagram of the four CPG oscillators used to generate the trot gait. The double-ended arrows indicate the mutual phase influence between each leg's CPG.

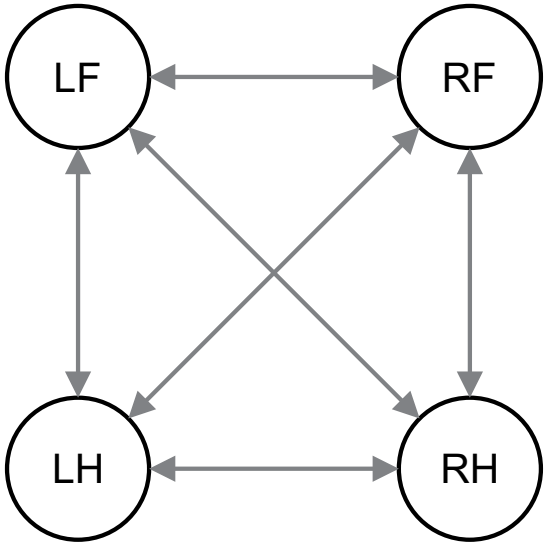

$$\begin{cases} \dot{x} = \alpha(\mu - r^2)x - \omega y \\ \dot{y} = \alpha(\mu - r^2)y + \omega x \\ r^2 = x^2 + y^2 \end{cases} \quad (2)$$

distance from the origin in the phase plane, directly related to the instantaneous amplitude of the oscillation. The parameter μ is a positive constant that defines the desired squared amplitude for a stable limit cycle. The dynamics of the oscillator, governed by the term $\alpha(\mu - r^2)$, continuously drive the system's amplitude r towards $\sqrt{\mu}$. The constant α influences the convergence speed to this limit cycle (stabilization), and ω defines the natural frequency of the oscillation. The frequency ω can be modified to generate asymmetric locomotion signals, so that the frequency of the stance phase (ω_{st}) is different from the swing phase (ω_{sw}), according to Equation 3, allowing the adoption of different gaits [1].

$$\omega = \frac{\omega_{st}}{e^{-ay}+1} + \frac{\omega_{sw}}{e^{ay}+1} \tag{3}$$

Another promising approach to gait control is based on the Van der Pol oscillator, a model that also relies on limit cycle theory for the generation of periodic and stable oscillation signals [16]. One of the main characteristics of this oscillator is its ability to converge to a single limit cycle, regardless of the initial conditions, resulting in a periodic and stable motion trajectory. The mathematical equation of the Van der Pol oscillator is given by Equation 4.

$$\ddot{x} - \alpha(p^2 - x^2)\dot{x} + \omega^2 x = 0 \tag{4}$$

Where the term $\alpha(p^2 - x^2)\dot{x}$ acts as a nonlinear damping, where α influences the shape of the output signal, p determines its amplitude, and ω defines the natural oscillation frequency. By adjusting the coupling topology and phase shift between multiple Van der Pol oscillators, it is possible to modulate the different phases of the robot's legs, allowing it to change its gait in a fluid and adaptable manner [16].

There is also the amplitude-controlled phase oscillator, presented by Ijspeert and colleagues [17], represented by Equations 5 and 6, where θ and r are the state variables, representing the phase and amplitude of the oscillator, respectively, while ω and μ represent its intrinsic frequency and amplitude, with a being a positive constant that interferes with the stabilization speed of the oscillator.

$$\ddot{r} = a\left(\frac{a}{4}(\mu - r) - \dot{r}\right) \tag{5}$$

$$\dot{\theta} = \omega \tag{6}$$

Applications of CPG in Quadruped Robots

Due to their simplicity and ability to generate natural movements, CPGs have been widely used to control the locomotion of quadrupedal robots. While some CPG applications in quadrupedal robots consist of using the signals generated by the CPG directly to control the robot's joints [14-16], another possibility is to use the CPG in combination with Inverse Kinematics [8], in which four coupled oscillators are used, one for each leg of the quadruped, so that the signals generated by each of these are converted into positions for the robot's legs, and subsequently converted into angular positions for the joints through the calculation of Inverse Kinematics [18] (Figure 2).

Due to the fact that, in essence, CPG is an open-loop control, strategies such as the one proposed in Righetti and Ijspeert [19] seek to close this loop to make the robot more adaptive. In this specific work, the loop is closed by changing the stance and swing phases of the legs only when the leg actually touches or leaves the ground, avoiding transitions at the wrong times that can destabilize the robot, especially on uneven terrain.

Another very efficient way to close the control loop and give the robot greater responsiveness and adaptability is by using hybrid control techniques. In recent years, CPG applications in combination with Reinforcement Learning have stood out, as they allow a trained agent to adapt to different conditions. Several studies focus on training an agent to parameterize CPG oscillators to ensure stable locomotion that is adaptable to different speed commands [8]. A similar study is proposed in [20], in which the CPG is kept fixed, while the agent learns corrections to the joint positions

Figure 2. Comparison of two hierarchical CPG control architectures: (a) the direct mapping approach, and (b) the inverse kinematics approach with a low-level PD feedback controller.

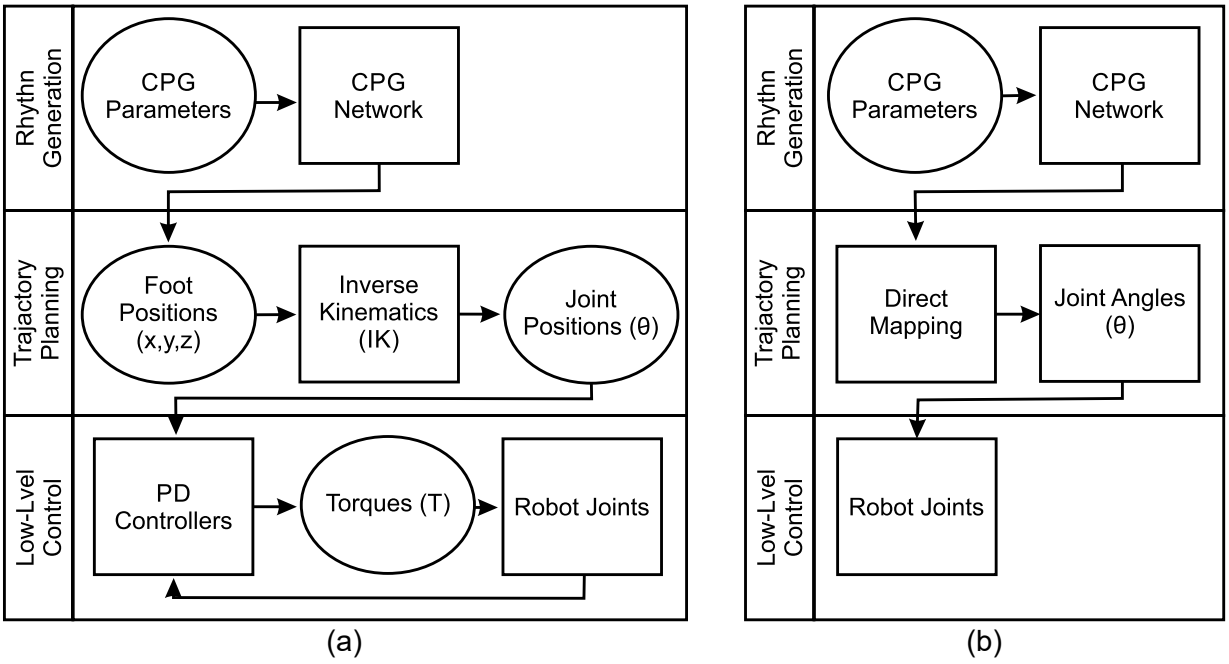

calculated by the CPG in conjunction with Inverse Kinematics, giving the robot greater adaptability and stability.

In addition, there are applications that explore the use of Reinforcement Learning to enable smooth transitions between different types of gait [21] or even to cross gaps in the ground [22] and navigate autonomously by using exteroceptive data [23].

Conclusion

This paper presented the main concepts of quadruped robot locomotion, with an emphasis on control methods based on Central Pattern Generators and their applications.

The use of CPGs in quadruped robotics represents a simple and efficient way to control this type of robot, enabling the adoption of different types of gaits by simply changing the coupling or difference between the oscillators, without the need for trajectory planners or optimizers. In addition, CPGs require low computational power for their application, not necessarily requiring a sensing system integrated with the control system to be implemented.

Hybrid control methods stand out, combining CPG techniques with learning-based methods, providing the robot with the ability to dynamically adapt to the environment and different terrains.

In future work, Central Pattern Generators will be applied to a real quadruped robot [17] to analyze their effectiveness in locomotion control.

Acknowledgement

This work is being developed at SENAI CIMATEC's Robotics and Autonomous Systems Competence Center as part of the scholarship program.

References

1. Dong S, et al. Gait planning and motion control methods for quadruped robots: achieving high environmental adaptability: a review. Comput Model Eng Sci. 2025;143(1):1–10. doi:10.32604/cmes.2025.062113.
2. Fankhauser P, Bjelonic M, Bellicoso D, Miki T, Hutter M. Robust rough-terrain locomotion with a quadrupedal robot. In: Proc IEEE Int Conf Robot Autom (ICRA); 2018. doi:10.1109/ICRA.2018.8460731.
3. Miao X, et al. PALO: learning posture-aware locomotion for quadruped robots. 2025 Mar 6.

4. Akki S, Chen T. Benchmarking model predictive control and reinforcement learning-based control for legged robot locomotion in MuJoCo simulation. IEEE Access. 2025;13:108732–108742. doi:10.1109/ACCESS.2025.3582523.
5. Ijspeert AJ. Central pattern generators for locomotion control in animals and robots: a review. Neural Netw. 2008;21(4):642–653.
6. Iscen A, Caluwaerts K, Tan J, Zhang T, Coumans E, Sindhwani V, et al. Policies modulating trajectory generators. arXiv [Preprint]. 2018. arXiv:1910.02812.
7. Carbone G, Ceccarelli M. Legged robotic systems. In: Kordic V, Lazinica A, Merdan M, editors. Cutting edge robotics. Vienna: ARS/PIV; 2005.
8. Bellegarda G, Ijspeert AJ. CPG-RL: learning central pattern generators for quadruped locomotion. IEEE Robot Autom Lett. 2022;7(4):12547–12554. doi:10.1109/LRA.2022.3218167.
9. Sentis L, Park J, Khatib O. Whole-body dynamic control of human-like robots. Auton Robots. 2010;33(1-2):13–39.
10. Vukobratović M, Borovac B. Zero-moment point—thirty five years of its life. Int J Humanoid Robot. 2004;1(1):157–173.
11. Pratt J, et al. Virtual model control: an intuitive approach for bipedal locomotion. Int J Robot Res. 2001;20(2):129–143.
12. Blickhan R. The spring-mass model for running and hopping. J Biomech. 1989;22(11-12):1217–1227.
13. Seto R, Li G, Kutsuzawa K, Owaki D, Hayashibe M. Two-stage learning of CPG and postural reflex toward quadruped locomotion on uneven terrain with simple reward. IEEE Access. 2025;13:106103–106114.
14. Lyu S, Zhao H, Wang D. A composite control strategy for quadruped robot by integrating reinforcement learning and model-based control. In: Proc IEEE/RSJ Int Conf Intell Robots Syst (IROS); 2023. p. 751–758.
15. Ma Z, Liang Y, Tian H. Research on gait planning algorithm of quadruped robot based on central pattern generator. In: Proc 39th Chin Control Conf (CCC); 2020; Piscataway (NJ): IEEE. p. 3948–3953.
16. Li F, Pang L, Dai T. CPG motion controller based on Van der Pol nonlinear oscillator for a quadruped robot. In: Proc 5th Int Conf Robot Intell Control Artif Intell (RICAI); 2023. p. 236–239. doi:10.1109/RICAI60863.2023.10489012.
17. Ijspeert AJ, Crespi A, Ryczko D, Cabelguen JM. From swimming to walking with a salamander robot driven by a spinal cord model. Science. 2007;315(5817):1416–1420. doi:10.1126/science.1138353.
18. Souza L, Mohr F, Alencar B. Analysis, prototyping and locomotion control of a quadruped robot. In: Latin American Robotics Symposium (LARS), Brazilian Symposium on Robotics (SBR), and Workshop on Robotics in Education (WRE); 2023; Salvador, Brazil. p. 129–134. doi:10.1109/LARS/SBR/WRE59448.2023.10333039.
19. Righetti L, Ijspeert AJ. Pattern generators with sensory feedback for the control of quadruped locomotion. In: Proc IEEE Int Conf Robot Autom (ICRA); 2008; Pasadena (CA). p. 819–824. doi:10.1109/ROBOT.2008.4543306.
20. Zhang X, Xiao Z, Zhang Q, Pan W. SYNLOCO: synthesizing central pattern generator and reinforcement learning for quadruped locomotion. arXiv [Preprint]. 2023. arXiv:2310.06606.
21. Bellegarda G, Shafiee M, Ijspeert AJ. AllGaits: learning all quadruped gaits and transitions. arXiv [Preprint]. 2024. arXiv:2411.04787.
22. Shafiee M, Bellegarda G, Ijspeert AJ. Puppeteer and marionette: learning anticipatory quadrupedal locomotion based on interactions of a central pattern generator and supraspinal drive. In: Proc IEEE Int Conf Robot Autom (ICRA); 2023. p. 1112–1119.
23. Bellegarda G, Shafiee M, Ijspeert AJ. Visual CPG-RL: learning central pattern generators for visually-guided quadruped locomotion. In: Proc IEEE Int Conf Robot Autom (ICRA); 2024; Yokohama, Japan. p. 1420–1427. doi:10.1109/ICRA57147.2024.10611128.

Instructions for Authors

The Authors must indicate in a cover letter the address, telephone number and e-mail of the corresponding author. The corresponding author will be asked to make a statement confirming that the content of the manuscript represents the views of the co-authors, that neither the corresponding author nor the co-authors have submitted duplicate or overlapping manuscripts elsewhere, and that the items indicated as personal communications in the text are supported by the referenced person. Also, the protocol letter with the number should be included in the submission article, as well as the name of sponsors (if applicable).

Manuscripts may be submitted within designated categories of communication, including:

- Original basic or clinical investigation (original articles on topics of broad interest in the field of bioengineering and biotechnology applied to health). We particularly welcome papers that discuss epidemiological aspects of international health, clinical reports, clinical trials and reports of laboratory investigations.
- Case presentation and discussion (case reports must be carefully documented and must be of importance because they illustrate or describe unusual features or have important practice implications).
- Brief reports of new methods or observations (short communications brief reports of unusual or preliminary findings).
- State-of-the-art presentations (reviews on protocols of importance to readers in diverse geographic areas. These should be comprehensive and fully referenced).
- Review articles (reviews on topics of importance with a new approach in the discussion). However, review articles only will be accepted after an invitation of the Editors.
- Letters to the editor or editorials concerning previous publications (correspondence relating to papers recently published in the Journal, or containing brief reports of unusual or preliminary findings).
- Editor's corner, containing ideas, hypotheses and comments (papers that advance a hypothesis or represent an opinion relating to a topic of current interest).
- Innovative medical products (description of new biotechnology and innovative products applied to health).
- Health innovation initiatives articles (innovative articles of technological production in Brazil and worldwide, national policies and directives related to technology applied to health in our country and abroad).

The authors should checklist comparing the text with the template of the Journal.

Supplements to the JBTH include articles under a unifying theme, such as those summarizing presentations of symposia or focusing on a specific subject. These will be added to the regular publication of the Journal as appropriate, and will be peer reviewed in the same manner as submitted manuscripts.

Statement of Editorial Policy

The editors of the Journal reserve the right to edit manuscripts for clarity, grammar and style. Authors will have an opportunity to review these changes prior to creation of galley proofs. Changes in content after galley proofs will be sent for reviewing and could be required charges to the author. The JBTH does not accept articles which duplicate or overlap publications elsewhere.

Peer-Review Process

All manuscripts are assigned to an Associate Editor by the Editor-in-Chief and Deputy Editor, and sent to outside experts for peer review. The Associate Editor, aided by the reviewers' comments, makes a recommendation to the Editor-in-Chief regarding the merits of the manuscript. The Editor-in-Chief makes a final decision to accept, reject, or request revision of the manuscript. A request for revision does not guarantee ultimate acceptance of the revised manuscript.

Manuscripts may also be sent out for statistical review ou *ad hoc* reviewers. The average time from submission to first decision is three weeks.

Revisions

Manuscripts that are sent back to authors for revision must be returned to the editorial office by 15 days after the date of the revision request. Unless the decision letter specifically indicates otherwise, it is important not to increase the text length of the manuscript in responding to the comments. The cover letter must include a point-by-point response to the reviewers and Editors comments, and should indicate any additional changes made. Any alteration in authorship, including a change in order of authors, must be agreed upon by all authors, and a statement signed by all authors must be submitted to the editorial office.

Style

Manuscripts may be submitted only in electronic form by www.jbth.com.br. Each manuscript will be assigned a registration number, and the author notified that the manuscript is complete and appropriate to begin the review process. The submission file is in OpenOffice, Microsoft Word, or RTF document file format for texts and JPG (300dpi) for figures.

Authors must indicate in a cover letter the address, telephone number, fax number, and e-mail of the corresponding author. The corresponding author will be asked to make a statement confirming that the content of the manuscript represents the views of the co-authors, that neither the corresponding author nor the co-authors have submitted duplicate or overlapping manuscripts elsewhere, and that the items indicated as personal communications in the text are supported by the referenced person.

Manuscripts are to be typed as indicated in Guide for Authors, as well as text, tables, references, legends. All pages are to be numbered with the order of presentation as follows: title page, abstract, text, acknowledgements, references, tables, figure legends and figures. A running title of not more than 40 characters should be at the top of each page. References should be listed consecutively in the text and recorded as follows in the reference list, and must follow the format of the National Library of Medicine as in Index Medicus and "Uniform Requirements for Manuscripts Submitted to Biomedical Journals" or in "Vancouver Citation Style". Titles of journals not listed in Index Medicus should be spelled out in full.

Manuscript style will follow accepted standards. Please refer to the JBTH for guidance. The final style will be determined by the Editor-in-Chief as reviewed and accepted by the manuscript's corresponding author.

Approval of the Ethics Committee

The JBTH will only accept articles that are approved by the ethics committees of the respective institutions (protocol number and/or approval certification should be sent after the references). The protocol number should be included in the end of the Introduction section of the article.

Publication Ethics

Authors should observe high standards with respect to publication ethics as set out by the International Committee of Medical Journal Editors (ICMJE). Falsification or fabrication of data, plagiarism, including duplicate publication of the authors' own work without proper citation, and misappropriation of the work are all unacceptable practices. Any cases of ethical misconduct are treated very seriously and will be dealt with in accordance with the JBTH guidelines.

Conflicts of Interest

At the point of submission, each author should reveal any financial interests or connections, direct or indirect, or other situations that might raise the question of bias in the work reported or the conclusions, implications, or opinions stated - including pertinent commercial or other sources of funding for the individual author(s) or for the associated department(s) or organizations(s), and personal relationships. There is a potential conflict of interest when anyone involved in the publication process has a financial or other beneficial interest in

the products or concepts mentioned in a submitted manuscript or in competing products that might bias his or her judgment.

Material Disclaimer

The opinions expressed in JBTH are those of the authors and contributors, and do not necessarily reflect those of the SENAI CIMATEC, the editors, the editorial board, or the organization with which the authors are affiliated.

Privacy Statement

The names and email addresses entered in this Journal site will be used exclusively for the stated purposes of this journal and will not be made available for any other purpose or to any other party.

Brief Policies of Style

Manuscript	Original	Review	Birief Comunication	Case Report	Editorial ; Letter to the Editor; Editor' s Corner	Innovative Medical Products	State-of-the-Art	Health Innovation Initiatives
Font Type	Times or Arial	Times or Arial	Times or Arial	Times or Arial	Times or Arial	Times or Arial	Times or Arial	Times or Arial
Number of Words – Title	120	90	95	85	70	60	120	90
Font Size/Space-Title	12; double space	12; double space	12; double space	12; double space	12; double space	12; double space	12; double space	12; double space
Font Size/Space-Abstracts/Key Words and Abbreviations	10; single space	10; single space	10; single space	10; single space	-	-	10; single space	10; single space
Number of Words – Abstracts/Key Words	300/5	300/5	200/5	250/5	-	-	300/5	300/5
Font Size/Space-Text	12; Double space	12; Double space	12; Double space	12; Double space	12; Double space	12; Double space	12; Double space	12; Double space
Number of Words – Text	5,000 including spaces	5,500 including spaces	2,500 including spaces	1,000 including spaces	1,000 including spaces	550 including spaces	5,000 including spaces	5,500 including spaces
Number of Figures	8 (title font size 12, double space)	3 (title font size 12, double space)	2 (title font size 12, double space)	2 (title font size 12, double space)	-	2 (title font size 12, double space)	8 (title font size 12, double space)	8 (title font size 12, double space)
Number of Tables/Graphic	7 title font size 12, double space	2 title font size 12, double space	2(title font size 12, double space)	1(title font size 12, double space)	-	-	7 title font size 12, double space	4 title font size 12, double space
Number of Authors and Co-authors*	15	10	5	10	3	3	15	10
References	20 (font size 10,single space	30(font size 10,single space	15 (font size 10,single space)	10 (font size 10,single space)	10 (font size 10,single space	5(font size 10,single space	20 (font size 10,single space	20

*First and last name with a sequencing overwritten number. Corresponding author(s) should be identified with an asterisk; Type 10, Times or Arial, single space. Running title of not more than 40 characters should be at the top of each page. References should be listed consecutively in the text. References must be cited on (not above) the line of text and in brackets instead of parentheses, e.g., [7,8]. References must be numbered in the order in which they appear in the text. References not cited in the text cannot appear in the reference section. References only or first cited in a table or figures are numbered according to where the table or figure is cited in the text. For instance, if a table is placed after reference 8, a new reference cited in table 1 would be reference 9.1 would be reference 9.

Checklist for Submitted Manuscripts

❑1. Please provide a cover letter with your submission specifying the corresponding author as well as an address, telephone number and e-mail.

❑2. Submit your paper using our website www.jbth.com.br. Use Word Perfect/Word for Windows, each with a complete set of original illustrations.

❑3. The entire manuscript (including tables and references) must be typed according to the guidelines instructions.

❑4. The order of appearance of material in all manuscripts should be as follows: title page, abstract, text, acknowledgements, references, tables, figures/graphics/diagrams with the respective legends.

❑5. The title page must include a title of not more than three printed lines (please check the guidelines of each specific manuscript), authors (no titles or degrees), institutional affiliations, a running headline of not more than 40 letters with spaces.

❑6. Acknowledgements of persons who assisted the authors should be included on the page preceding the references.

❑7. References must begin on a separate page.

❑8. References must be cited on (not above) the line of text and in brackets instead of parentheses, e.g., [7,8].

❑9. References must be numbered in the order in which they appear in the text. References not cited in the text cannot appear in the reference section. References only or first cited in a table or figures are numbered according to where the table or figure is cited in the text. For instance, if a table is placed after reference 8, a new reference cited in table 1 would be reference 9.

❑10. Reference citations must follow the format established by the "Uniform Requirements for Manuscripts Submitted to Biomedical Journals" or in "Vancouver Citation Style".

❑11. If you reference your own unpublished work (i.e., an "in press" article) in the manuscript that you are submitting, you must attach a file of the "in press" article and an acceptance letter from the journal.

❑12. If you cite unpublished data that are not your own, you must provide a letter of permission from the author of that publication.

❑13. Please provide each figure in high quality (minimum 300 dpi: JPG or TIF). Figure must be on a separate file.

❑14. If the study received a financial support, the name of the sponsors must be included in the cover letter and in the text, after the author's affiliations.

❑15. Provide the number of the Ethics Committees (please check the guidelines for authors).